The Use of a Novel Antioxidant Compound, WN1316, for the Treatment of Experimental Glaucoma

Leyla Pourang

Thesis submitted to the University of Ottawa
in partial fulfillment of the requirements for the
MSc. degree in Neuroscience

Department of Cellular and Molecular Medicine
Faculty of Medicine
University of Ottawa

ABSTRACT

Glaucoma is a leading cause of irreversible blindness worldwide, characterized by the death of retinal ganglion cells (RGCs). Accumulating evidence has revealed that in addition to elevated intraocular pressure (IOP), oxidative stress also plays a significant role in glaucomatous pathology. In this respect, this thesis assessed whether a novel antioxidant compound, WN1316, could offer functional and structural protection of RGCs in the magnetic microbead mouse model of glaucoma. WN1316 has been previously shown to protect against oxidative stress-induced cell death in other disease models. Sustained IOP elevations were achieved in microbead-injected eyes; however, confounding lens and corneal damage developed, complicating the disease phenotype and the interpretation of WN1316's effects on RGCs. Trends in the electrophysiological and histological data were therefore not consistent and the therapeutic efficacy of WN1316 remains inconclusive. Future studies should thus refine the glaucomatous disease model to better assess the clinical potential of WN1316.

TABLE OF CONTENTS

LIST OF FIGURES

CHAPTER 1. INTRODUCTION

CHAPTER 3. RESULTS

ABBREVIATIONS

8-OH-dG	8-hydroxy-2'-deoxyguanosine
AD	Alzheimer's disease
AIF	Apoptosis-inducing factor
ALS	Amyotrophic lateral sclerosis
AOND-QSAR	Anti-Oxidative Neuronal Cell Death Quantitative Structure Activity Relationship
APAF-1	Apoptosis-inducing factor-1
ARE	Antioxidant response element
ARVO	Association for Research in Vision and Ophthalmology
ATP	Adenosine triphosphate
BBB	Blood-brain barrier
BCL-2	B-cell CLL/lymphoma 2
BDNF	Brain-derived neurotrophic factor
BMPs	Bone morphogenic proteins
BRB	Blood-retina barrier
CAIs	Carbonic anhydrase inhibitors
cKO	Conditional knockout
CNS	Central nervous system
CNTF	Ciliary neurotrophic factor
CSF	Cerebrospinal fluid
ECM	Extracellular matrix
ELAM-1	Endothelial leukocyte adhesion molecule-1
ER	Endoplasmic reticulum
ERG	Electroretinography
FADD	Fas-associated death domain
ffERG	Full-field scotopic flash ERG
GCL	Ganglion cell layer

GDDs	Glaucoma drainage devices
GSH	Glutathione
HLA-DR	Human leukocyte antigen-DR
HMSCs	Hyper-mature senile cataracts
HO-1	Heme oxygenase-1
IAPs	Inhibitory apoptosis proteins
ICP	Intracranial pressure
IL-1β	Interleukin-1 beta
IMS	Intermembrane space
INL	Inner nuclear layer
iNOS	Inducible nitric oxide synthase
IOP	Intraocular pressure
JNK	c-Jun N-terminal kinase
Keap1	Kelch-like erythroid cell-derived protein
LIG	Lens-induced glaucoma
MHC	Major histocompatibility complex
MMPs	Matrix metalloproteinases
MOMP	Mitochondrial outer membrane permeabilization
mtDNA	Mitochondrial DNA
MYOC	Myocilin
NAIP	Neuronal apoptosis inhibitory protein
$NADH^+$	Nicotinamide adenine dinucleotide + hydrogen
NGF	Nerve growth factor
NQO1	NAD(P)H quinone oxidoreductase
NO	Nitric oxide
NTF	Neurotrophic factor
NTG	Normotensive glaucoma

Nrf2	Nuclear factor-erythroid 2-related factor 2
OAG	Open-angle glaucoma
OCT	Optical coherence tomography
ONL	Outer nuclear layer
OPL	Outer plexiform layer
OPs	Oscillatory potentials
PACG	Primary angle-closure glaucoma
PARP	Poly(ADP-ribose) polymerase
PAS	Peripheral anterior synechiae
PERG	Pattern ERG
PGAs	Prostaglandin analogs
PI3K	Phosphotidylinosol-3 kinase
PMG	Phacomorphic glaucoma
POAG	Primary open-angle glaucoma
RBPMS	RNA-binding protein with multiple splicing
RGCs	Retinal ganglion cells
RIPK1	Receptor-interacting protein kinase-1
RIPK3	Receptor-interacting protein kinase-2
RNFL	Retinal nerve fibre layer
ROS	Reactive oxygen species
SC	Superior colliculus
SDS-PAGE	SDS/polyacrylamide gel electrophoresis
SMAC	Second mitochondria-derived activator of caspase
SOD	Superoxide dismutase
SOD2	Superoxide dismutase 2
TGF-β2	Transforming growth factor beta-2
TM	Trabecular meshwork

TMC	Trabecular meshwork cell
TNF-α	Tumor necrosis factor alpha
TNF-R1	Tumor necrosis factor receptor-1
TRAIL	Tumor necrosis factor-related apoptosis-inducing ligand
VEPs	Visual evoked potentials
WN1316	2-[mesityl(methyl)amino]-N-[4(pyridine-2-yl] acetamide trihydrochloride
XIAP	X-linked inhibitor of apoptosis

ACKNOWLEDGEMENTS

I would firstly like to thank my supervisor, Dr. Catherine Tsilfidis, for her guidance throughout this project. I also extend my gratitude to my thesis advisory committee, Dr. Pierre Mattar and Dr. David Picketts, for their detailed feedback and encouragement.

My sincere thanks go out to Adam Baker and Dr. Pamela Lagali for their contributions to this project, for teaching me laboratory techniques, and for being encouraging and supportive mentors. Adam, thank you for the technical assistance with surgeries and electroretinography, and for your encouragement during challenging experiments. Pam, thank you for assisting during sampling and for your wisdom and mentorship throughout my time in the lab. I could not have asked for better mentors who made me look forward to coming into the lab every day. I also thank my lab mates Batoul Jomaa and Mayar Alkhbuli for their contributions.

I cannot thank my family and friends enough for always encouraging me and for believing in me even when I felt I could not believe in myself. Your support means more to me than you could ever know.

This thesis is dedicated to the memory of my childhood best friend, Florie. I miss you all the time.

CHAPTER 1. INTRODUCTION

1.0 The Sense of Sight

Vision is often regarded as the most complex of the five senses; the visual perception of an organism's external environment is a multi-step process that involves the orchestration of ocular refraction, phototransduction, and the processing of visual information. As light passes through the eye, it is first refracted by the cornea and lens onto the retina, where light stimulation in the form of photons is converted into visual information in the form of action potentials. These neural impulses are conveyed by optic nerve fibres to several higher-order vision centres in the brain for processing; thirty to fifty-five percent of the mammalian brain is dedicated to vision (reviewed by Ptito et al., 2021). Damage at any point along the visual pathway can lead to a variety of debilitating ocular diseases that can hinder an individual's ability to perceive and interact with the external environment, in turn resulting in poor quality of life.

1.1 Gross Anatomy of the Eye

The mammalian eye is anatomically divided into two distinct regions: the anterior and posterior segments. The cornea, iris, pupil, conjunctiva, ciliary body, anterior chamber, trabecular meshwork, and lens comprise the anterior segment, while the posterior segment is composed of the vitreous humour, sclera, choroid, retina, macula, and optic nerve (Figure 1.1) (Addo, 2016). As light first enters the eye, it is refracted by the cornea, the outermost region of the eye that accounts for two-thirds of the total ocular refractory power (Figure 1.1) (Addo, 2016).

After passing through the anterior chamber, light enters the pupil, the diameter of which is reflexively regulated by the iris depending on the degree of light exposure. Behind the pupil, the elastic lens further refracts light by expanding or contracting, a process known as accommodation. Light then enters the posterior segment where it passes through the vitreous, a transparent, gelatinous liquid that

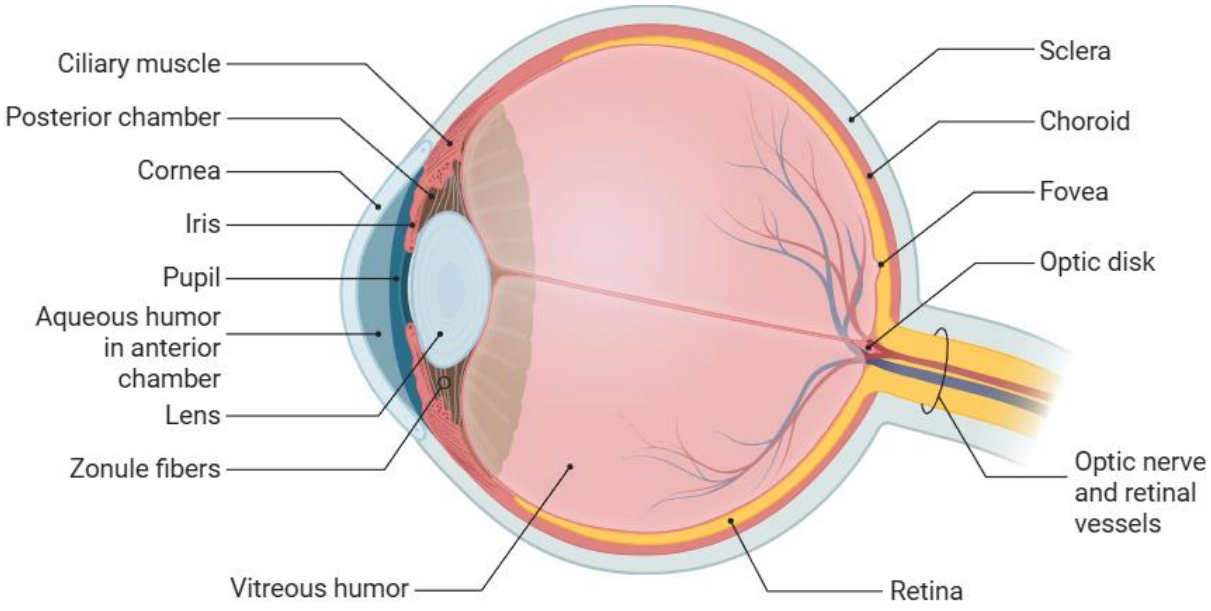

Figure 1.1. Gross anatomy of the eye. The cornea and lens refract light to focus it onto the retina, a photosensitive tissue located at the posterior end of the eye where visual signals in the form of photons are converted into electrical signals. Adapted from "Anatomy of the Human Eye" by BioRender.com. Retrieved from https://app.biorender.com/biorender-templates/figures. 29.2

fills the space between the lens and retina akin to how aqueous humour fills the space between the cornea and iris. The refracted light is ultimately focused onto the retina where phototransduction transpires (Figure 1.1) (Sharif, 2021).

1.2 The Retina

The retina is a photosensitive tissue located at the posterior end of the eye. It is at the level of the retina where the transduction of light in the form of photons to electrical signals occurs. Retinal cell types are divided into three broad classes based on function: photoreceptor cells, neuronal cells, and glial cells (Addo, 2016). These cells are discretely organized into three distinct nuclear layers punctuated by two synaptic layers (Figure 1.2) (Masland, 2012).

The outer nuclear layer (ONL), the nuclear layer located furthest from the front of the eye, is primarily composed of photoreceptor cell bodies, the rod and cone cells. Rod cells are highly specialized for low-light detection as well as motion detection, and they outnumber cone cells by 20-fold in most mammalian retinas (Masland, 2012). Cone cells are primarily responsible for visual acuity and processing colour vision and, in primates, come in three different types that each process different wavelengths of light (Masland, 2012). Ultimately, rods and cones work in tandem to transform light stimulation into graded potentials that are synaptically transmitted through the outer plexiform layer (OPL) to bipolar, amacrine, and horizontal interneurons whose nuclei are located in the inner nuclear layer (INL). Through the inner plexiform layer (IPL), interneurons then relay the photoreceptor-derived electrical signals to retinal ganglion cells (RGCs). RGC nuclei compose the ganglion cell layer (GCL) alongside displaced amacrine cells, and their axons comprise the retinal nerve fibre layer (RNFL). RGCs are central nervous system (CNS) neurons that serve to convert photoreceptor- and interneuron-derived graded potentials into action potentials that travel along their long-projecting axons extending to the visual cortex (Figure 1.2).

1.3 The Optic Nerve

The axons of approximately 1.2 million human RGCs bundle together at the optic disc to form the optic nerve, which connects the retina to the brain (Smith & Czyz, 2025). The optic nerve exits the back of the eye through the lamina cribrosa, a mesh-like structure that provides structural support to the unmyelinated RGC axons. After passing through the lamina cribrosa, the optic nerve passes through the skull through an opening known as the optic foramen and continues to travel along the optic chiasm within the middle cranial fossa (Figure 1.2). At the optic chiasm, nerve fibers originating from the nasal retina cross over to the contralateral optic tract, and temporal retinal fibers continue to travel along the ipsilateral optic tract; this anatomical organization of the retinal fibres causes each optic tract to relay visual information from the contralateral visual fields. The majority of the optic tract fibres culminate in the lateral geniculate nucleus (LGN) of the thalamus, while a small minority project to the pretectal nucleus of the midbrain and the superior colliculus (SC) which regulate the pupillary light reflex and saccadic eye movements, respectively (Smith & Czyz, 2025). LGN axons form the optic radiations, or geniculocalcarine tracts, which project to the primary visual cortex of the occipital lobe where visual information is processed and relayed to other visual association areas for further processing (Smith & Czyz, 2025).

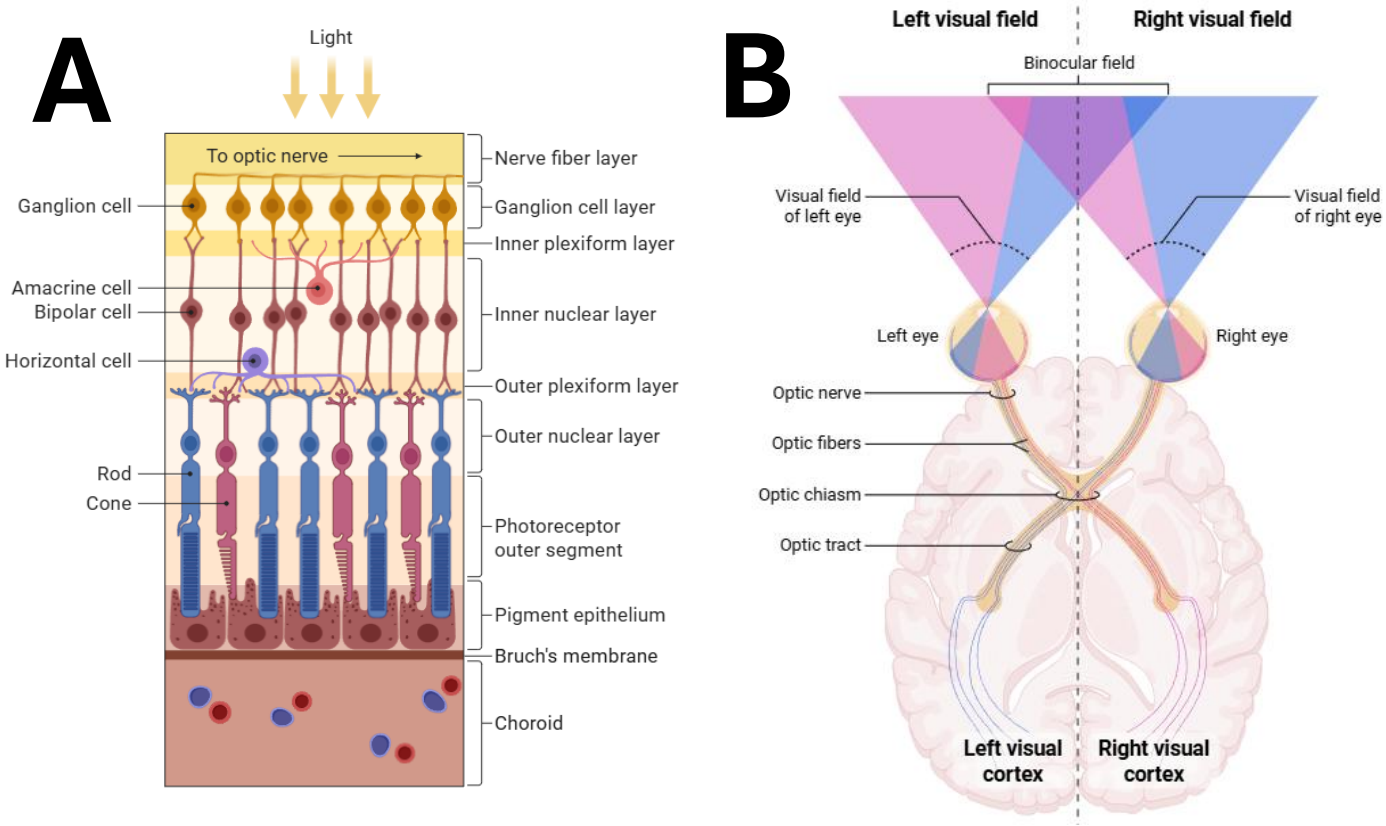

Figure 1.2. Overview of the visual pathway. (A) The retina is a laminar tissue, with distinct types of neurons and glia residing within each layer. As light enters the retina, it is first processed by rod and cone photoreceptors in the outer nuclear layer (ONL), which produce graded potentials and synaptically relay the visual signals through the outer plexiform layer (OPL) to bipolar cell interneurons in the inner nuclear layer. Amacrine cells are another neuronal cell type found within the INL and ganglion cell layer (GCL) that assist bipolar cells in synaptically transmitting visual signals to retinal ganglion cells (RGCs) in the GCL. RGCs are central nervous system (CNS) neurons and are the only neuronal cell type to produce action potentials, which are conducted through the optic nerve to visual centres in the brain for processing. Adapted from "Structure of the Retina" by BioRender.com. Retrieved from https://app.biorender.com/biorender-templates/figures. (B) The visual pathway extends from the eye to the visual cortex in the brain for processing. Visual information from the left or right visual field is relayed through the contralateral optic tract. Adapted from "Integration of Information in the Human Visual System" by BioRender.com. Retrieved from https://app.biorender.com/biorender-templates/figures.

1.4 Intraocular Pressure

The space between the cornea and the iris, the anterior chamber, is filled with a clear fluid known as aqueous humour, which maintains the globular shape of the eye, provides nutrition to the cornea to compensate for its avascular nature, eliminates metabolic waste products, and transports neurotransmitters (Addo, 2016). Aqueous humour is produced by the ciliary body, secreted by the ciliary epithelium, and drained conventionally through the trabecular meshwork and Schlemm's canal and unconventionally through the uveoscleral outflow pathway (Figure 1.3) (Weinreb et al., 2014). The trabecular meshwork is a fenestrated structure located in the iridocorneal angle of the anterior chamber and is made up of connective tissues that are surrounded by endothelial-like cells. Three distinct parts constitute the trabecular meshwork: the uveal meshwork, characterized by elongated connective tissue derived from the iris and ciliary body stroma, the corneoscleral meshwork, identified by the presence of endothelium-covered lamellae, and the juxtacanalicular meshwork, comprised of cells that are embedded in an elaborate extracellular matrix (ECM) (Buffault et al., 2020). The balance between the production and outflow of aqueous humour is essential for the maintenance of intraocular pressure (IOP).

1.5 Glaucoma

Glaucoma is a group of ocular neurodegenerative diseases and a leading cause of irreversible blindness worldwide. The cornerstone of glaucomatous pathology is the death of RGCs and the degeneration of their axons that form the optic nerve. Degeneration of RGC axons results in a phenomenon known as "cupping" of the optic nerve, in which a distinct depression forms in the central optic disk (Weinreb et al., 2014). Glaucoma currently affects 80 million individuals, with projections indicating a substantial surge in prevalence in the next few decades; it is anticipated that 112 million people will be diagnosed with glaucoma by 2040 in part due to the increasingly aging world

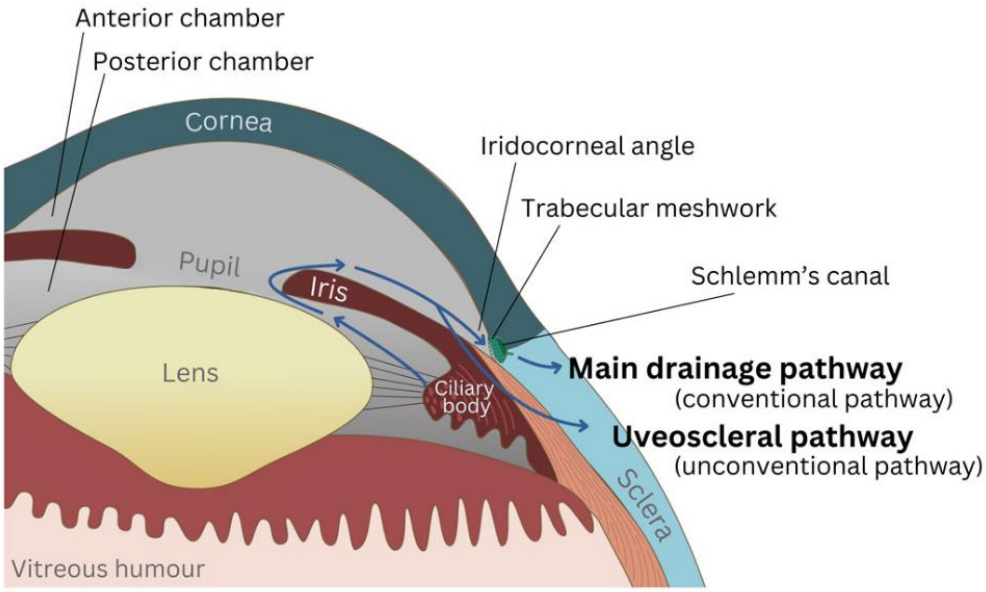

Figure 1.3. Aqueous humour dynamics. Aqueous humour, a clear fluid that maintains the shape of the anterior chamber and provides nourishment to the cornea, is produced by the ciliary body and drained primarily through the conventional pathway and secondarily through the unconventional pathway. In the conventional pathway, aqueous humour exits the anterior chamber through the trabecular meshwork and Schlemm's canal, while in the uveoscleral pathway, aqueous humour passes through the ciliary muscle and into the supraciliary and suprachoroidal spaces. Reproduced with permission from Souzeau et al., 2024.

population (Sharif, 2021). Approximately 400,000 Canadians are living with glaucoma, with direct costs of glaucomatous vision loss estimated at $300 million annually (Cruess et al., 2011). It is likely that many more individuals are affected by glaucoma; it is often referred to as the "silent thief of sight" as symptoms of vision loss typically do not present until the optic nerve has undergone severe and irreparable damage (Sharif, 2021). Hence, glaucoma presents as a major socioeconomic burden accounting for decreased quality of life and morbidity (WHO, 2019), underscoring the need for novel and holistic therapeutic avenues; a one-size-fits-all therapeutic approach cannot exist for glaucoma, as it is a multifactorial disease with a wealth of known risk factors such as advanced age, genetics, high blood pressure, diabetes, prolonged corticosteroid use, elevated IOP, and oxidative stress (Weinreb et al., 2014).

1.5.1. Subtypes of Glaucoma

Glaucoma is a heterogeneous disease and is broadly divided into three major categories: open-angle glaucoma, angle-closure glaucoma, and normotensive glaucoma. The "angle" term is in reference to the angle between the iris and the cornea, known as the iridocorneal angle, where the drainage of aqueous humour occurs (Sunderland & Sapra, 2025). Open-angle glaucoma accounts for the vast majority of cases and is characterized by resistance to aqueous humour outflow through the trabecular meshwork, leading to the accumulation of aqueous humour in the anterior chamber and subsequent increases in IOP, typically above 21 mmHg (Kaushik et al., 2024). Angle-closure glaucoma, though less common than the open-angle subtype, disproportionately accounts for severe cases of glaucomatous vision loss and is classified by the physical occlusion of the drainage canals in the anterior chamber, in turn leading to elevations in IOP outside the normal range. Open-angle and angle-closure glaucoma can be further subdivided into primary and secondary subtypes, with the secondary form attributed to known external factors such as diabetes, inflammation, and physical

injury. Normotensive glaucoma is the rarest and most elusive subtype, in which glaucomatous optic neuropathy persists despite patients continuously showing IOP levels within the normal range (Kaushik et al., 2024).

1.5.1.2. Primary Open-Angle Glaucoma

Primary open-angle glaucoma (POAG) is the most prevalent of the glaucoma subtypes, accounting for approximately 90% of diagnosed glaucoma cases in Canada (Jin et al., 2024). The majority of POAG patients are diagnosed around the ages 55-74. POAG remains asymptomatic until advanced stages of the disease, when patients may begin to notice blurred vision in one or both eyes, gradual loss of peripheral vision, and lack of contrast sensitivity. The initial diagnosis of POAG is speculative, and consistent findings over the course of several years such as visual field defects, a 0.3 or greater cup-to-disk ratio, nerve fibre deficits observed by optical coherence tomography (OCT), and IOP readings over 21 mmHg are required to confirm the diagnosis (Michels & Ivan, 2023).

In POAG, RGC death is attributed to elevations in IOP caused by the imbalance between the secretion and outflow of aqueous humour. POAG patients show reduced outflow of aqueous humour through the trabecular meshwork, the main drainage pathway, leading to the accumulation of aqueous humour in the anterior chamber. An established mechanism for the increased resistance of the trabecular meshwork to aqueous humour outflow remains elusive, but proposed factors include extracellular matrix (ECM) remodelling, trabecular meshwork cell (TMC) senescence and apoptosis, actin cytoskeleton dynamic changes in connective tissue, and changes in the expression levels of transforming growth factor β2 (TGF-β2) and bone morphogenic protein (BMP) antagonists (Buffault et al., 2020). Clinical studies with POAG patients have observed trabecular stiffening indicated by the marked increase in presence of extracellular sheath-derived plaques compared to age-matched normal subjects; the increase in these plaques is caused by fibrils and ECM components adhering to elastic

fibre sheaths along the inner wall of the trabecular meshwork endothelium (Buffault et al., 2020). Furthermore, reductions in TMC numbers have been observed in POAG patients, consequently causing trabecular lamellae to fuse and thicken (Tektas & Lütjen-Drecoll, 2009). In addition to ECM remodelling, there have been observed increases in actin cytoskeleton contractility within connective tissue cells of the juxtacanalicular region of the trabecular meshwork, in turn causing the inner wall of Schlemm's canal to stiffen (Tian et al., 2009). Furthermore, TGF-β2 has been shown to be increased in the trabecular meshwork of POAG patients and was experimentally found to increase IOP by causing TMCs to secrete non-degradable ECM components that reduce the outflow of aqueous humour (Tripathi, 1977). BMP antagonists have also been found to be highly expressed in the TMC of POAG patients; under basal conditions, BMPs serve to repress TGF-β2-induced fibrosis in the trabecular meshwork (Tovar-Vidales et al., 2016). Ultimately, the reduced capacity of aqueous humour outflow through the trabecular meshwork leads to global increases in pressure throughout the eye, placing mechanical stress on the axons of RGCs and driving them towards cell death.

1.5.1.3. Primary Angle-Closure Glaucoma

Though not nearly as prevalent as POAG, primary angle-closure glaucoma (PACG) can be considered just as debilitating as it carries triple the risk of bilateral blindness (Sun et al., 2017). Among Chinese, Mongolian, and Inuit individuals, PACG has been considered the predominant form of glaucoma as opposed to POAG (Clemmesen & Alsbirk, 1971). While POAG is considered as a chronic optic neuropathy, PACG is classified as either acute or chronic depending on the timing of the onset of symptoms (Sun et al., 2017). In acute PACG, an attack transpires in which the iris rapidly bulges and completely blocks the trabecular meshwork, producing rapid, and sometimes painful, elevations in IOP followed by noticeable vision loss. Chronic PACG differs from acute PACG in that the iris gradually covers the trabecular meshwork, eventually leading to a phenomenon known as

peripheral anterior synechiae (PAS) in which the iris adheres to structures in the iridocorneal angle. Like POAG, chronic PAGC involves progressively increasing IOP levels that are usually asymptomatic until advanced stages (Sun et al., 2017).

Much remains to be uncovered with regards to the exact mechanisms that lead to angle closure and vision loss in PACG. It is currently known, however, that both pushing and pulling forces lead the iris to come into physical contact with the trabecular meshwork. The pushing forces are known as pupillary block, caused by the proximity between the lens and posterior iris that forces the peripheral iris to tilt anteriorly due to an increased pressure gradient (Sun et al., 2017). Pulling forces are known as non-pupillary block and are caused by distinct anatomical features such as a thick peripheral iris or an anteriorly rotated iris. As in POAG, elevations in IOP produce optic neuropathy, but patterns of optic nerve degeneration differ in PACG. In PACG, the optic disk typically appears pale and diffusely depressed rather than exhibiting the distinct cupped shape characteristic of POAG (Sun et al., 2017), Furthermore, PACG eyes tend to exhibit more diffuse visual field loss as opposed to localized vision loss in the superior hemifield as often seen in POAG patients (Wang et al., 2008). In essence, though POAG and PACG are distinct in terms of their clinical presentation, both diseases lead to elevations in IOP that cause RGC death and subsequent vision loss.

1.5.1.4. Normotensive Glaucoma

Normotensive glaucoma (NTG), the rarest form of glaucoma, presents a unique phenotype in which RGC apoptosis and peripheral vision loss persist despite IOP levels within the statistically normal range (Ho et al., 2024). Diagnosis of NTG can be challenging in that there is a spectrum of clinical presentations of NTG, from non-progressive and asymptomatic to full bilateral blindness (Gosling & Meyer, 2025). Treatment for NTG is another hurdle, as most currently available glaucoma

treatments constitute IOP-lowering medications. Hence, the existence of NTG begs the question of whether other factors in addition to elevated IOP play a role in glaucomatous pathology.

There have been multiple proposed theories as to the mechanisms underlying pathology in NTG, though none are all-encompassing (H. Killer & Pircher, 2018). Propositions include, but are not limited to, elevated sensitivity to normal IOP levels, vascular dysregulation, abnormal translaminar pressure gradient, and impaired cerebrospinal fluid (CSF) circulation (Killer & Pircher, 2018). In favour of a genetic component underlying increased sensitivity to normal IOP levels, one study conducted in a Zulu population from South Africa found that 57.1% of glaucoma patients had consistent IOP levels in the normal range, while it was observed in other studies involving Caucasian glaucoma patients from the United States and some European countries that 30-39% of glaucoma subjects showed normal IOP levels (Bonomi et al., 1998; Dielemans et al., 1994; Klein et al., 1992; Rotchford & Johnson, 2002). With regards to the vascular dysregulation theory of NTG, it has been observed that comorbid vascular diseases such as migraines and optic nerve hemorrhages are risk factors for rapid progression of visual field loss in NTG patients (De Moraes et al., 2011; Drance et al., 2001). Furthermore, an abnormal translaminar pressure gradient can arise due to imbalances between IOP and intracranial pressure (ICP) at the site of the lamina cribrosa, where the axons of RGCs exiting the eye are unmyelinated; studies performed in Asian and American populations have found significantly lower ICP in NTG patients relative to POAG and control subjects (Berdahl et al., 2008; Ren et al., 2010). One key factor influencing ICP is CSF turnover, and studies have noted CSF stagnation particularly in the optic canals of NTG patients (H. E. Killer et al., 2012; Pircher et al., 2017). It is evident that NTG is a complex, multifactorial disease that necessitates novel treatment avenues that extend beyond the conventional IOP-lowering therapies.

1.6 Mechanisms of Glaucomatous Pathology

As previously mentioned, vision loss in glaucoma is the product of selective RGC cell death and axonal degeneration. In glaucoma, RGC axons undergo both retrograde and anterograde (Wallerian) degeneration, leading to the loss of cell bodies in the retina and the degeneration of all associated visual pathways, respectively (Dias et al., 2022). RGC soma and axons do not regenerate, hence the damage is irreversible. Though much remains to be elucidated in terms of the specific molecular mechanisms that facilitate RGC degeneration in glaucoma, two predominant schools of thought, the mechanical pressure and vascular hypotheses, have been established to attempt to conceptualize these mechanisms. According to the mechanical pressure theory, sustained IOP elevation places mechanical stress on the unmyelinated axons of RGCs by deforming the lamina cribrosa, the delicate mesh-like structure that houses the RGC axons as they exit the eye. Conversely, the vascular hypothesis suggests that RGC damage in glaucoma is the result of inadequate blood supply to the retina and optic nerve that arises due to both IOP-dependent and independent factors (Boccaccini et al., 2023; Sharif, 2021; Weinreb et al., 2014).

Elevations in IOP have been shown to promote RGC damage by instigating numerous pathological processes such as axonal transport failure and neuroinflammation. In a healthy eye, RGCs expressing tropomyosin receptor kinase (Trk) receptors receive neurotrophic factor (NTF) support from Müller glia in the retina and from brain areas such as the LGN through retrograde axonal transport (Boccaccini et al., 2023). NTFs are vital diffusible peptides that regulate survival during development, adulthood, and injury (Claes et al., 2019). Anterograde transport from the RGC cell body to the distal branches of the axons is also necessary for the transport of mitochondria and regulatory proteins. Ocular hypertension studies have found that axonal transport failure is one of the early hallmarks of glaucoma that precedes cell body degeneration (Burgoyne, 2011; Knox et al., 2007).

Brain-derived neurotrophic factor (BDNF) loss of expression has been observed during IOP elevation, and its deprivation instigates RGC apoptosis through c-Jun N-terminal kinase (JNK) signaling, which in turn activates the BCL-2 protein family of proapoptotic proteins that act to promote mitochondrial dysfunction (Lambuk et al., 2022). As RGC axons degenerate, crosstalk between RGCs and retinal glial cells ensues, triggering the onset of neuroinflammation in glaucoma (Boccaccini et al., 2023). Microgliosis and astrocytosis ravage the optic nerve head by instigating the secretion of matrix metalloproteinases (MMPs) and pro-inflammatory cytokines such as interleukin-1 beta (IL-β) and tumor necrosis factor alpha (TNF-α) that induce remodeling and excavation of the optic nerve head (Miao et al., 2023).

Not only does IOP elevation subject RGC axons to detrimental levels of mechanical stress, but it can also lead to vascular dysregulation and oxidative stress via the constriction of blood vessels that supply the optic nerve (McMonnies, 2018). Ocular hypoperfusion and reperfusion caused by IOP fluctuations leads to the disruption of mitochondrial electron chain transport, a critical step in the vital oxidative phosphorylation process that harnesses oxygen to produce the energy currency for the cell, adenosine triphosphate (ATP). The retina is one of the most metabolically active tissues in the body, and adequate mitochondrial functioning is essential for these demands to be fulfilled (Boccaccini et al., 2023). During reperfusion, spikes in oxygen levels trigger excessive reactive oxygen species (ROS) production by mitochondria (McMonnies, 2018). ROS, also known as free radicals, are molecules with an unpaired electron that, at high levels, instigate a number of pathological processes that drive the cell towards an apoptotic fate such as DNA fragmentation, lipid peroxidation, and protein degradation. Under such conditions, a pathological phenomenon known as oxidative stress ensues, whereby the cellular antioxidant capacities are outpaced by excessive ROS production. POAG patients have been shown to exhibit high serum and aqueous humour levels of ROS, correlated with vision loss (Nucci et al., 2013). Reduced antioxidant capacities have also been observed in POAG patients,

as it was found that the null-allele mutation of *GTSM1,* which encodes the prevalent cellular antioxidant glutathione, was shown to be significantly more expressed in POAG patients relative to healthy controls (Izzotti et al., 2003).

1.6.1. Oxidative Stress as a Key Factor in Glaucomatous Pathology

Oxidative stress promotes RGC death in glaucoma through both direct and indirect mechanisms (Figure 1.4). At high intracellular levels, ROS can directly induce RGC cell death through caspase-independent mechanisms such as through the activation of poly(ADP-ribose) polymerase (PARP) and apoptosis-inducing factor (AIF) (Li & Osborne, 2008). Furthermore, oxidative stress has been shown to directly disrupt the functioning of glutamine synthetase, an enzyme that plays a critical role in converting retinal glutamate into non-toxic forms, leading to the accumulation of neurotoxic glutamate (Tezel et al., 2005). Abnormally high intracellular glutamate levels in turn lead to the overstimulation of NMDA receptors, leading to disruptions in Na^+/K^+ homeostasis and excessive Ca^{2+} influx. Accumulation of Ca^{2+} subsequently drives the activation of enzymes that damage cellular components such as proteases, phospholipases, and endonucleases, leading the cell towards an apoptotic fate (Boccaccini et al., 2023). Moreover, oxidative stress indirectly promotes RGC degeneration by mediating pathological immune responses and concomitant retinal glial cell dysfunction (Chrysostomou et al., 2013). In experimental models of glaucoma, ROS have been shown to initiate aberrant immune responses by enhancing the antigen-presenting ability of retinal microglia and astrocytes (Tezel, 2009). Glia derived from rat retinae and optic nerves have been shown to overexpress major histocompatibility complex (MHC) class II antigen-presenting molecules after pre-treatment with ROS in culture, and T cells showed significant proliferation and activation during co-incubation with these glial cells (Tezel et al., 2007). Intriguingly, T cells that were isolated from ocular hypertensive rats demonstrated a robust response to retinal proteins indicated by increased

proliferation and cytokine secretion, which was found to be correlated with RGC damage (Tezel et al., 2009). Upregulation of human leukocyte antigen-DR isotype (HLA-DR), a type of MHC class II molecule, was also observed in microglia and astrocytes in the human glaucomatous retina and optic nerve head (Tezel et al., 2003; Yang et al., 2001). Moreover, during periods of prolonged oxidative stress, glial cells also facilitate RGC death in glaucoma by secreting neurotoxic substances such as the pro-inflammatory cytokine tumor necrosis factor alpha (TNF-α). TNF-α has been observed to be upregulated in human and experimental glaucomatous eyes and exacerbates RGC damage through a wealth of mechanisms such as receptor-mediated caspase cascade activation, promoting mitochondrial dysfunction, and activating matrix metalloproteinases (MMPs) that further drive IOP elevation (Tezel et al., 2008). Oxidative stress-induced neuroinflammation further exacerbates mitochondrial damage in RGCs and subsequent increases in ROS production, in turn generating a vicious and pathological inflammatory cycle (Boccaccini et al., 2023).

In glaucoma, oxidative damage is not limited to the retina and optic nerve but also extends to the trabecular meshwork (Izzotti et al., 2006), compromising its outflow facility. Oxidative DNA damage was shown to be significantly greater in the trabecular meshwork cells of POAG patients compared to age-matched controls, as indicated by increases in the levels of 8-hydroxy-2'-deoxyguanosine (8-OH-dG), an abundant oxidative nucleotide modification (Izzotti et al., 2003). Trabecular meshwork cells play a critical role in regulating aqueous humour outflow and have been shown to be among the most ROS-sensitive cells in the anterior chamber (M. Wang & Zheng, 2019). Importantly, positive correlations were found between 8-OH-dG levels, IOP, and visual field deficits in glaucomatous patients, though the directionality of the relationship between these factors remains to be further elucidated (Saccà et al., 2005). Elevation of ROS levels has been shown to damage mitochondrial DNA (mtDNA), proteins, and membrane lipids in trabecular meshwork cells, in turn

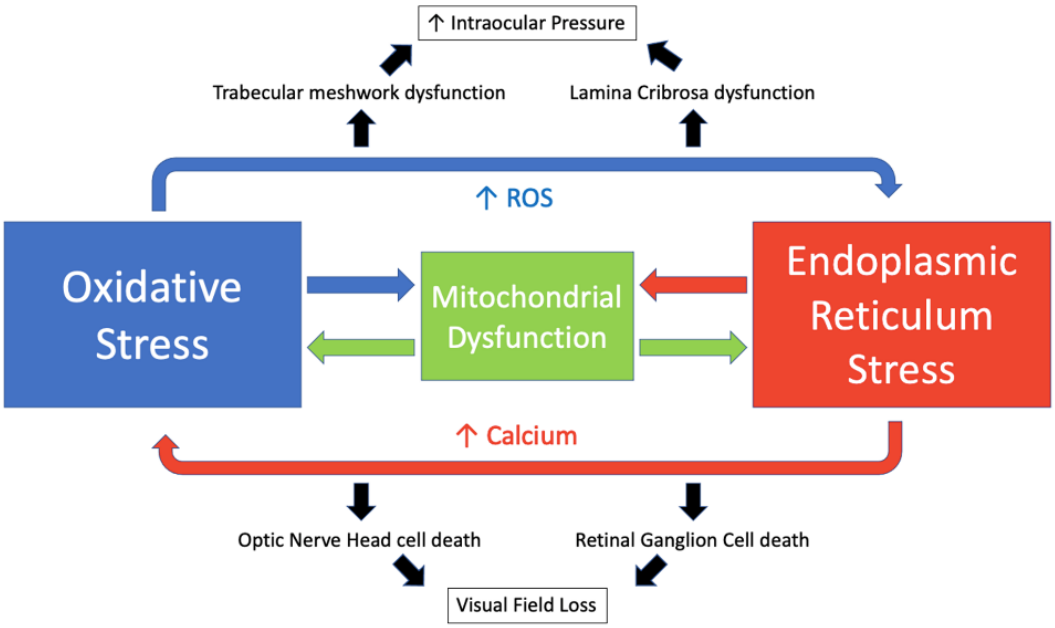

Figure 1.4. Oxidative stress plays a major role in glaucomatous pathology. (A) The multi-directional interactions between oxidative stress and other pathological factors such as mitochondrial dysfunction and endoplasmic reticulum stress contributes to elevations in intraocular pressure (IOP), optic nerve degeneration, and retinal ganglion cell (RGC) death in glaucoma, culminating in visual field loss. Reproduced with permission from Hurley et al., 2022.

increasing resistance to aqueous humour outflow (Abu-Amero et al., 2006; Izzotti et al., 2003). In glaucomatous patients, mtDNA damage and lipid peroxidation products in the trabecular meshwork were found to be significantly more elevated compared to healthy controls, and visual field loss was reported to be directly proportional to oxidative damage in the trabecular meshwork (Babizhayev, 1989; Izzotti et al., 2003; Zanon-Moreno et al., 2008). Moreover, in addition to directly damaging the components of trabecular meshwork cells, oxidative stress has also been shown to indirectly exacerbate glaucomatous trabecular meshwork cell damage *in vivo* by increasing the expression of inflammatory mediators such as interleukins and endothelial leukocyte adhesion molecule-1 (ELAM-1) (Tourtas et al., 2012). Ultimately, the oxidative stress-induced changes in the integrity of the trabecular meshwork can lead to further elevations in IOP due to reduced aqueous humour outflow, producing another vicious positive feedback loop of pathology in glaucoma.

1.6.2. RGC Apoptosis: Intrinsic and Extrinsic Pathways

The interplay between the aforementioned pathological factors in glaucoma results in RGC death by apoptosis, a pre-programmed genetic intracellular cascade that orchestrates the destruction of the cell through a number of processes such as DNA and plasma membrane fragmentation, organelle breakdown and mitochondrial dysfunction. The apoptotic process is executed through two fundamental pathways, the intrinsic and extrinsic pathways, that act through the mitochondria and death receptors, respectively (Figure 1.5) (Levkovitch-Verbin, 2015). These pathways can act independently or in tandem to activate downstream effector caspases, which are cysteine proteases that are responsible for protein degradation during the apoptotic process (Levkovitch-Verbin, 2015).

In the intrinsic pathway of RGC apoptosis, insults such as neurotrophic factor deprivation and oxidative stress first induce the oligomerization and mitochondrial outer membrane insertion of BAX and BAK, proapoptotic members of the B-cell CLL/lymphoma 2 (BCL-2) protein family. In

mice, BAX deficiency has been shown to promote a three-fold increase in the number of RGCs in the adult retina attributed to less RGC elimination during development (Mosinger Ogilvie et al., 1998). The activation of BAX and BAK subsequently triggers the release of the apoptosis-promoting factor cytochrome *c* into the cytoplasm from the mitochondrial intermembrane space, which then proceeds to form the apoptosome complex by binding to apoptosis-inducing factor-1 (Apaf-1) and procaspase-9. Procaspase-9 is then cleaved and enters its active form, the initiator caspase-9, which then activates effector caspases 3- and 7 (Qu et al., 2010). Effector, or executioner, caspases then go on to initiate self-destruction of the cell by degrading cellular contents. Notably, procaspase-9, caspase-9, and caspase-3 have been observed to be upregulated in experimental glaucoma models (Hänninen et al.,2002; Visuvanathan et al., 2022). It was also found that the inhibition of proapoptotic factors such as caspases through the upregulation of X-linked inhibitor of apoptosis (XIAP) resulted in the rescue of RGC dysfunction and degeneration in the mouse magnetic microbead model of glaucoma (Visuvanathan et al., 2022).

In contrast to the intrinsic pathway, the extrinsic pathway is mediated by Fas and tumor necrosis factor (TNF) death receptors found on the cytoplasmic membrane (Levkovitch-Verbin, 2015). The binding of the Fas ligand (Fas) or TNF cytokines to their respective receptors causes the death domains of the receptors to bind procaspase-8 and cleave it to produce its active form, caspase-8, which further goes on to activate executioner caspases that carry out the apoptotic cascade (Qu et al., 2010). Glaucomatous eyes have been observed to exhibit increased Fas signaling as well as elevated mRNA expression of caspases 3 and 8 (Kim & Park, 2005; Tezel & Wax, 1999). Furthermore, the glial production of TNF-α and expression of the respective receptor TNF-R1 have been shown to be increased in the retina and optic nerve head of glaucomatous human donor eyes (Tezel, 2008). When RGCs and retinal glia were co-cultured and exposed to glaucomatous stimuli, the inhibition of TNF-α bioactivity by a neutralizing antibody caused reductions in RGC apoptosis (Tezel & Wax, 2000). In

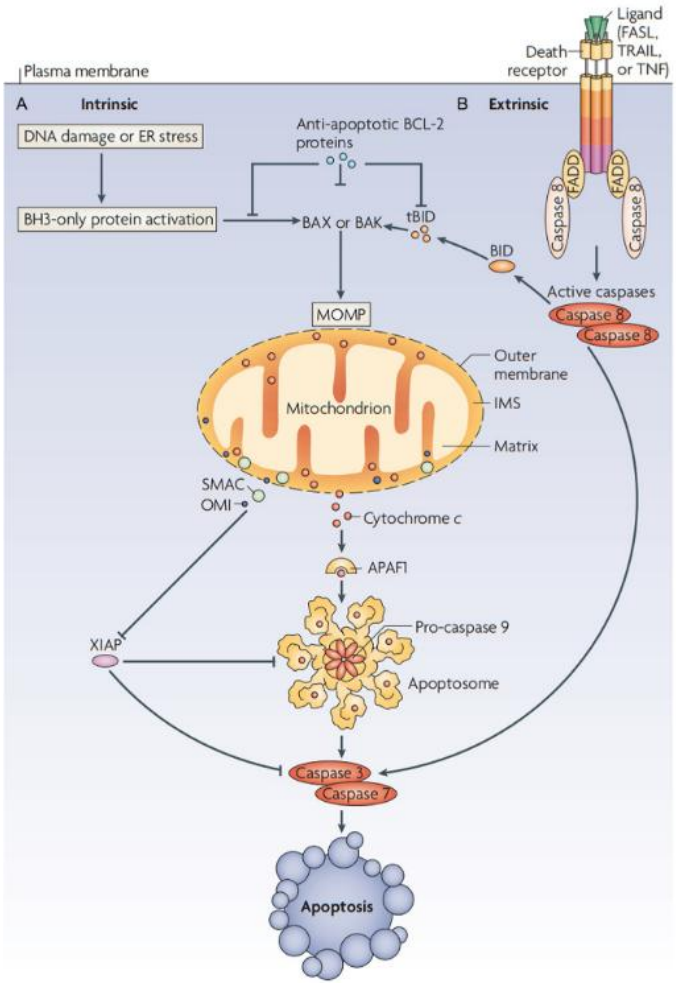

Figure 1.5. Overview of the key cellular regulators involved in the intrinsic and extrinsic pathways of apoptosis. The intrinsic apoptotic pathway is triggered by external factors such as DNA damage, endoplasmic reticulum (ER) stress, and neurotrophic factor deprivation, leading to the activation of pro-apoptotic proteins BAK or BAX. Conversely, the extrinsic pathway is facilitated by the activation of death receptors on the cytoplasmic membrane, which in turn activates caspases that carry out the apoptotic cascade. Reproduced with permission from Levkovitch-Verbin, 2015.

essence, the prevention of apoptosis is a major aim for neuroprotective glaucoma management strategies.

1.7 Current Glaucoma Therapies

Given that elevated IOP remains as the most widely accepted main risk factor for glaucoma progression, first-line treatment constitutes topical IOP-lowering medications. However, it has been reported that up to 30% of POAG patients fail to achieve normal IOP levels <21 mmHg within a year of IOP-lowering medication treatment and continue to progress towards blindness. In the event that IOP elevation and vision loss persists despite the continued use of IOP-lowering pharmacotherapies, laser therapy and surgical treatments are employed as a second line of defense (Wagner et al., 2022). Experimental studies are also currently underway to address the underlying neurological underpinnings of glaucomatous pathology.

There are four major classes of IOP-lowering drugs: prostaglandin analogs (PGAs), carbonic anhydrase inhibitors (CAIs), beta blockers, and alpha agonists. Each medication has a unique mechanism of action. PGAs are the most commonly prescribed medications for ocular hypertension and reduce IOP by increasing aqueous humour outflow through the uveoscleral pathway, which indirectly accounts for reduced outflow through the trabecular meshwork. Rather than targeting the outflow pathways, CAIs act by reducing aqueous humour production by the ciliary body by reducing bicarbonate ion production in the ciliary body epithelium. Similarly, beta blockers decrease the production of aqueous humour by antagonizing β1 receptors on sympathetic nerve endings found in the epithelium of the ciliary body. Alpha-adrenergic agonists effectively lower IOP by improving aqueous humour outflow and reducing aqueous production by the ciliary body (Lusthaus & Goldberg, 2019).

Laser treatment and surgical interventions are measures taken when IOP-lowering drugs fail to effectively reduce IOP levels. Laser therapy is considered more favourable than surgical means as it is less costly and invasive (Wagner et al., 2022). For open-angle glaucoma (OAG) patients, selective laser trabeculoplasty (SLT) is the most common type of laser therapy, which involves the use of a low-energy green (523 nm) laser to specifically eradicate melanin-containing cells in the trabecular meshwork (Freitas et al., 2016) and spare TMCs. Angle-closure glaucoma (ACG) patients require different laser therapies known as a laser peripheral iridotomy and laser peripheral iridoplasty, with the former involving laser-induced perforation of the peripheral iris to reduce pupillary block, and the latter constituting of low-power laser burns to shrink the iris and alleviate angle closure caused by abnormal positioning of the iris. When pharmacotherapy and laser treatments are deemed ineffective at producing the desired IOP-lowering effects, surgical means such as trabeculectomies and shunt implantations are used. Trabeculectomies are the surgical gold standard for POAG in which a new, artificial drainage pathway from the anterior chamber to the subconjunctival space is created by excision of a segment of the trabecular meshwork. Shunt implantations act as glaucoma drainage devices (GDDs) that drain aqueous humour into the subconjunctival space (Binibrahim & Bergström, 2017; J. Wang & Barton, 2017).

1.8 Neuroprotective Strategies for Glaucoma Management

The current commercially available therapies treat the symptoms of glaucoma but do not directly target the underlying neurodegeneration of the retina and optic nerve. Hence, emerging novel neuroprotective strategies aim to protect against retinal and optic nerve degeneration. Notable neuroprotective therapies include but are not limited to neurotrophic factor supplementation and antioxidants (Boccaccini et al., 2023).

As mentioned previously, the mechanical pressure theory of glaucomatous pathology posits that the IOP-induced mechanical stress on the unmyelinated RGC axons within the lamina cribrosa disrupts transport of neurotrophic factors, leading to RGC cell death (Hakim et al., 2023). In POAG patients, visual field loss has been linked to reduced serum and aqueous humour levels of neurotrophic factors such as brain-derived neurotrophic factor (BDNF), nerve growth factor (NGF), and ciliary neurotrophic factor (CNTF). BDNF treatment has been shown to promote RGC survival in animal models of ocular hypertension by activating the BDNF-TrkB pathway (Osborne et al., 2018). NGF acts on the TrkA receptor found in RGCs and promotes survival and proliferation by reducing oxidative stress through the phosphotidylinosol-3-kinase (PI3K)/AKT pathway (H. Wang et al., 2014). CNTF is expressed in retinal glial cells and promotes neurite outgrowth by activating the CNTF receptor on neurons; exogenous CNTF application has been demonstrated to protect against photoreceptor and RGC death in animal models of retinal diseases and POAG clinical trials are currently ongoing to evaluate the therapeutic efficacy of the delivery of genetically modified human cells that have been engineered to secrete CNTF (Do Rhee et al., 2022; Goldberg et al., 2023).

In addition to neurotrophic factor deprivation, oxidative stress also plays a major role in glaucomatous neurodegeneration as previously discussed. In this regard, the use of antioxidants as neuroprotective therapies for glaucoma have been investigated. Plants are one of the most abundant sources of antioxidants and have been used medicinally for centuries. The extracts of the leaves of the ancient tree *Ginkgo biloba* have been experimentally shown to protect RGCs against vascular dysregulation, optic nerve crush, IOP elevations, and apoptosis (Boccaccini et al., 2023; Cho et al., 2019; Di Meo et al., 2020; Hirooka et al., 2004; Ma et al., 2010). EGb761, an extract of *Gingko biloba* leaves that has been used in clinical trials for other neurodegenerative diseases, acts as a ROS scavenger and also increases the activities of the prominent antioxidants superoxide dismutase (SOD) and glutathione (GSH), the levels of which have been shown to be decreased in the serum and aqueous

humour of glaucomatous patients (Boccaccini et al., 2023; Bridi et al., 2001; Chen et al., 1999; Rimbach et al., 2001). Synthetic antioxidants also show therapeutic potential for glaucoma; rapamycin was found to promote RGC survival in a rat chronic hypertensive glaucoma model by suppressing the production of NO and TNF-α, repressing microgliosis, and directly inhibiting glutamate-induced apoptosis (Henderson et al., 2024; Su et al., 2014). Hence, antioxidants present as promising treatments for glaucoma given that they target several factors that have been shown to be implicated in glaucomatous pathology.

1.9 WN1316 Antioxidant Compound for the Treatment of Glaucoma

WN1316, 2-[mesityl(methyl)amino]-N-[4(pyridine-2-yl] acetamide trihydrochloride, is a novel small molecule antioxidant compound. *In vitro,* WN1316 was found to robustly and selectively protect against oxidative-stress induced cell death in SH-SY5Y neuroblastoma cells (Tanaka et al., 2014). In later *in vivo* experiments in which WN1316 was tested in a mouse model of late-stage amyotrophic lateral sclerosis (ALS), a neurodegenerative disease in which oxidative stress plays a significant role in pathology as in glaucoma, WN1316 was found to significantly protect against motor neuron loss in the anterior horn of the lumbar spinal cord, preserve motor function, and prolong post-onset survival (Tanaka et al., 2014). The neuroprotective effects of WN1316 are twofold; it upregulates antioxidant and anti-apoptotic agents, and suppresses a number of pathological factors such as gliosis and neuroinflammation (Tanaka et al., 2014).

WN1316 exerts its neuroprotective effects by upregulating the nuclear factor-erythroid 2-related factor 2 (Nrf2) pathway, neuronal apoptosis inhibitory protein (NAIP), and glutathione (GSH) (Tanaka et al., 2014). Nrf2 is a critical transcription factor that regulates the expression of several genes encoding antioxidant enzymes and anti-inflammatory agents. Under basal conditions, Nrf2 forms a complex with Kelch-like erythroid cell-derived protein (Keap1) in the cytoplasm where it facilitates

proteasome degradation (M. Wang et al., 2020). During periods of oxidative stress, Keap1 undergoes conformational changes, allowing Nrf2 to translocate into the nucleus where it binds to the antioxidant response element (ARE), in turn leading to the upregulation of antioxidants including heme oxygenase-1 (HO-1) and NAD(P)H quinone oxidoreductase (NQO1) (M. Wang et al., 2020). Following WN1316 treatment, increases in Nrf2-regulated genes as well as increases in cytoplasmic Nrf2 nuclear translocation were observed in SH-SY5Y cells (Tanaka et al., 2014). Nrf2 also plays a role in glaucomatous pathology; reduced Nrf2 expression has been observed in glaucomatous trabecular meshwork cells, and Nrf2 overexpression promoted cell survival and reduced apoptosis of TMCs (Cheng et al., 2017). Independently of the Nrf2 pathway, WN1316 showed a dose-dependent upregulation of a member of the inhibitory apoptosis proteins (IAPs) family, NAIP, in THP-1 cells (Tanaka et al., 2014). NAIP overexpression has been shown to selectively protect against oxidative stress-induced cell death in a hippocampal model of ischemia (Xu et al., 1997). Moreover, WN1316 upregulates GSH in a dose-dependent manner in SH-SY5Y cells (Tanaka et al, 2014). GSH is an abundant ROS-scavenging antioxidant, and mass spectrometry studies have observed decreased GSH levels in the aqueous humour of POAG and NTG patients, correlated with visual field defects (Sato et al., 2023).

Additionally, WN1316 was found to suppress the activation of microglia and astrocytes as well as the production of inflammatory factors interleukin-1 beta (IL-1β) and inducible nitric oxide synthase (iNOS) in the lumbar spinal cord of ALS mice (Tanaka et al., 2014); both gliosis and neuroinflammation are key contributors to glaucomatous pathology (Tezel et al., 2008). In an experimental rat model of glaucoma, expression of MHC class II by activated microglia in the optic nerve head was found to be correlated with severe RGC degeneration (Chidlow et al., 2016). Importantly, microglial activation has been identified as one of the earliest events in glaucomatous neurodegeneration, as it has been shown to begin as early as four days post IOP elevation in

experimental glaucoma models (Miao et al., 2023). Astrocytic activation has also been found to precede RGC injury in glaucomatous experimental models; activated astrocytes become highly ramified and induce extracellular matrix (ECM) remodelling, in turn inducing cupping of the optic nerve head and RGC axonal damage (Miao et al., 2023). Furthermore, POAG patients have been observed to exhibit elevated blood and aqueous humour levels of pro-inflammatory cytokine IL-1β, and IL-1β has been demonstrated in rodent models of glaucoma to induce RGC death through the Toll-like receptor 4-NOD-like receptor protein 1/NOD-like receptor protein 3-caspase 8 (TLR4-NLRP1/NLRP3-CASP8) axis (Benitez-Del-Castillo et al., 2019; Chi et al., 2014; Wooff et al., 2019). In addition, iNOS, a key regulator of immune activation and inflammation that produces the free radical nitric oxide (NO) from L-arginine, has been observed to be elevated in the optic nerve head of donor POAG patients; selective inhibition of iNOS in co-cultures of rat RGCs and glia was shown to be effective at reducing rates of RGC apoptosis (Neufeld et al., 1997, 1999, p. 19; Tezel & Wax, 2000). In essence, WN1316 has proved to be a potent inhibitor of oxidative stress and neuroinflammation, which are major factors in glaucomatous pathology.

WN1316 was additionally selected as the therapeutic candidate of choice for this study due to its favourable safety and efficacy profile. The compound was identified by an *in-silico* drug design technique known as Anti-Oxidative Neuronal Cell Death Quantitative Structure Activity Relationship (AOND-QSAR), a computational approach that predicts a chemical compound's efficacy to protect neurons from oxidative stress-induced cell death based on their molecular structure. Against other compounds that were identified using this strategy, WN1316 was not only identified as the most potent suppressor of oxidative stress-induced cell death, but also showed the highest blood-brain barrier (BBB) permeability, the greatest water solubility, and the lowest toxicity (Tanaka et al., 2014). Further nanospectroscopy studies conducted by the Tsilfidis lab demonstrated that WN1316 also exhibits high blood-retina barrier (BRB) permeability (C. Tsilfidis, pers. comm.). Therefore, given its

remarkable ability to protect against oxidative stress and neuroinflammation, as well as its ideal therapeutic profile, WN1316 shows promise as a potential neuroprotective treatment for glaucoma.

1.10 Animal Models of Glaucoma

It is essential that animal models accurately recapitulate the human glaucomatous phenotype to ensure the translatability of experimental findings. The vast majority of glaucomatous animal models involve IOP elevation through either genetic or inducible means due to the fact that elevated IOP is the most well-characterized and modifiable risk factor for the disease. However, given the emerging evidence that glaucoma is a multifactorial disease and can still develop in the absence of IOP elevation, interest has been garnered towards developing glaucomatous animal models through IOP-independent methods (Almasieh & Levin, 2017).

Genetic animal models of glaucoma are useful for the understanding of how genetic factors contribute to glaucoma development and progression, though major caveats with genetic models are long time courses for the emergence of the disease phenotype and high phenotypic variability between animals. An example of a genetic model that is relevant to human glaucoma is the transgenic myocilin (MYOC) rodent model; *MYOC* was identified as a causative gene for up to 8% of adult-onset POAG and familial juvenile OAG. Transgenic knock-in mice carrying the Tyr437His mutation ($MYOC^{Y437H}$) have been observed to display IOP elevation and RGC death around 18 months, and gene editing studies involving deletion of the mutant *MYOC* allele revealed protection against IOP elevation and RGC loss (Jain et al., 2017; Zhou et al., 2008). Though perhaps not as directly relevant to human glaucoma, the DBA/2J mouse model is the most widely used model for chronic, age-related glaucoma (Loo et al., 2024). In this model, inbreeding produces spontaneous mutations in the Tyrp1 and Gpnmb genes, which in turn cause the mice to naturally develop iris pigment dispersion and iris stromal

atrophy, respectively. IOP elevations typically begin around 6 to 9 months of age, and by 12 months, most animals show severe optic nerve degeneration and RGC death (Loo et al., 2024).

Inducible models allow for acute glaucoma progression and short, cost-effective experimental time courses in contrast to genetic models. An added benefit of inducible models is that glaucoma is often induced in one eye, allowing the contralateral eye to act as a control. One example of an inducible model is the cautery of extraocular veins to induce IOP elevation. This technique is not favourable, as cauterization of vortex veins in rats can also produce undesirable side effects in addition to ocular hypertension including ischemia, which can lead to outer retinal damage (Pang & Clark, 2020). Cauterization of extraocular veins can also produce varying IOP elevations between animals, as the regrowth of blood vessels can cause IOP levels to drop to baseline levels after a few weeks post-surgery (Pang & Clark, 2020). Obstruction of the outflow pathways is another animal model that involves IOP elevation and subsequent RGC degeneration. Laser photocoagulation of the trabecular meshwork is one such technique, which has been shown to yield IOP elevations, RGC apoptosis and optic nerve degeneration, but the model is technically challenging in that frequent lasering is often required for sustained IOP elevation (Pang & Clark, 2020). A preferable technique is the intracameral injection of various agents, such as viscoelastic materials and microbeads, to block the outflow pathway. For this study, the intracameral injection of magnetic microbeads was selected as the model of choice. Upon the injection of the magnetic microbeads into the anterior chamber, a handheld magnet is moved in a circular motion to evenly disperse the microbeads around the iridocorneal angle where the drainage canals of the anterior chamber are located, effectively interfering with the outflow of aqueous humour from the anterior chamber and subsequently leading to acute IOP elevations. Previous studies have shown that a single injection of the magnetic microbeads produced sustained IOP elevations up to 6-weeks post-surgery, and caused significant RGC dysfunction and optic nerve degeneration (Ito et al., 2016; Visuvanathan et al., 2022).

1.11 Electroretinography

Electroretinography (ERG) is an *in vivo* physiological test that evaluates the functionality of retinal cells by measuring their responsiveness to light stimulation. ERG involves the use of corneal stimulators, which present bright flashes of light to the eye at varying intensities. Retinal cells generate electrical responses to the light stimulation, which are recorded by electrodes at the corneal surface and processed by a computer that generates waveform traces representing the sum of the electrical responses produced by the retinal cells. The waveforms are composed of various components that each represent the functioning of a specific retinal cell type. The mean peak amplitudes of the components can be quantified and statistically analyzed, allowing for comparisons of retinal cell functionality between experimental groups. This experiment utilized two distinct ERG tests, the full-field scotopic flash ERG (ffERG) and the pattern ERG (PERG) to evaluate the functionality of outer retinal cells and RGCs, respectively.

The ffERG measures the electrical responses of retinal neurons and glia located in the outer layers of the retina. The a-wave is the initial negative deflection and represents the hyperpolarization of rod and cone photoreceptors. Under scotopic (dark-adapted) conditions, the a-wave is more reflective of rod activity, whereas in photopic (light-adapted) scenarios, cone function is emphasized. Following the a-wave is the b-wave, a positive deflection that is indicative of the combined activities of ON-bipolar cell interneurons and Müller glia. Superimposed on the rising phase of the b-wave are the oscillatory potentials (OPs), which are three small wavelets that originate from amacrine cells. Reductions in the aforementioned components of the ffERG are typically not observed in glaucomatous patients, as glaucoma is primarily a disease of RGCs, though some studies involving the use of the microbead glaucoma model in rodents have reported reductions in the a- and b-wave components (Pang & Clark, 2020; Wu et al., 2019).

To evaluate the functioning of RGCs specifically, the PERG test is performed. During the PERG, alternating black-and-white checkerboard or grating patterns are presented to the eye as opposed to diffuse flashes of light. During pattern reversal, local luminance varies, but the overall mean luminance remains unchanged. As a result, the linear components of the ERG, namely the a- and b-waves, are effectively cancelled out, isolating the nonlinear components of the response. These nonlinear signals, which constitute the PERG, are closely related to the functionality of RGCs; RGCs respond more to changes in contrast and patterns rather than incremental changes in overall brightness as do photoreceptors (Miura et al., 2009; Tanimoto, 2018). The murine PERG constitutes three major components: the negative N1, the positive P1, and the negative N2. The P1 amplitude, which is the difference from the trough of N1 to the peak of P1, represents RGC soma function, while the N2 amplitude, measured between the peak of P1 and the trough of N2, reflects RGC axon function (Miura et al., 2009).

Glaucomatous damage can extend from the retina to the visual cortex of the brain, hence visual evoked potentials (VEPs) have been performed to evaluate the functional integrity of the visual pathway in the magnetic microbead mouse model of glaucoma (Prabhakaran et al., 2021). The VEP is performed simultaneously with the ffERGs. During VEPs, recording electrodes placed underneath the scalp near the occipital lobe measure the electrical activity of the visual cortex. Three components make up the murine VEPs: the positive P1, negative N1, and positive P2. The P1-N1 amplitude is an indicator of early-arriving visual signals in the primary visual cortex (V1) and is influenced by retinal input and optic nerve radiations. The N1-P2 amplitude reflects cortical excitability, and the P1-P2 amplitude is thought to reflect intracortical connectivity between the visual cortex and other cortical regions (Marenna et al., 2023).

Taken together, the ffERGs, PERGs, and VEPs provide valuable insights into how glaucoma affects the functioning of the entire visual pathway, extending from the retina to the visual cortex and association areas.

1.12 Rationale and Hypothesis

Glaucoma is an asymptomatic group of optic neuropathies and a leading cause of irreversible vision loss worldwide, characterized by the death of retinal ganglion cells and the degeneration of their axons that form the optic nerve. It is a multifactorial disease that necessitates novel neuroprotective treatment avenues that extend beyond the conventional IOP-lowering therapies, which are solely symptomatic and do not directly target the underlying neurodegeneration of retinal ganglion cells in glaucoma. Surmounting evidence has revealed that oxidative stress is among the major factors that contribute to glaucomatous pathology. In this regard, this study aimed to investigate the use of a novel antioxidant compound, WN1316, for the treatment of experimental glaucoma. WN1316 is a potent suppressor of oxidative stress and neuroinflammation and presents an ideal therapeutic profile. We hypothesize that through the upregulation of neuroprotective antioxidant proteins, WN1316 treatment would be effective at protecting against retinal ganglion cell dysfunction and cell death in the magnetic microbead mouse model of glaucoma.

CHAPTER 2. MATERIALS AND METHODS

2.1 Animals

Two-month-old C57BL/6J mice (n=48; 24 males, 24 females) were purchased from Jackson Laboratories (Bar Harbor, Maine). Animals were housed under standard 12-hour light/dark conditions and were given one week to acclimate prior to the start of the experiment. Procedures were performed in compliance with the University of Ottawa Animal Care and Veterinary service guidelines and the Association for Research in Vision and Ophthalmology (ARVO) statement for the Use of Animals in Ophthalmic Research. The experimental groups were as follows:

- Glaucoma + saline (6 males, 6 females)
- Glaucoma + WN1316 (6 males, 6 females)
- Sham + saline (6 males, 6 females)
- Sham + WN1316 (6 males, 6 females)

2.2 Surgeries

2.2.1. Surgery Preparation

Mice were anesthetized with 2% isoflurane gas for the duration of the surgeries. Subcutaneous injections of Meloxicam (1 mg/kg) were given for pain management prior to the commencement of the surgeries. 1% tropicamide dilation drops (Mydriacyl, Alcon) were applied to the surgical (left) eyes, and 0.5% proparacaine hydrochloride (Alcaine, Alcon) was administered for topical anesthetization of the cornea. Contralateral (right) eyes received Systane gel (Systane, Alcon) for hydration purposes.

2.2.2. Microbead and Sham Injections

Half of the 48 mice (12 males and 12 females) received microbead injections to the left eye; contralateral eyes were not injected. A Nanofil 10 uL microsyringe (World Precision Instruments) attached to a Nanofil 34-gauge beveled needle (World Precision Instruments) was used for the injections. For microbead-injected animals, a 0.6 uL suspension of microbeads (Dynabeads, M-450, Life Technologies) at a concentration of $1.6x10^6$ beads/uL was injected intracamerally into the anterior chamber of the left eye. A handheld magnet was moved in a circular motion around the periphery of the cornea to evenly disperse the microbeads around the iridocorneal angle. The other half of the 48 mice (12 males and 12 females) received an equal injected volume of 0.6 uL of balanced salt solution (BSS) to the left eyes as a control.

2.2.3. Post-Surgery Recovery

Mice were placed in a heated incubator to recover from the anesthetic. Systane gel (Systane, Alcon) was periodically applied to the corneas to ensure that the eyes remained hydrated throughout the recovery period.

2.3 WN1316 Treatment

Animals were subjected to a one-week training period prior to the surgeries in which 100 uL of saline was delivered daily by oral gavage. 1cc Syringes (Fisher Scientific) and 20 gauge 38 mm barrel shaped stainless steel feeding needles (Fine Science Tools) were used to perform the oral gavage. Beginning one day before the surgical injections, 24 mice (12 glaucoma, 12 sham) were given 100 uL of WN1316 at a dose of 50 ug/kg by oral gavage on a daily basis up to 12 weeks post-surgery. The WN1316 stock solution was prepared biweekly by dissolving 1 mg of WN1316 in 1 mL of Milli-Q water, and the solution was stored in an amber light-resistant tube at 4 degrees Celsius. The remaining 24 mice (12 glaucoma, 12 sham) received saline as a control up to 12 weeks post-surgery. All animals were weighed on a weekly basis to ensure accurate dosing.

2.4 IOP Measurements

IOP measurements were taken in awake mice using a TonoLab device (iCare, Finland). Measurements were recorded across a span of four days; IOP measurements were taken for only one experimental group per day and always taken between 9am-12pm to mitigate the diurnal effects on IOP. The tonometer probe was placed approximately 1-4 mm away from the centre of the cornea and the recording button was pressed six times to generate a mean IOP measurement; five mean measurements were recorded for both the left and right eyes. IOP measurements were taken at baseline one week prior to the surgeries, weekly up to 4 weeks post-surgery, and bi-weekly after 4-weeks post-surgery up until 12 weeks post-surgery.

2.5 Visual Electrophysiology and Fundus Imaging

Electroretinograms (ERGs) were the *in vivo* physiological tests used to evaluate the functioning of retinal cells and were performed at baseline one week prior to the surgeries and every three weeks until 12 weeks post-surgery. The Celeris ERG System running Espion software (Diagnosys LLC) was used to perform the ERG tests. Animals were subjected to two separate and consecutive tests of visual function, the simultaneous full-field ERG and visual evoked potentials (VEP), and the pattern ERG (PERG). Prior to the testing, animals were first dark-adapted overnight under red safelight conditions. Immediately prior to the tests, animals were anesthetized through intraperitoneal injections of 50 mg/kg ketamine and 1 mg/kg medetomidine. Eyes were subsequently dilated with 1% tropicamide (Mydriacyl, Alcon) and 2.5% phenylephrine hydrochloride (Mydfrin, Alcon) and anesthetized with a drop of 0.5% proparacaine hydrochloride (Alcaine, Alcon). Periodically throughout the tests, hypromellose gel (Systane Gel, Alcon) was topically applied to the eyes for hydration. At the end of the measurements and fundus images, animals were intraperitoneally injected with 2.5 mg/kg atipamezole hydrochloride to reverse the anesthetic, subcutaneously injected with 1-2 mL of saline to

maintain hydration, and placed on a heating pad set to 37 degrees Celsius to prevent reductions in body temperature.

2.5.1. Simultaneous Full-Field ERG and VEP

Two Ag/AgCl corneal stimulators (Diagnosys, LLC) were placed in contact with the center of the left and right corneas. A homemade gold looped electrode was placed in the mouth as the VEP reference electrode, a needle electrode was placed subcutaneously in the tail as the VEP ground electrode (Chalgren, product #112-812-48TP), and an active VEP needle electrode (Chalgren, product #112-812-48TP) was placed subcutaneously near the visual cortex. The Ag/AgCl corneal stimulators presented an alternating scotopic 6ms flash stimulus to each eye at an intensity of 0.05 cd.s/m^2. Measurements were recorded from 10ms pre-stimulus to 300 ms post-stimulus, and a single trace was generated from the average of 100 sweeps.

2.5.2. Pattern ERG (PERG)

Immediately following the simultaneous full-field ERG and VEP tests, the PERG test was performed. A Celeris pattern ERG stimulator (Diagnosys, LLC) was placed in front of the experimental eye and presented alternating horizontal black and white bars, at 100% contrast, at a distance of 1100 mm from the eye, with 0.155 cycles per second, and an intensity of 50 cd.s/m^2. The contralateral eye was also tested. A single trace was generated from the average of 300 independent traces. The Ag/AgCl corneal reference electrode was placed in contact with the eye not being stimulated by the PERG stimulator.

2.5.3. Fundus Imaging

After the completion of the PERG tests, animals were transferred to a brightly lit room for fundus imaging. One drop of 0.3% Hypromellose gel (Systane Gel, Alcon) was applied topically to

each cornea to prevent damage and dehydration during imaging and to increase the resolving power of the objective of the imaging microscope. A MICRON® III retinal imaging microscope (Phoenix Research Laboratories) was paired with StreamPix III software (NorPix) to obtain fundus images.

2.6 Tissue Harvesting and Fixation

Eyecups and optic nerves were harvested and fixed at two timepoints: at 6 weeks, with four animals per experimental group, and at 12 weeks with the remaining 25 animals. Initially, 32 animals were to be sampled at the 12-week timepoint, but 7 animals died prior to this endpoint. Mice were sacrificed through intraperitoneal injections of 65 mg/mL Euthanyl at a dosage of 390 mg/kg. Transcardial perfusion was then performed using 4% paraformaldehyde (PFA). The head was removed, and the skin surrounding the skull was cut and peeled away. Following two lateral cuts and one central cut, the upper skull bones were cut and peeled away to expose the brain. A tweezer was used to lift the brain and expose the optic chiasm under a dissecting microscope. A cut was made 1-2 mm distal to the optic chiasm to release the optic nerves from the brain. Using fine tweezers, the orbital bones were removed to expose the entirety of the optic nerves. Micro-scissors were used to separate the two optic nerves and to release them from the eye (by cutting at 0.5 mm from the back of each eyeball. Optic nerves were then placed in vials containing Karnovsky's fixative (4% PFA, 2% glutaraldehyde, 0.1 M sodium cacodylate in PBS, pH 7.4) to fix overnight. The next day, the optic nerves were post-fixed in 2% OsO_4 in distilled water for 1 hour and 30 minutes and washed twice with distilled water. The optic nerves were dehydrated in 50%, 70%, and 100% ethanol for 1 hour each and subsequently transferred into a 1:1 Spurr's resin:acetone mixture for 1 hour. The nerves were cured in Spurr's resin overnight. The following day, the optic nerves were embedded in fresh Spurr's resin and polymerized in small rectangular moulds overnight at 65 degrees Celsius.

For eyecup harvesting, eyes were scored (for later orientation), removed from the skull and placed in small petri dishes filled with 1X phosphate-buffered saline (PBS) under a dissecting microscope. A needle was used to puncture a small hole in the cornea, and micro-scissors were used to cut away the cornea. Tweezers were used to remove and discard the cornea, lens, and iris. Each eyecup was placed for 15 minutes in a plastic labelled vial filled one-quarter of the way with 4% PFA. Eyecups were then washed with 1X PBS twice for 30 minutes each wash. The eyecups were subsequently incubated in 30% sucrose at 4 degrees Celsius overnight, followed by incubation in a 1:1 mixture of 30% sucrose:optimal cutting temperature (OCT) compound at 4 degrees Celsius overnight. During embedding, eyecups were placed in appropriately labelled small plastic cassettes filled with a 1:1 mixture of 30% sucrose:OCT. Eyecups were oriented with the opening of the eye facing downwards, and the nasal side of the eye facing a marking made on the left side of the cassette. Samples were stored at -80 degrees Celsius prior to sectioning.

2.7 Optic Nerve Processing and Axon Counts

Optic nerves were cut at 500 nm using a Leica Ultracut R Ultramicrotome to produce cross-sections. Four sections per nerve were mounted onto glass slides and stained with 1% toluidine blue. Sections were imaged with a 63x plan apochromat oil immersion objective using a Zeiss M2 Imager microscope (Zeiss). GNU image manipulation program (GIMP) software was used to stitch the optic nerve images into one merged image that contained the full face of the cross-section. ImageJ software was used to enhance the contrast of the images to facilitate axon counts. Axon counts were performed using Axonet 2.0 software, which counts the total number of axons within the full optic nerve cross-section. Axon counts from 3-4 left optic nerve sections were averaged to give the mean axon count for each optic nerve.

2.8 *Retina Processing and Immunohistochemical Analysis*

Left eyecups were sectioned at 12 μm along the sagittal plane using a Leica cryostat. Six sections per eye were mounted onto Fisherfrost™ Superfrost™ slides and air-dried for 2 hours prior to storage at -20 degrees Celsius. Immunohistochemistry was performed on left eye cryosections. Sections were post-fixed in 70% ethanol for 5 minutes, washed 3x in PBS for 10 minutes each, and blocked for 1 hour in a solution of 10% donkey serum and 0.1% Triton-X 100 in TBLS. After discarding the blocking solution, primary antibody solutions in 10% donkey serum and 0.1% Triton-X 100 in TBLS were immediately applied to the slides. Primary antibodies were incubated overnight. The following day, slides were washed 3x in PBS for 10 minutes each and incubated for 1 hour in a secondary antibody solution of 0.1% Triton-X 100 in TBLS. Slides were washed again 3x in PBS for 10 minutes each, counterstained with DAPI for 20 minutes, again washed 3x in PBS for 10 minutes each wash, mounted with Dako fluorescent mounting medium, and coverslipped. The primary antibodies used for immunostaining were rabbit anti-RBPMS (1:200; Phosphosolutions, Inc.) and rabbit anti-caspase-3 (1:200; Cell Signalling). The secondary antibody used was Alexa Fluor™ 594 donkey anti-rabbit IgG (1:500; Invitrogen). Central retina sections were imaged with a 20x objective using a Zeiss M2 Imager microscope (Zeiss).

2.9 Western Blots

Western blots were performed using C57BL6/J mouse retinas harvested from a preliminary WN1316 feeding experiment and 661W cells exposed to menadione (0 μM, 15 μM, or 25 μM) following pretreatment with WN1316 (0 μM, 3 μM, or 5 μM) to evaluate the expression levels of the neuroprotective antioxidant heme oxygenase-1 (HO-1) that WN1316 has been previously shown to upregulate (Tanaka et al., 2014). Protein concentrations of each sample were firstly determined using the DC protein assay. Following protein separation by SDS/polyacrylamide gel electrophoresis (SDS-

PAGE), proteins were transferred to an Immobilon-P membrane. Prior to transfer, the membrane was activated in methanol for 15 seconds, rinsed in deionized water for 2 minutes, and equilibrated in 1x transfer buffer (5.8 g Tris base, 2.95 g glycine, 3.75 mL SDS, 200 mL ethanol, and deionized water to 1 L) for 5 minutes. Components of the transfer cassette were simultaneously equilibrated in 1x transfer buffer for 15 minutes. For assembly of the transfer cassette, a fibre pad was first placed on the black side of the cassette, followed by thick blot paper (Bio-Rad), SDS-PAGE gel, transfer membrane, thick blot paper (Bio-Rad), and a fibre pad. The transfer cassette was then placed in a tank and submerged in 1x transfer buffer at 30 mV overnight. Following the disassembly of the transfer cassette and discarding of the SDS-PAGE gel, membrane blots were blocked overnight in 5% bovine serum albumin (BSA) in TBS-T. The next morning, blots were quickly rinsed twice with TBS-T, washed once for 15 minutes, and washed twice for 5 minutes each wash. Blots were then incubated with primary antibodies diluted in block solution for 1 hour. After incubation of the primary antibody, blots were washed again in TBS-T following the previously mentioned washing protocol. Secondary antibodies diluted in block solution were then applied for 20 minutes, and blots were subsequently washed in TBS-T with the same washing protocol but with two additional washes for 5 minutes each. Clarity™ Western ECL Substrate detection reagents (Bio-Rad) were mixed 1:1 and then applied for 5 minutes for immunodetection. The primary antibody used for immunodetection was rabbit anti-HO-1 (1:5000; Abcam). The secondary antibody used was peroxidase goat anti-rabbit (1:2000, Jackson Laboratories).

2.10 Statistical Analysis

For IOP measurements, the Student's t-test was performed in Microsoft Excel to evaluate the differences in average IOP between experimental groups. GraphPad Prism 10 was used to conduct two-way ANOVAs with Šidák correction for ERG, optic nerve axon count, and RGC soma count

statistical analyses. Data is presented as mean ± standard error of the mean (SEM). $p<0.05$ denotes statistical significance, and asterisks represent the following significance thresholds: * = $p<0.05$, ** = $p<0.01$, *** = $p<0.001$, **** = $p<0.0001$.

2.11 Nanospectroscopy

The following nanospectroscopy experiments were conducted by Sarah Tompkins, a former student in the Tsilfidis lab, whose study aimed to evaluate whether WN1316 crosses the blood-retina barrier:

2.111 Sample preparation

Between 15 mg to 50 mg of retinal tissue sample was homogenized in a Wheaton micro tissue grinder. Ground up tissue was extracted with 250 µL of tert-butyl methyl ether twice and the extract was transferred to a 5 mL glass centrifuge tube. 250 µL of 0.1 mM ammonium acetate/acetic acid in LC/MS grade H2O (100:0.01, v/v), 150 µL of LC/MS grade H2O and 500 µL of tert-butyl methyl ether were added to the supernatant and vortexed for 1 minute. Vortexed samples were centrifuged at 2000 g and 4°C for 5 min, after which 900 µL of top organic phase was transferred to a glass vial and evaporated in a Savant SpeedVac SPD111 at 35°C overnight. Samples were reconstituted in 100 µL of acetonitrile/H2O (2:8, v/v) and 1% formic acid. Samples were then passed through a 0.2 µm PTFE filter and injected into LC/MS. For liquid samples, 150 µL of H2O was replaced with an equivalent volume of the sample.

2.112 LC-MS/MS

All experiments were performed on an Orbitrap Fusion (Thermo Scientific) coupled to an Ultimate3000 nanoRLSC (Dionex). The analysis was performed on an in-house packed column (polymicro technology), 15 cm x 70 µm ID, Luna C18(2), 3 µm, 100 Å (Phenomenex) employing a

water/acetonitrile/0.1% formic acid gradient. Samples were loaded onto the column for 52 min at a flow rate of 0.30 µl/min. Peptides were separated using 10% acetonitrile in the first 7 min and then using a linear gradient from 10 to 98 % of acetonitrile for 31 min, then at 98 % of acetonitrile for 5 min, followed by a gradient from 98 to 2% of acetonitrile for 4 min and wash 5 min at 10 % of acetonitrile. Eluted compounds were directly sprayed into mass spectrometer using positive electrospray ionization (ESI) at an ion source temperature of 250°C and an ionspray voltage of 2.1 kV. Orbitrap Fusion Tribrid was run in top speed mode. Full-scan MS spectra (m/z 300–400) were acquired at a resolution of 60 000. Precursor ions were filtered according to monoisotopic precursor selection, charge state (+1 to + 3), and dynamic exclusion (10 s with a ± 10 ppm window). The automatic gain control settings were 1e6 for full FTMS scans and 5e4 for MS/MS scans. Fragmentation was performed with higher energy collision dissociation (HCD). Precursors were isolated using a 2 m/z isolation window and fragmented with a normalized collision energy of 35%.

2.113 Data Analysis

Areas of the WN1316 isolated precursor ions were analyzed using XCalibur Qual Browser 3.0 (Thermo Fisher Scientific) with mass tolerance set at 10 ppm and integration boundaries were manually verified for all peaks.

CHAPTER 3. RESULTS

This study aimed to evaluate the therapeutic use of a novel antioxidant small molecule compound, WN1316, in the experimental mouse magnetic microbead model of glaucoma. Baseline IOP and ERG measurements were taken in advance of the ocular injection surgeries to screen for any physical defects that may confound the results of the study; no animals presented with ocular irregularities at baseline. Beginning one week in advance of the surgeries, animals were given 100 μL of saline delivered by oral gavage on a daily basis to acclimate them to the procedure. WN1316 delivery by oral gavage at a dosage of 50 μg/kg began one day prior to the glaucoma induction surgeries, and WN1316 was also delivered immediately before the injections.

Magnetic microbeads were delivered by intracameral injection to 24 animals (12 males and 12 females) to induce ocular hypertension. A handheld magnet was used to direct the microbeads and allow them to settle into the iridocorneal angle where the aqueous outflow pathways are located. Blockage of the outflow canals by the magnetic microbeads was expected to lead to elevations in IOP as a result of aqueous humour buildup in the anterior chamber, subsequently leading to RGC dysfunction, axon loss, and apoptosis. The remaining 24 animals (12 males and 12 females) served as controls and received intracameral saline injections. Only the left eyes received injections of microbeads or saline to reduce stress on the animals; contralateral eyes were not subjected to injections.

The day following the surgical injections, WN1316 was delivered at a dosage of 50 μg/kg by oral gavage on a daily basis to half of the animals until they were sacrificed at either 6- or 12-weeks post-surgery. The remainder of the animals received daily saline treatment as controls. The experimental groups are illustrated as follows, with an equal ratio of males to females in each group:

- Glaucoma + WN1316 (n=12)

- Glaucoma + saline (n=12)
- Sham + WN1316 (n=12)
- Sham + saline (n=12)

3.1 WN1316 crosses the blood-retina barrier

To evaluate whether WN1316 is able to pass through the blood-retina barrier, preliminary nanospectroscopy experiments were performed by a former member of the Tsilfidis lab. When WN1316 was loaded into the chromatographic column, its retention time was 19.52 seconds, with a base peak of 350 m/z (Figure 3.1 A). Retention time, which is the amount of time a compound spends in the column after it was loaded, is unique for different compounds and allows for the identification of the presence of a compound in tissue samples. A control retina sample from a rat that was not fed WN1316 was passed through the column, and a peak of 350 m/z was not observed at 19.52 seconds, indicating the absence of WN1316 in this control retina sample as expected (Figure 3.1 B). When a retina sample from a rat that was fed WN1316 was loaded into the column, a base peak of 350 m/z was observed at 19.11 seconds, confirming that WN1316 had crossed the blood-retina barrier in this rat (Figure 3.1 C). Therefore, the preliminary nanospectroscopy studies confirmed that WN1316 is able to cross the blood-brain barrier in rats.

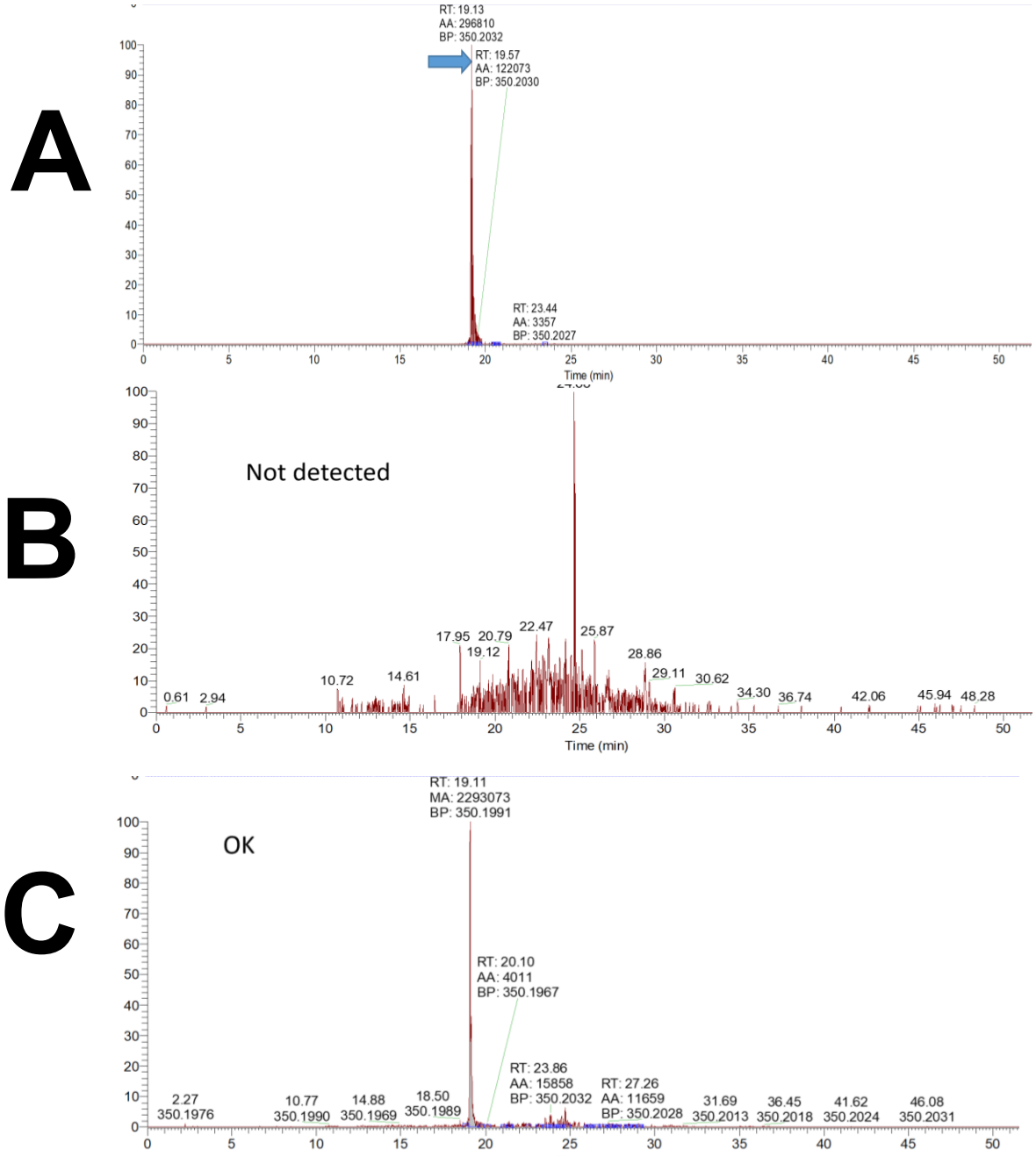

Figure 3.1. WN1316 crosses the blood-retina barrier. (A) A control sample of WN1316 loaded into the column has a retention time of 19.52 seconds and a base peak of 350 m/z. (B) WN1316 is not detected in a control retina sample. (C) A base peak of 350 m/z and retention time of 19.11 appears when a WN1316-treated retina sample was loaded into the column, indicating that WN1316 crossed the blood-brain barrier. These are representative samples, but similar results were obtained in all samples tested (N=5-6).

3.2 WN1316 enhances HO-1 protein expression in 661W cells following oxidative stress, and in a time-dependent manner in intact mouse retinas

Given that WN1316 has been previously shown to upregulate the neuroprotective antioxidant HO-1 *in vitro* (Tanaka et al., 2014), Western blot analysis was performed on protein extracts from 661W cells following WN1316 pre-treatment and menadione exposure. Protein samples were collected from 661W cells by another student in the Tsilfidis lab. Representative Western blot images show that WN1316 increases HO-1 protein expression, particularly under conditions of oxidative stress (Figure 3.2 A). 661W cells that were treated with 5 μM WN1316 and 25 μM menadione showed the greatest expression of HO-1, with a normalized ratio of 1.08 compared to 0.65 in cells treated with 0 μM WN1316 and 25 μM menadione as revealed by quantitative densitometric analysis of HO-1 band intensities normalized to β-actin (Figure 3.2 C). When 661W cells were treated with 3 μM WN1316 and 25 μM menadione, the normalized ratio of HO-1 expression was lower compared to the 5 μM WN1316 and 25 μM condition, at 0.81. HO-1 expression was moderately enhanced (0.18) when cells were treated with 5 μM WN1316 and 15 μM menadione condition (Figure 3.2 C). These findings demonstrate that *in vitro*, WN1316 induces HO-1 protein expression in a dose- and oxidative stress-dependent manner. To determine whether WN1316 induces HO-1 expression *in vivo*, Western blot analysis was performed using intact retinas harvested from a preliminary WN1316 feeding study. In the feeding study, animals were fed WN1316 at a dosage of 100 μg/kg and sacrificed at 4-, 6-, 8-, and 16-hours post-feeding. The representative Western blot image revealed that WN1316 appeared to induce HO-1 protein expression in a time-dependent manner in intact mouse retinas (Figure 3.2 B). Quantitative densitometric analysis of band intensities normalized to β-actin revealed that at 4-, 6-, 8- and 16-hours post-feeding, normalized ratios were 1.2, 1.0, 0.93, and 0.35, respectively (Figure 3.2 D). It cannot be definitively confirmed that these bands were truly HO-1 bands, as these bands had migrated faster than the 661W HO-1 protein control band.

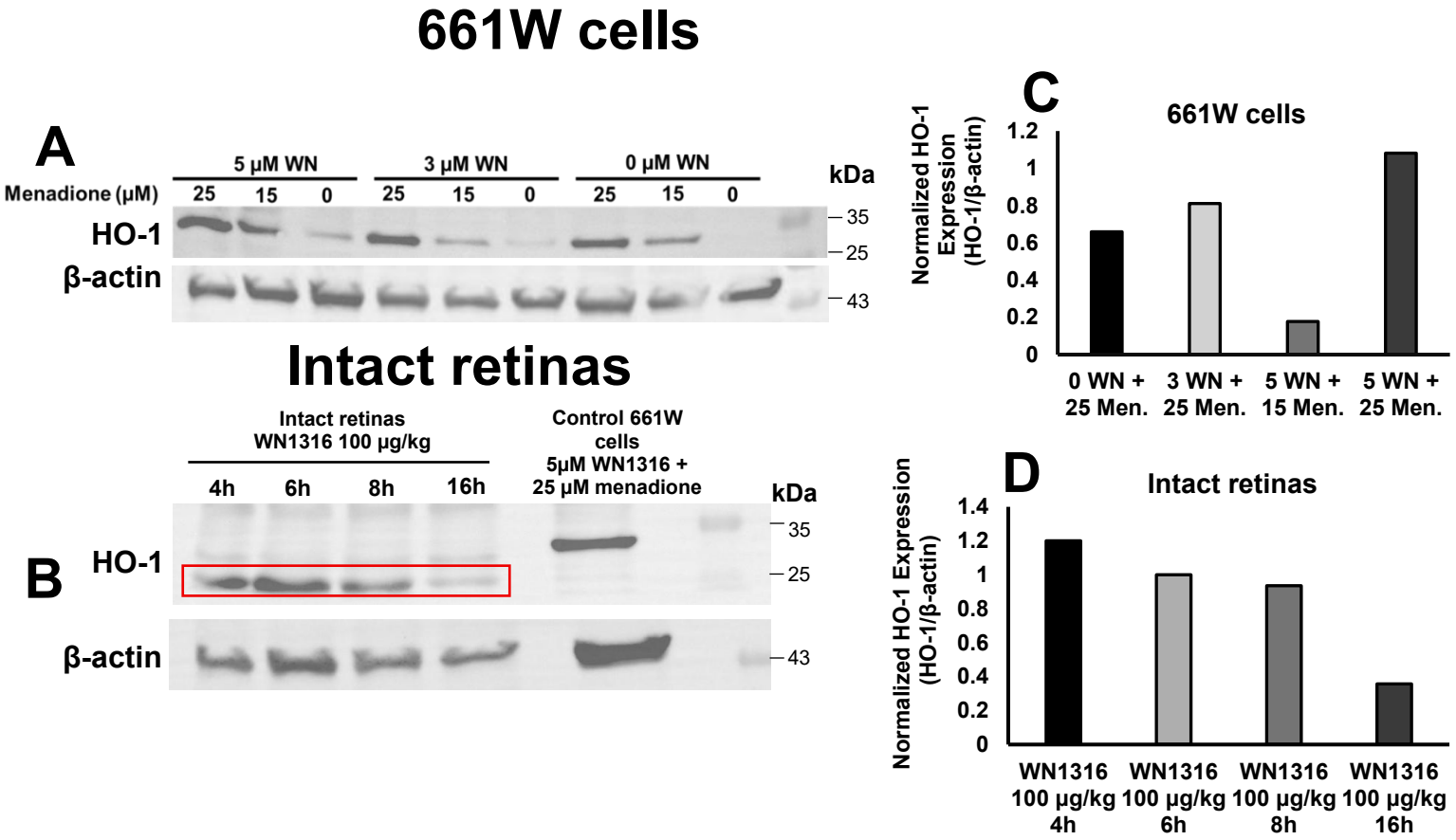

Figure 3.2. WN1316 induces HO-1 protein expression in 661W cells during oxidative stress, and in a time-dependent manner in intact mouse retinas. (A) Representative Western blot photos of HO-1 and β-actin protein levels in 661W cells that were exposed to menadione (15 µM or 25 µM) following pre-treatment with different concentrations of WN1316 (0, 3, or 5 µM). (B) Representative Western blot photos of HO-1 and β-actin protein levels in intact C57BL/6 mouse retinas harvested from a preliminary feeding study. Animals were fed WN1316 by oral gavage at a dosage of 100 µg/kg and sacrificed at 4-, 6-, 8-, and 16-hours post-feeding. Protein extracts from 661W cells treated with 5 µM WN1316 and 25 µM menadione were represented as a control to confirm the location of the HO-1 band. It is uncertain if the highlighted bands represent HO-1, as these bands do not align with the 661W control band. (C) Quantitative densitometry of HO-1 band intensities normalized to β-actin in 661W cells. Bars represent the ratio of HO-1 to β-actin loading control expression. Data suggests that WN1316 enhances HO-1 protein expression in a dose- and stress-dependent manner. (D) Quantitative densitometry of HO-1 band intensities normalized to β-actin in intact C57BL6/J mouse retinas. Bars represent the ratio of HO-1 to β-actin loading control expression. Data indicates that WN1316 upregulates HO-1 in intact mouse retinas in a time-dependent manner, with expression peaking at 4 hours post-feeding.

3.3 Microbead injections cause severe and unexpected corneal and lens damage

The goal of the microbead injections was to induce glaucoma by IOP elevation. Ideally, the beads would have settled in the iridocorneal angle and blocked the outflow pathways, leading to aqueous humour buildup in the anterior chamber without causing damage to ocular structures such as the cornea and lens, as was the case in the study conducted by the developers of the magnetic microbead model of glaucoma (Ito et al., 2016). Unexpectedly, corneal abrasions and lens opacities were observed in the majority of the eyes that received the microbead injections. These damages were clearly observable beginning the day following the surgeries and were confirmed by fundus imaging at 3 weeks. The damages persisted up until the point of sampling. At week 6, all of the 16 glaucomatous animals that were sampled exhibited irregularly shaped and clouded corneas, dense central cataracts in the lenses, and degraded irises (Figure 3.3 A). The observations of microbead-injected eyes that were harvested at week 12 were similar, however the lens and corneal opacities were not as severe in these animals (Figure 3.3 B). The animals that showed the most severe ocular damage and worst ERG performance were sampled at 6 weeks, which explains the difference in severity in the damage between the 6- and 12-week timepoints. Only two microbead-injected animals, which were sampled at week 12, exhibited clear lenses and corneas, allowing observation of the retina by fundus imaging. Surprisingly, all sham injected animals displayed light-coloured regions throughout their retinas as observed by fundus imaging, which indicate retinal damage in their injected eyes, noted as early as 3 weeks post-injection and persisting until 6- (Figure 3.3 C) or 12-weeks (Figure 3.3 D) post-surgery when animals were sampled.

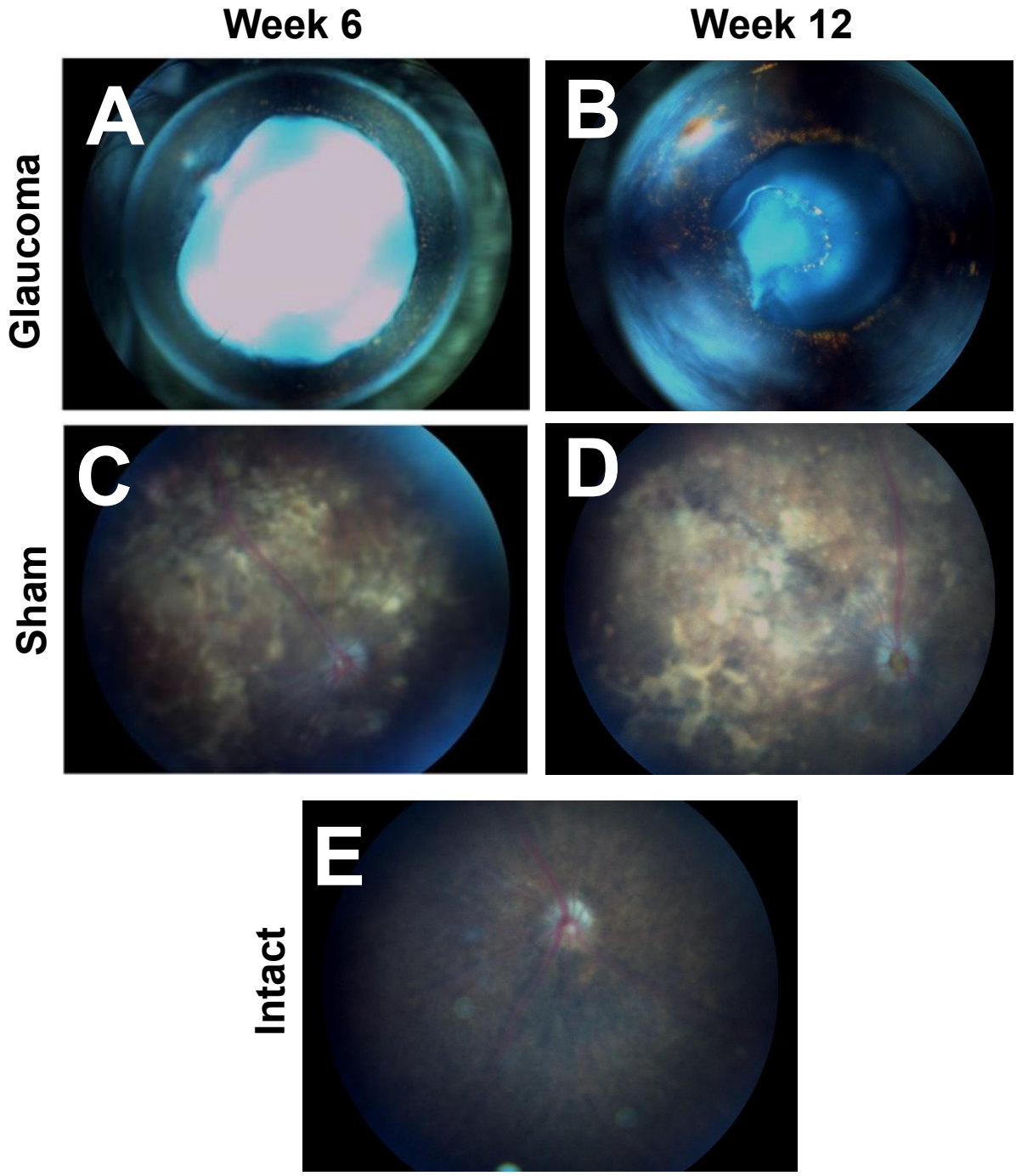

Figure 3.3. Representative fundus images exhibiting ocular damage caused by injection surgeries. (A) Representative fundus image of a microbead-injected eye demonstrating dense lens and corneal opacity at week 6. (B) Representative fundus image of a microbead-injected eye showing moderate corneal opacity at week 12. (C) Representative fundus image of a sham-injected eye at week 6, displaying light-coloured patches indicative of retinal damage. (D) Representative fundus image of a sham-injected eye at week 12; light-coloured patches reflect retinal damage. (E) Example fundus image of an uninjected eye. All images were taken of the dilated left eyes of anesthetized C57BL6/J mice.

3.4 Microbead injections successfully induce and sustain IOP elevations

Given that elevated IOP is the most widely recognized risk factor for clinical glaucoma, IOP measurements were taken in awake mice to ensure that the magnetic microbead model resembles clinical glaucoma. Measurements were taken weekly in awake mice until 4 weeks post-surgery and bi-weekly until 12 weeks using rebound tonometry. One week post-bead injections, IOPs were elevated by 64% in WN1316-treated glaucomatous animals (Figure 3.4 A) and 91% in saline-treated glaucomatous animals (Figure 3.4 B) relative to baseline. IOP elevations were sustained at an average of 25.3 ± 5.9 mmHg (mean ± SD) until 12 weeks post-surgery in WN1316-treated glaucomatous mice (Figure 3.2 A) and 24.8 ± 6.23 mmHg in saline-treated glaucomatous mice (Figure 3.4 B). WN1316-treated (Figure 3.4 A) and saline-treated (Figure 3.4 B) control animals showed consistent IOP averages of 12.6 ± 2.3 mmHg and 13.2 ± 2.6 mmHg up to 12 weeks post-injections, respectively. As anticipated, the intracameral injections of microbeads into the anterior chamber produced significantly sustained elevations in IOP up to 12 weeks post-surgery in glaucomatous mice that were treated with WN1316 or saline relative to their respective controls (Figure 3.4 A,B), confirming that the magnetic microbead model is effective at inducing sustained IOP elevations.

3.5 WN1316 treatment does not affect IOP levels

The relationship between WN1316 treatment and IOP has not been previously investigated in the literature. However, a preliminary 6-week study performed by the Tsilfidis lab found that WN1316 did not provide significant protection against IOP elevation. As elevated IOP is a major risk factor for clinical glaucoma, a goal of this study was to evaluate whether WN1316 treatment would have any protective effects against IOP elevation throughout the longer 12-week experiment. As

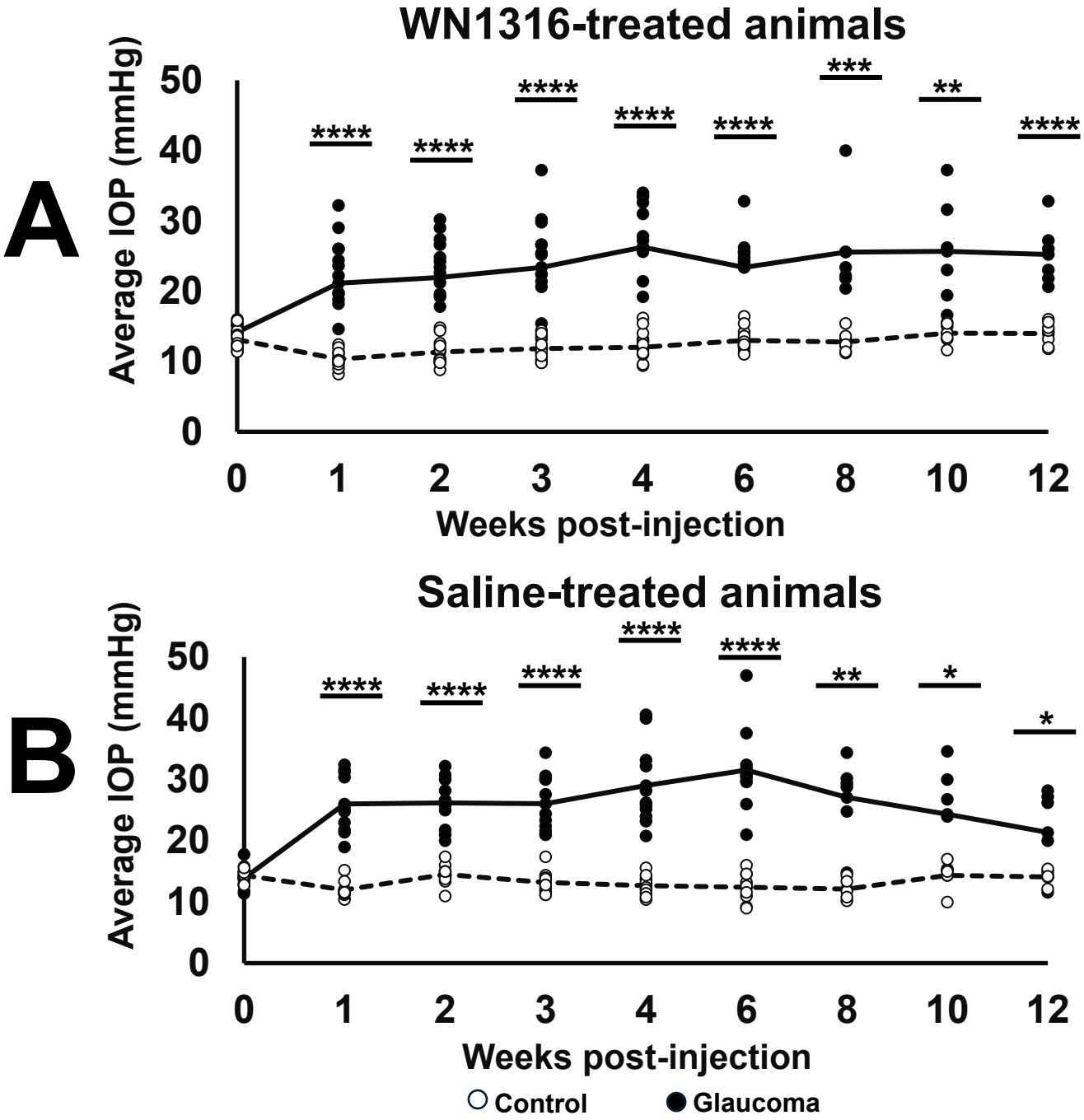

Figure 3.4. Microbead injections successfully induce and sustain elevations in IOP up to 12 weeks post-injection. Mean IOP (mmHg) is significantly elevated in (A) WN1316-treated glaucomatous animals and (B) saline-treated glaucomatous animals relative to their respective sham controls up to 12 weeks post-surgery. All measurements were taken from the left eyes of awake animals. Each data point represents the mean of five IOP measurements taken for each animal. Statistical analysis was performed using the Student's t-test. * = $p<0.05$, ** = $p<0.01$, *** = $p<0.001$, **** = $p<0.0001$.

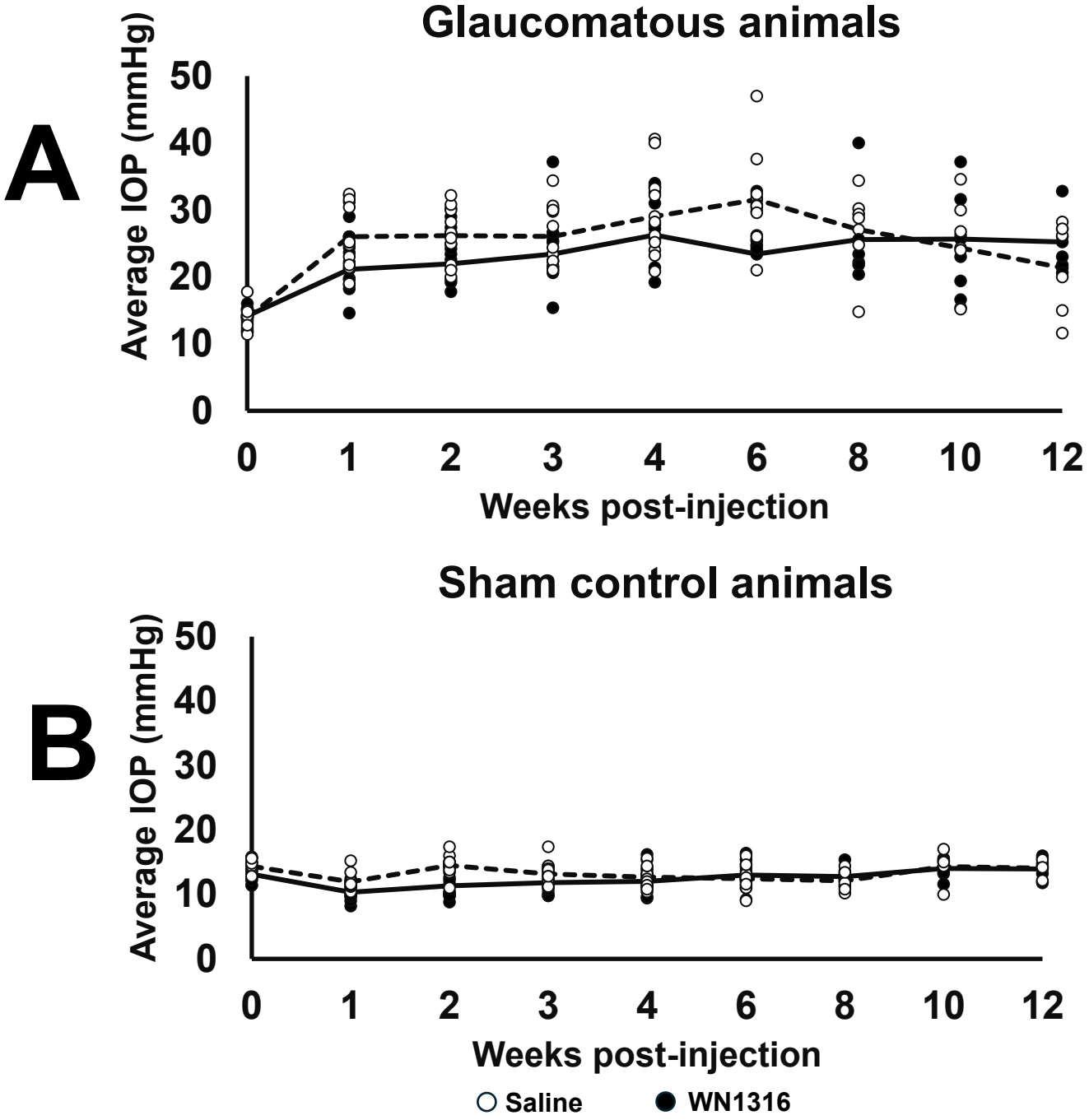

Figure 3.5. WN1316 treatment does not influence IOP levels. (A) Glaucomatous and (B) sham animals treated with WN1316 do not show significant differences in IOP compared to animals treated with saline ($p>0.05$). All measurements were taken from the left eyes of awake animals. Each data point represents the mean of five IOP measurements taken for each animal. Statistical analysis was performed using the Student's t-test.

illustrated in Figure 3.5 A, there were no significant differences between the mean IOP of saline-treated and WN1316-treated glaucomatous mice across all timepoints. Furthermore, significant differences were also not observed between the mean IOP of saline-treated and WN1316 sham mice (Figure 3.5 B). Hence, WN1316 treatment does not appear to influence IOP levels.

3.6 Glaucoma induction impairs outer retinal function

Glaucoma is characterized as a degenerative disease of the optic nerve and dysfunction of cells in the outer retinal layers is typically not observed. To determine whether the magnetic microbead model of glaucoma affects outer retinal functioning, an *in vivo* physiological test known as the dark-adapted full-field electroretinogram (ffERG) was performed at baseline, 3-, 6-, 9-, and 12-weeks post-surgery. The amplitudes of the a-wave, b-wave, and oscillatory potential (OP) components of the ffERG reflect the functioning of photoreceptors, the inner retina (including bipolar cells and Muller cells), and amacrine cells, respectively.

In terms of photoreceptor functioning, glaucoma induction appeared to diminish the mean peak amplitude of the a-wave at some but not all timepoints. At 6 weeks, significant reductions in the a-wave amplitude were observed in both saline-treated ($p<0.01$) and WN1316-treated ($p<0.001$) glaucomatous animals relative to their respective sham controls (Figure 3.6 C). At 9 and 12 weeks, no significant differences were found between the a-wave amplitudes across all treatment groups (Figure 3.6 D,E). Interestingly, at 3 weeks, the a-wave amplitude in WN1316-treated glaucomatous animals was not significantly different from the saline-treated sham control but was significantly reduced ($p<0.0001$) relative to WN1316-treated sham controls (Figure 3.6 B). This result may be due to the fact that the a-wave amplitudes were significantly elevated ($p<0.05$) in the WN1316-treated sham control group relative to the saline-treated sham control group, suggesting that WN1316 may be able

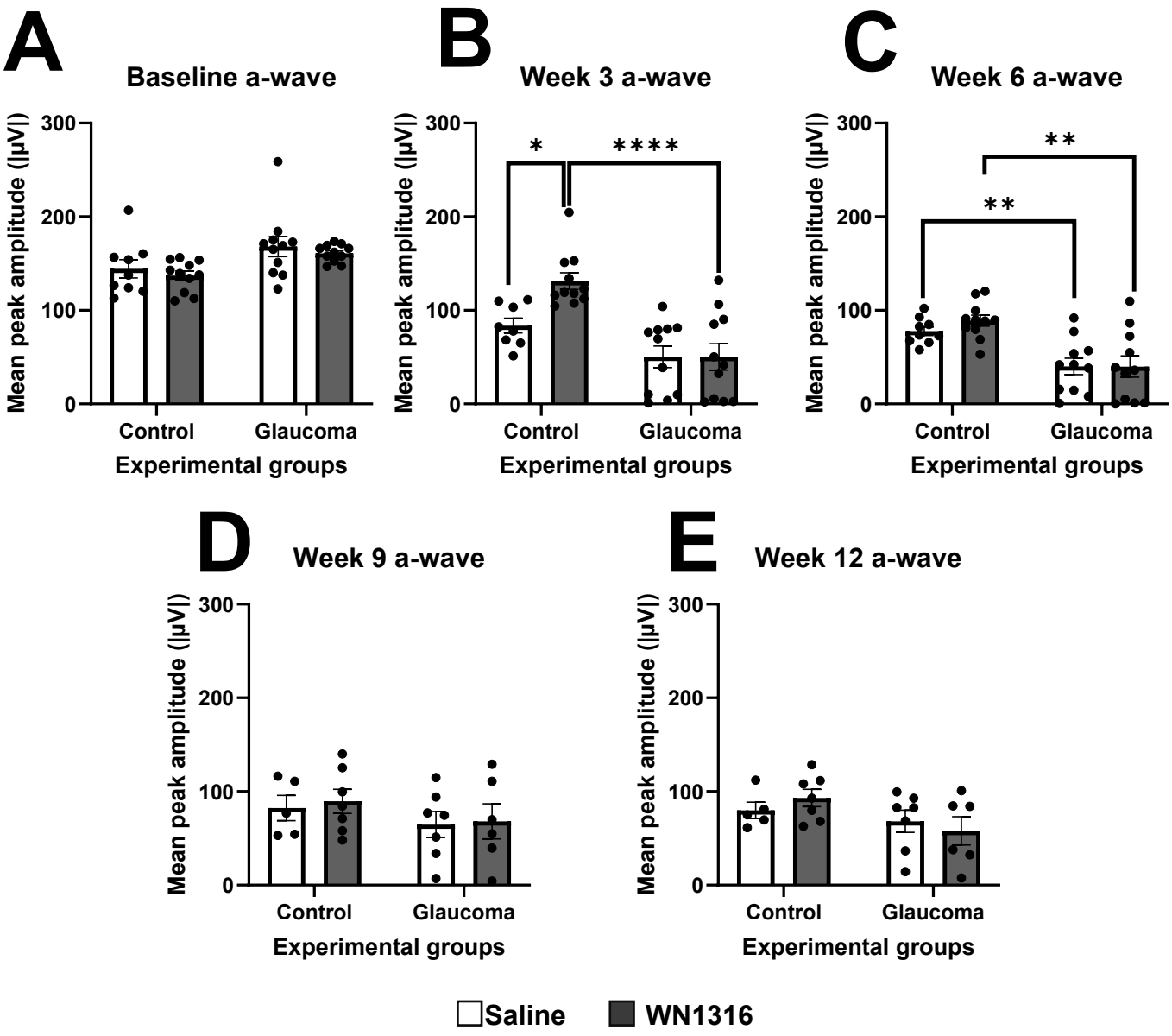

Figure 3.6. Photoreceptor function is reduced in glaucomatous animals at 3- and 6-weeks post-surgery. Mean peak amplitude of the a-wave at (A) baseline, (B) 3-weeks, (C), 6-weeks, (D) 9-weeks, and (E) 12-weeks post-surgery. All measurements were taken from only the left eyes of anesthetized animals. Statistical analysis was performed using a two-way ANOVA with Šidák correction. Error bars represent the standard error of the mean (SEM). *p<0.05, **p<0.01, ***p<0.001, ****p<0.0001.

to protect against photoreceptor dysfunction in cases where retinal damage is less severe, as would be the case with a sham injection (Figure 3.6 B). It is important to note that there is bias between the pre- and post- 6-week timepoints because at 6 weeks, animals that showed the most severe ocular damage were sampled.

Similarly, inner retinal cell function appeared to be negatively impacted in the WN1316-treated glaucomatous group. At 3- and 6-weeks post-surgery, WN1316-treated glaucomatous animals showed significant reductions ($p<0.001$, $p<0.05$) in the mean peak amplitude of the b-wave relative to WN1316-treated sham control animals (Figures 3.7 B,C). However, this may be due to the fact that the mean peak amplitude of the b-wave was higher in the WN1316-treated sham control group compared to the saline-treated sham control group. As was seen with the a-waves, the b-wave amplitudes of the WN1316-treated sham control animals were significantly elevated ($p<0.02$) compared to the saline-treated sham control animals at 3 weeks, again suggesting that WN1316 treatment may be protective in cases of mild retinal damage (Figure 3.7 B).

Amacrine cell function, represented by the amplitudes of the oscillatory potentials (OPs), was also reduced at certain timepoints in glaucomatous animals. At week 3, OP1 was significantly diminished ($p<0.0001$) in WN1316-treated glaucomatous animals relative to WN1316-treated sham controls, and at week 6, OP1 was significantly reduced in both saline-treated ($p<0.01$) and WN1316-treated glaucoma animals ($p<0.001$) (Figures 3.8 B,C). At week 6, there was a significant reduction ($p<0.05$) in OP2 in the WN1316-treated glaucoma condition compared to the WN1316-treated control group (Figure 3.8 H). There were no significant differences ($p>0.05$) in the mean peak amplitude of OP3 between any of the experimental groups throughout all timepoints (Figures 3.8 K-O).

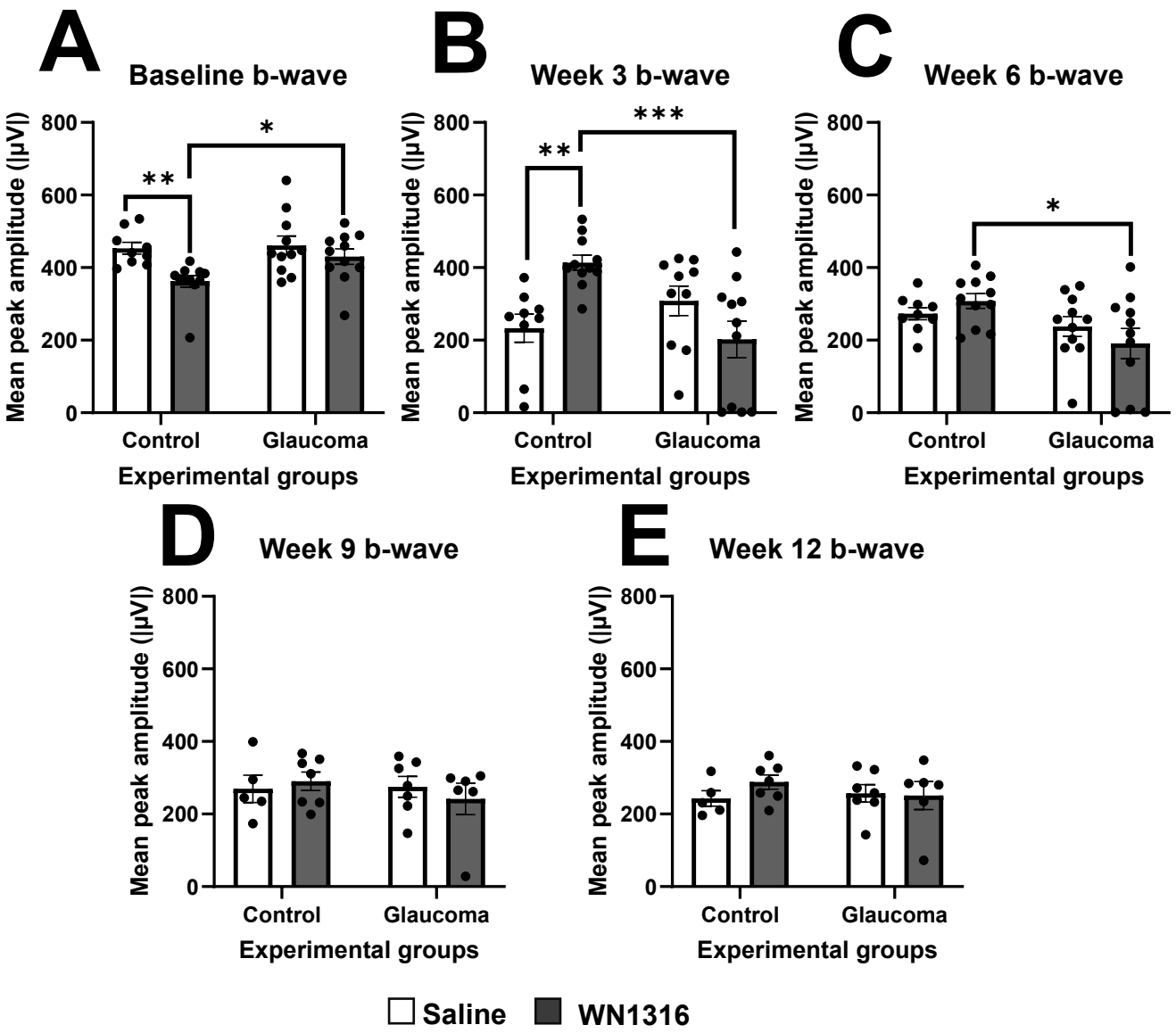

Figure 3.7. Bipolar cell function is diminished in WN1316-treated glaucomatous animals at 3- and 6-weeks post-surgery. Mean peak amplitude of the b-wave at (A) baseline, (B) 3-weeks, (C), 6-weeks, (D) 9-weeks, and (E) 12-weeks post-surgery. All measurements were taken from only the left eyes of anesthetized animals. Statistical analysis was performed using a two-way ANOVA with Šidák correction. Error bars represent the standard error of the mean (SEM). *$p<0.05$, **$p<0.01$, ***$p<0.001$.

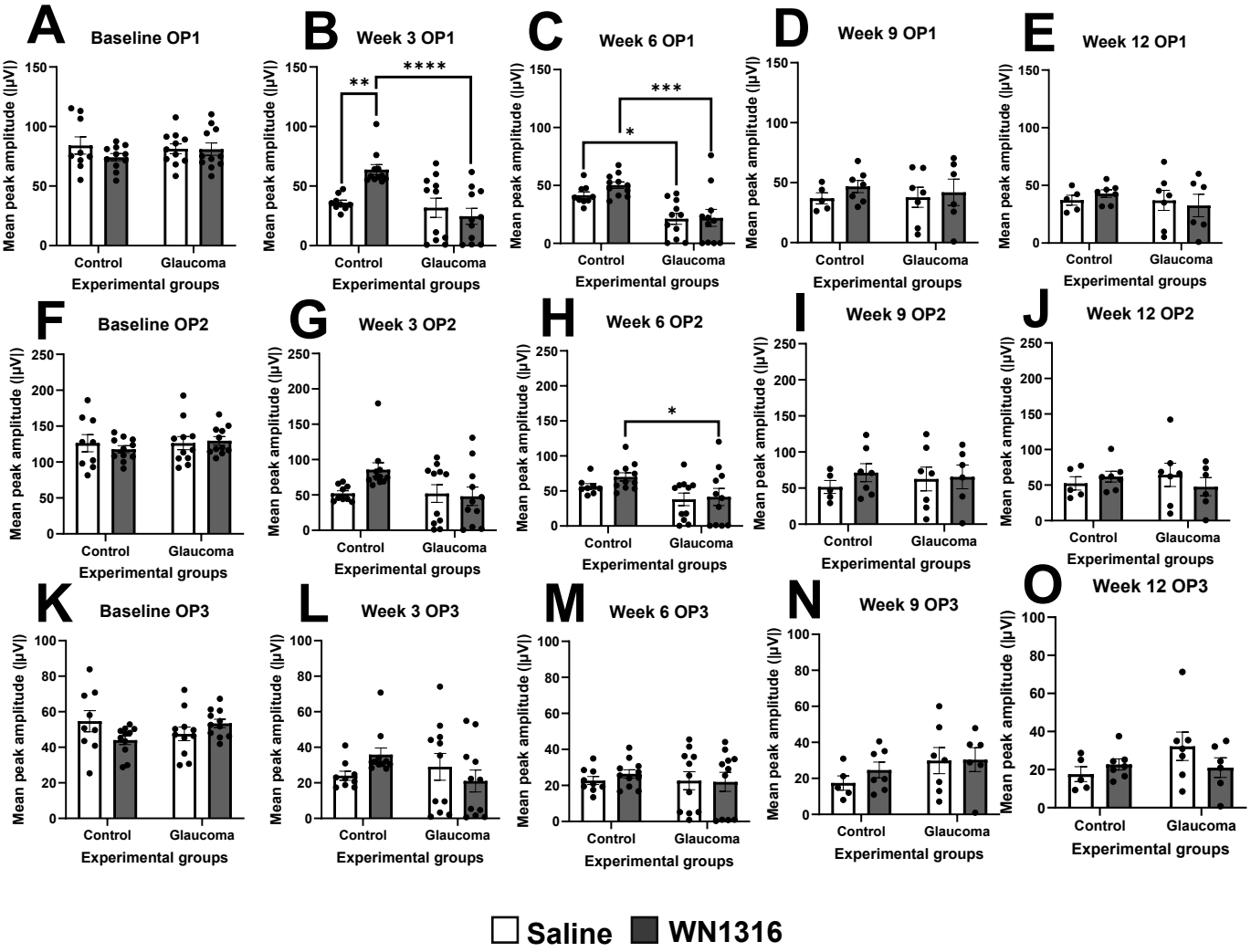

Figure 3.8. Amacrine cell function is impaired in glaucomatous eyes. (A-E) Mean peak amplitude of OP1 at (A) baseline, (B) 3-weeks, (C) 6-weeks, (D) 9-weeks, and (E) 12-weeks post-surgery. (F-J) Mean peak amplitude of OP2 at (F) baseline, (G) 3-weeks, (H) 6-weeks, (I) 9-weeks, and (J) 12-weeks post-surgery. (K-O) Mean peak amplitude of OP3 at (K) baseline, (L) 3-weeks, (M) 6-weeks, (N) 9-weeks, and (O) 12-weeks post-surgery. All measurements were taken from only the left eyes of anesthetized animals. Statistical analysis was performed using a two-way ANOVA with Šidák correction. Error bars represent the standard error of the mean (SEM). *p<0.05, **p<0.01, ***p<0.001, ****p<0.0001.

These findings suggest that IOP elevation, particularly in tandem with severe lens and corneal damage, can cause outer retinal dysfunction in glaucomatous animals. WN1316 did not appear to provide significant protection against outer retinal dysfunction in bead-injected eyes, but trends hinted that WN1316 may be protective in cases of less severe retinal damage as was observed with the sham control eyes.

3.7 WN1316 does not protect against RGC dysfunction in glaucoma

To evaluate whether IOP elevation causes RGC dysfunction in glaucoma and whether WN1316 treatment offers functional protection, the pattern ERG (PERG) test was performed at 3-, 6-, 9-, and 12-weeks post-glaucoma induction. The PERG corneal stimulator presents alternating black-and-white horizontal bars to the eyes, and this specific type of visual pattern elicits responses from RGCs. The P1 and N2 components of the PERG waveform reflect the functioning of RGC soma and axons, respectively. At 3 weeks, saline-treated and WN1316-treated glaucomatous animals exhibited significant reductions ($p<0.05$, $p<0.0001$) in the mean peak amplitudes of P1 and N2 in relation to WN1316-treated controls (Figure 3.9 B,G) , while P1 and N2 amplitudes were significantly elevated ($p<0.05$, $p<0.01$) in the WN1316-treated control group relative to the saline-treated control group at this timepoint (Figure 3.9 B,G). P1 and N2 remained significantly reduced in the WN1316-treated glaucomatous animals relative to WN1316-treated controls at 6 and 9 weeks (Figure 3.9 C,D). At 12 weeks, no significant reductions were observed for P1 (Figure 3.9 E), while N2 was significantly diminished ($p<0.05$) in the WN1316-treated glaucoma group at 12 weeks (Figure 3.9 J). Overall, these results demonstrate that the microbead model appeared to impair RGC function, as would be expected, but that WN1316 does not protect against RGC dysfunction in glaucoma.

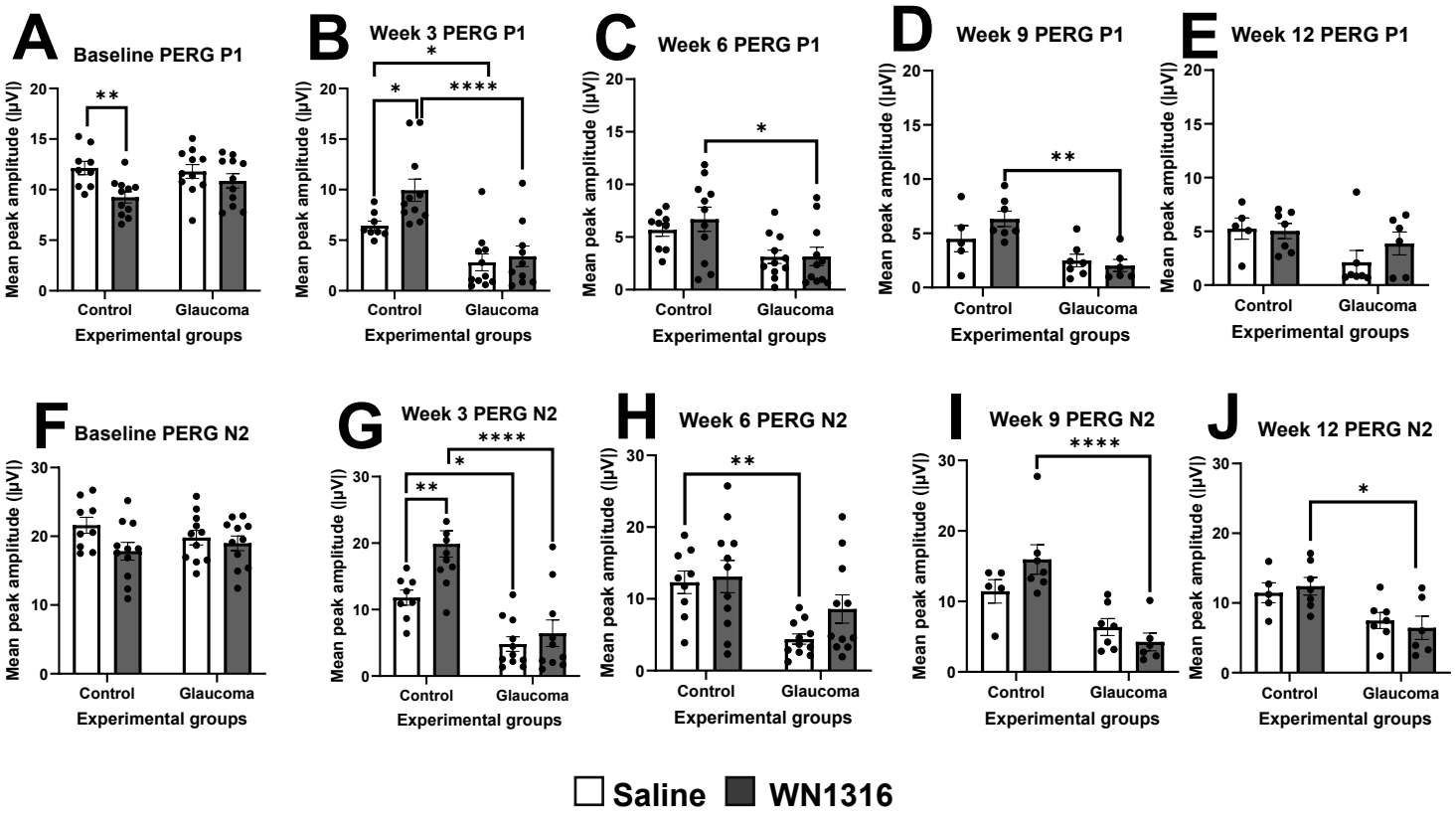

Figure 3.9. WN1316 does not protect against RGC soma and axon dysfunction in glaucoma. (A-E) Mean peak amplitude of the P1 component of the pattern electroretinogram (PERG), which represents RGC soma function, at (A) baseline, (B) 3-weeks, (C) 6-weeks, (D) 9-weeks, and (E) 12-weeks post-surgery. (F-J) Mean peak amplitude of the N2 component of the PERG, which reflects RGC axon function, at (F) baseline, (G) 3-weeks, (H) 6-weeks, (I) 9-weeks, and (J) 12-weeks post-surgery. All measurements were taken from only the left eyes of anesthetized animals. Statistical analysis was performed using a two-way ANOVA with Šidák correction. Error bars represent the standard error of the mean (SEM). *p<0.05, **p<0.01, ***p<0.001, ****p<0.0001.

3.8 WN1316 does not protect against visual cortex dysfunction in glaucoma

The visual pathway culminates in the visual cortex of the occipital lobe where visual perception is generated, and evidence has shown that signalling to the visual cortex is impaired in glaucoma. Hence, visual evoked potentials (VEPs) were recorded to evaluate whether visual cortex signalling is affected in the mouse magnetic microbead model of glaucoma and if WN1316 treatment can preserve the functionality of the visual pathway that extends from the retina to the visual cortex. During the VEP test, an active electrode placed subcutaneously under the scalp near the occipital lobe records electrical responses elicited by the visual cortex in response to bright flashes of light presented to the eyes by corneal stimulators. Two components of the VEP were analyzed in this study: the N1 and P2. The N1 represents early-arriving signals to the primary visual cortex (V1) derived from the retina, while P2 represents intracortical visual signalling. At 3- and 6-weeks post-surgery, WN1316-treated glaucomatous animals showed significant reductions in the mean peak amplitude of N1 compared to WN1316-treated sham controls ($p<0.001$) (Figure 3.10 B,C). At week 12, N1 was reduced in saline-treated glaucomatous relative to saline-treated controls ($p<0.01$) while this was not the case with WN1316-treated glaucomatous animals at week 12 ($p>0.05$) (Figure 3.10 E). There were no significant reductions ($p>0.05$) in P2 in glaucomatous animal groups across all experimental timepoints (Figure 3.10 F-J). It is difficult to discern whether WN1316 had any effect on visual cortex function in glaucoma based on these results, as the VEP test often comes with high inter-animal variability due to variations in electrode placement.

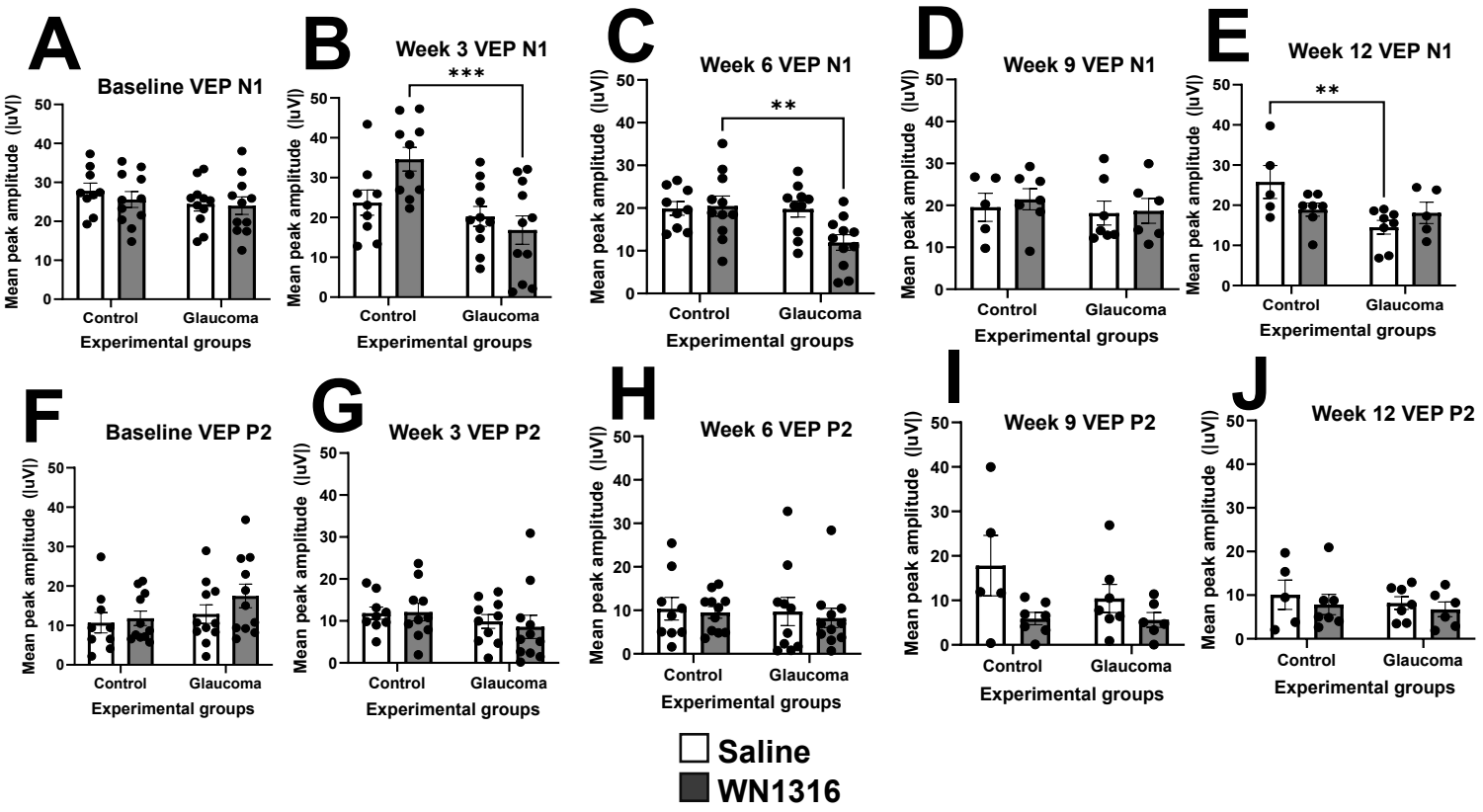

Figure 3.10. WN1316 does not protect against visual cortex dysfunction in glaucoma. (A-E) Mean peak amplitude of the N1 component of the visual evoked potential (VEP) which represents early-arriving signals at the level of the visual cortex, at (A) baseline, (B) 3-weeks, (C) 6-weeks, (D) 9-weeks, and (E) 12-weeks post-surgery. (F-J) Mean peak amplitude of the P2 component of the PERG, which intracortical visual signalling, at (F) baseline, (G) 3-weeks, (H) 6-weeks, (I) 9-weeks, and (J) 12-weeks post-surgery. All measurements were taken from only the left eyes of anesthetized animals. Statistical analysis was performed using a two-way ANOVA with Šidák correction. Error bars represent the standard error of the mean (SEM). **$p<0.01$, ***$p<0.001$.

3.9 WN1316 does not protect against optic nerve axon loss in glaucoma

In addition to functional protection, a goal of this study was to determine whether WN1316 could offer structural protection for RGCs in glaucoma. At 6- and 12-weeks post-surgery, retinas and optic nerves were harvested. Optic nerves were stained with toluidine blue and imaged with light microscopy, and axon counts were conducted on full optic nerve cross-sections. Analyses revealed a significant 75% axon count reduction ($p<0.05$) in WN1316-treated glaucomatous animals in relation to WN1316-treated control animals at week 6 post-surgery (Figure 3.11 I). Axon counts were also significantly reduced by 73% ($p<0.05$) in WN1316-treated glaucomatous animals compared to saline-treated glaucomatous animals at week 6 post-surgery (Figure 3.11 I). Surprisingly, the axon counts of saline-treated glaucomatous animals were not significantly reduced compared to those of saline-treated controls at week 6, indicating that sustained IOP elevation was not sufficient to induce axon loss in this group (Figure 3.11 I). At 12 weeks post-surgery, there were no significant differences ($p>0.05$) in optic nerve axon counts between control and glaucoma animals (Figure 3.11 J); this was highly unexpected given the sustained IOP elevations in glaucomatous animals. To confirm these findings, a secondary evaluator conducted axon counts on five equally sized frames from five different regions of each optic nerve, and counts from each frame were averaged to give a mean count for each optic nerve. Similar to the aforementioned findings, the secondary evaluator found a significant 68% reduction in the average axon counts of 6-week WN1316-treated glaucomatous optic nerves relative to WN1316-treated control optic nerves ($p<0.05$) (Figure 3.11 K), as well as a 61% reduction in WN1316-treated glaucomatous optic nerves compared to saline-treated glaucomatous optic nerves ($p<0.05$) (Figure 3.11 K). The secondary evaluator also found no significant differences between any of the treatment groups at week 12 (Figure 3.11 L). The difference in axon counts between the 6- and 12-week timepoints may be due to the fact that at 6 weeks, animals that showed the greatest extent of ocular damage (i.e., cornea and lens opacities) as well as the poorest PERG performance were sampled.

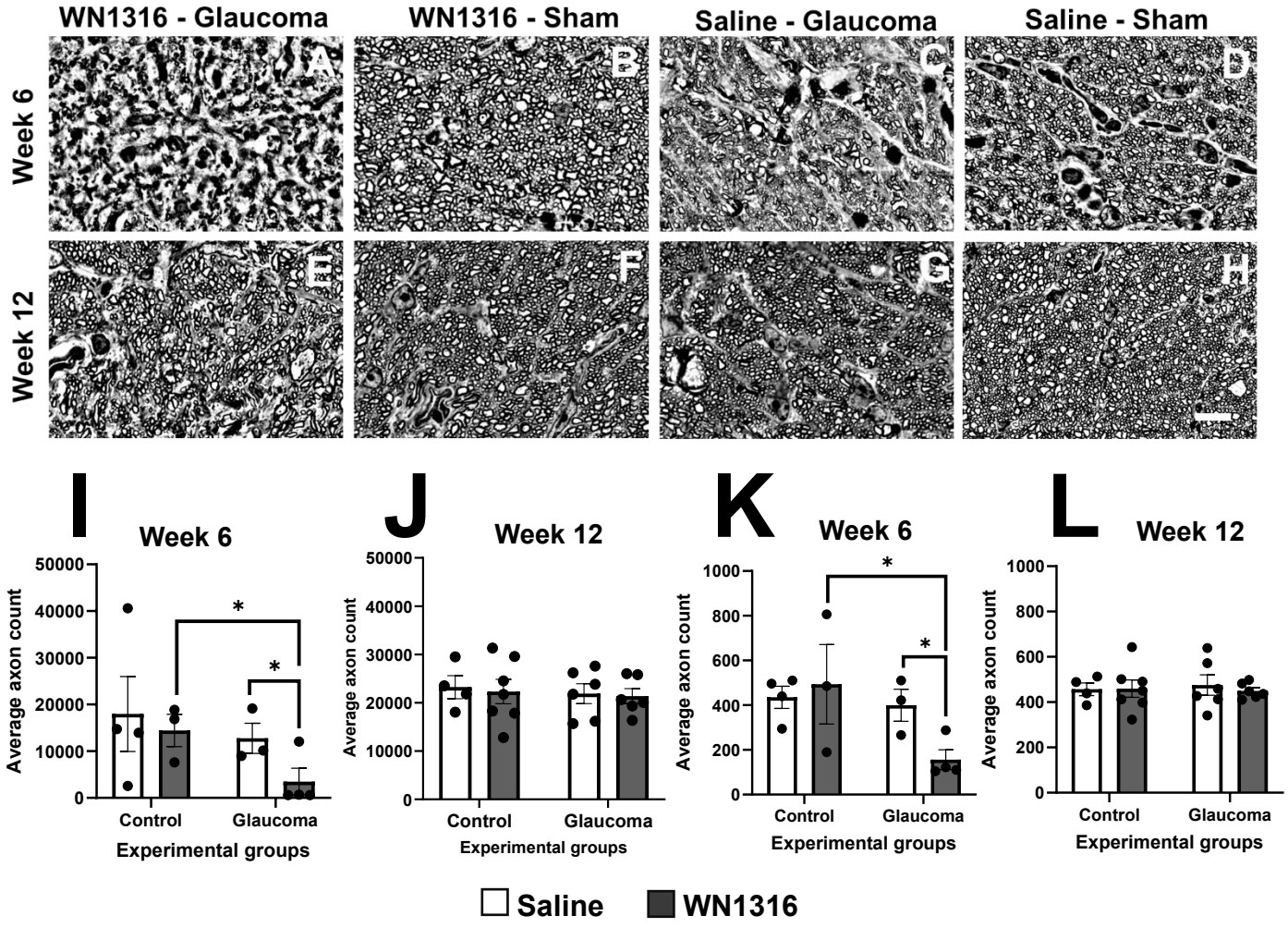

Figure 3.11. Optic nerve axon counts are significantly reduced in WN1316-treated glaucomatous animals at 6-weeks but not at 12-weeks post-surgery. (A-D) Representative magnified 6-week optic nerve images of (A) WN1316-treated glaucomatous mice, (B) WN1316-treated sham-mice, (C) saline-treated glaucomatous mice, and (D) saline-treated sham mice (E-H) Representative magnified 12-week optic nerve images of (E) WN1316-treated glaucomatous mice, (F) WN1316-treated sham mice, (G) saline-treated glaucomatous mice, and (H) saline-treated sham mice. (I) At 6-weeks post-surgery, optic nerve axon counts are significantly reduced in WN1316-treated glaucomatous mice compared to WN1316-treated controls and saline-treated glaucomatous mice. (J) Optic nerve axon counts are not reduced in glaucomatous mice at 12-weeks post-surgery. (K) Average axon counts from five different regions of the optic nerve, conducted by a secondary evaluator, are significantly reduced in WN1316-treated glaucomatous animals relative to saline-treated glaucomatous animals as well as WN1316-treated control animals at week 6. (L) At week 12, average axon counts conducted by the secondary evaluator were similar between treatment groups All axon counts were performed on left optic nerve cross-sections and averaged from 3-4 sections per animal. Scale bar represents 5 μm. Statistical analysis was performed using a two-way ANOVA with Šidák correction. Error bars represent the standard error of the mean (SEM). *$p<0.05$.

However, given the sustained IOP elevations throughout the 12-week period, it is surprising that reductions in axon counts were not detected at 12 weeks.

3.10 RGC somata are unaffected by IOP elevation

In glaucoma, optic nerve axon loss typically precedes RGC soma loss in the retina. In previous glaucoma studies conducted by the Tsilfidis lab that utilized the same magnetic microbead model of glaucoma, RGC soma loss was not observed in glaucomatous animals by 6 weeks post-bead injections, even though reductions in axon counts were noted. Hence, to determine if RGC soma loss occurred after the 6-week timepoint, this study sought to determine whether the IOP-induced damage would extend to the retina at 12 weeks post-glaucoma induction and if WN1316 treatment could protect against soma loss. Retinal cross-sections were stained with RNA-binding protein with multiple splicing (RBPMS), a marker of RGCs, and cell counts were performed manually in the central region of the sections. All of the glaucomatous retina sections that were harvested at 6 weeks were completely degraded and neuronal layers were entirely detached from the retinal pigment epithelium (RPE), hence these 6-week sections could not be used for cell counting. At 12 weeks post-surgery, WN1316-treated and saline-treated glaucomatous animals showed no significant losses ($p>0.05$) in RGC somata relative to sham controls (Figure 3.12 E). This was again highly unexpected given the consistent IOP elevations, but it was unlikely for RGC soma loss to occur as optic nerve axon loss was also not observed. DAPI counts were also performed in the GCL of central retina sections to confirm the RGC counts, and no significant differences were found between treatment groups ($p>0.05$) (Figure 3.12 F). Given that the trends in the ERG data indicated that the magnetic microbead model can cause RGC dysfunction, cleaved caspase-3 immunostaining was performed to determine if glaucomatous RGCs were in the process of undergoing apoptosis at week 12. Cleaved caspase-3 was not detected in WN1316-treated or saline-treated glaucomatous retinas (Figure 3.13 A,B). To evaluate the

functionality of the anti-caspase-3 primary antibody, positive control staining was done on postnatal day 5 (P5) Chd4 conditional knockout (cKO) mouse retinas; the Mattar lab found positive caspase-3 staining in these samples using the same primary antibody. Caspase-3 was indeed observed in P5 Chd4 cKO mouse retinas, confirming that the anti-caspase-3 primary antibody is functional (Figure 3.13 C). It therefore remains inconclusive as to whether WN1316 can protect against structural damage in glaucoma.

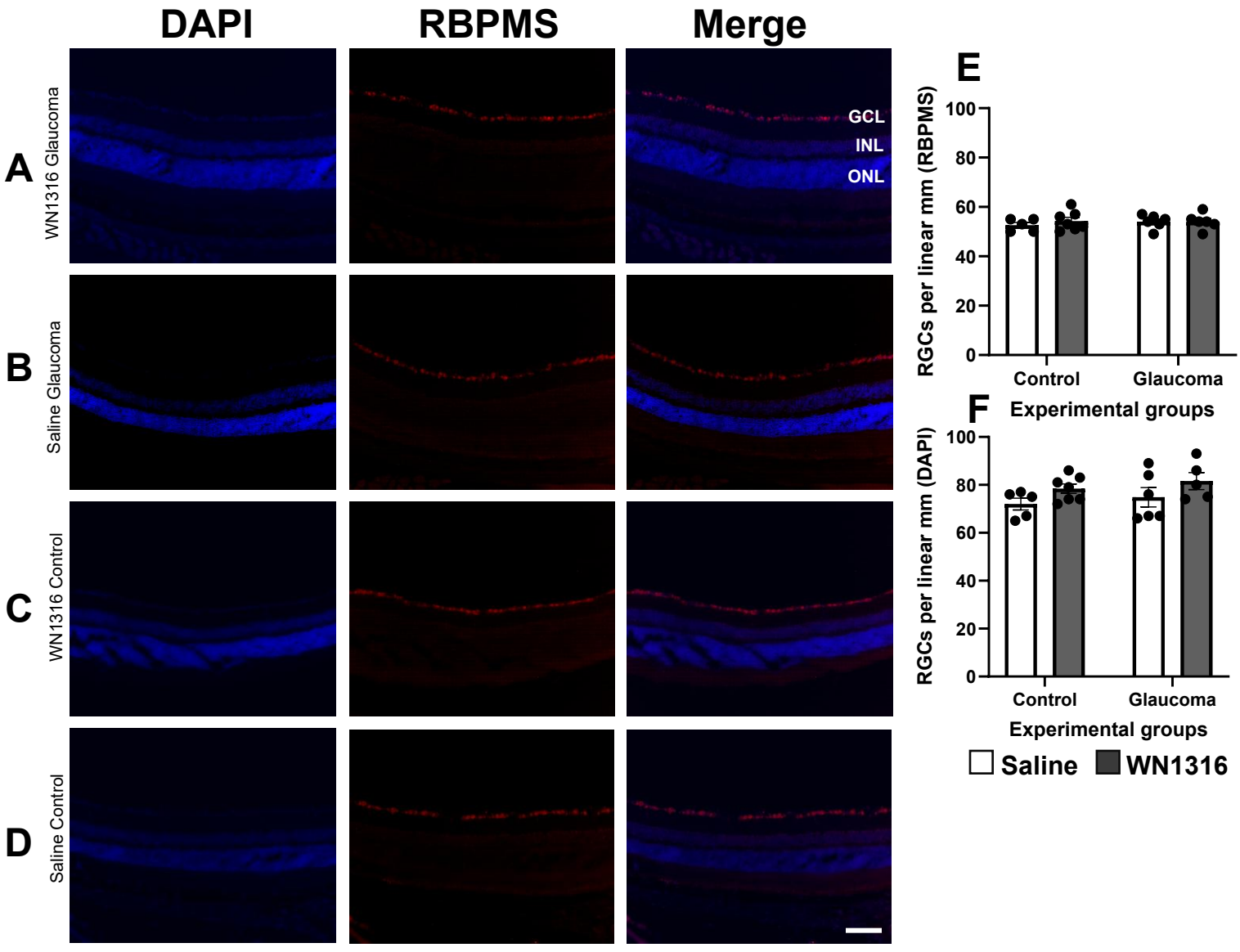

Figure 3.12. RGC somata are unaffected by IOP elevation at 12-weeks post-surgery. Representative RBPMS-immunolabelled central retina sections of (A) WN1316-treated glaucomatous animals, (B) saline-treated glaucomatous animals, (C) WN1316 control animals, and (D) saline-treated control animals at 12-weeks post-surgery. Sections were counterstained with DAPI. (E) Quantification of average RBPMS-labelled RGCs reveals no significant differences between control and glaucomatous animals ($p>0.05$). (F) No significant differences between average GCL DAPI-stained nuclei counts were observed between treatment groups ($p>0.05$). Each data point represents the mean RGC count averaged from 4-6 sections per animal. Scale bar represents 50 μm. Statistical analysis was performed using a two-way ANOVA with Šidák correction. Error bars represent the standard error of the mean (SEM).

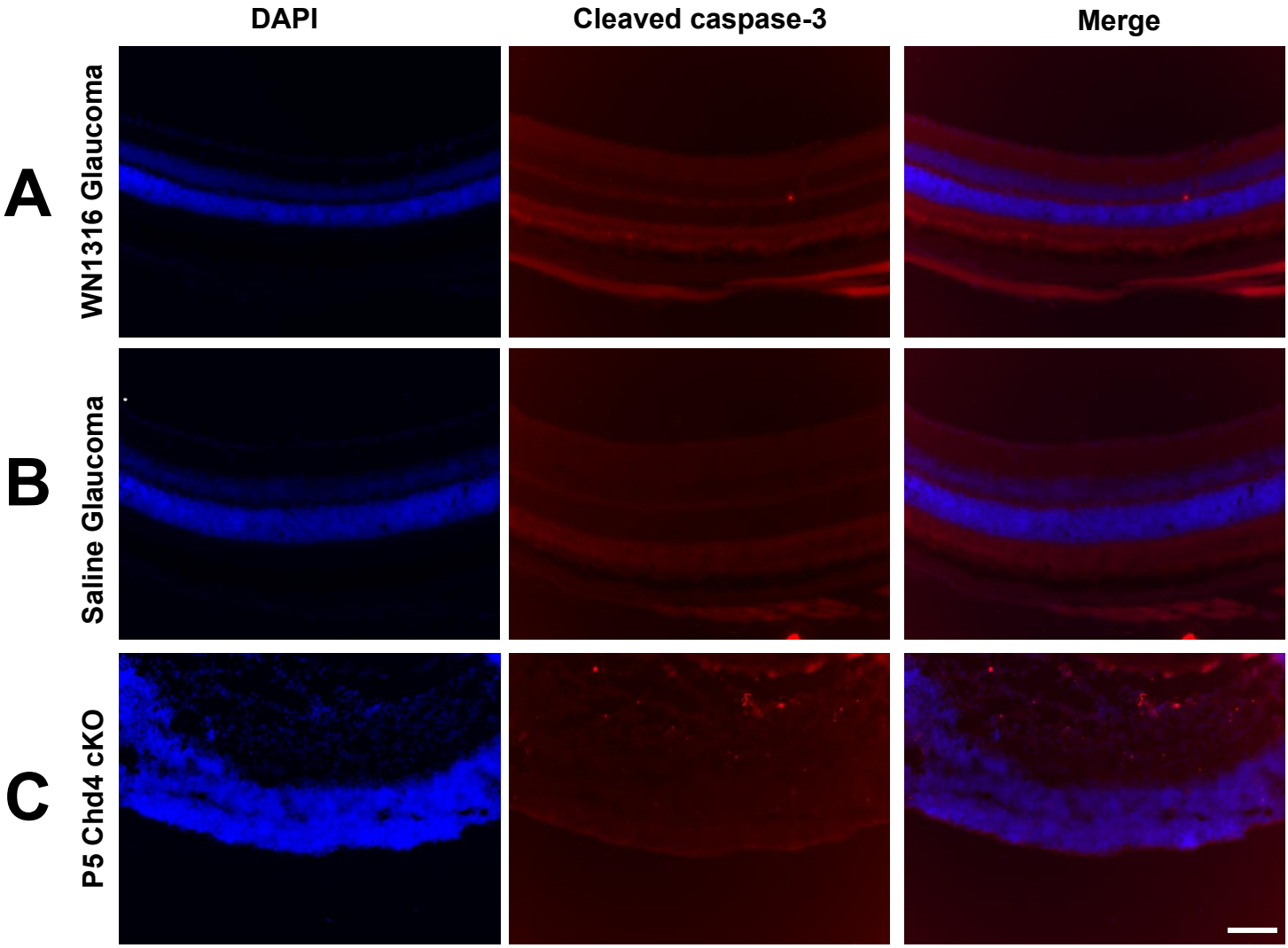

Figure 3.13. RGC somata in glaucomatous retinas do not show caspase-3 activation at week 12 post-surgery. Sections were counterstained with DAPI. Central retinal sections immunolabelled for cleaved caspase-3 in (A) WN1316 glaucoma, (B) saline glaucoma, and (C) P5 Chd4 cKO positive control animals. Only the P5 Chd4 cKO retinas stained positive for cleaved caspase-3. Scale bar represents 50 μm.

CHAPTER 4. DISCUSSION

WN1316 is a novel small molecule compound with antioxidant and anti-inflammatory properties, and this thesis aimed to evaluate WN1316's ability to provide protection against IOP elevation, RGC dysfunction, and RGC axon and soma degeneration in the magnetic microbead mouse model of glaucoma. While the magnetic microbead model was effective at inducing sustained elevations in IOP, microbead-injected eyes rapidly and unexpectedly developed secondary insults such as lens and corneal opacities and abrasions. Hence, it is not possible to discern whether the observed RGC dysfunction was caused by IOP elevations or by these secondary ocular damages. Moreover, despite the sustained IOP elevations and ocular damages, microbead-injected eyes showed no reductions in RGC axons and somata as well as no caspase-3 activation at 12-weeks post-injection. Therefore, due to the complications of the magnetic microbead model of glaucoma that rendered it an ineffective model of the disease, it currently remains inconclusive as to whether WN1316 can provide functional and structural protection in glaucoma.

WN1316 was selected as the therapeutic candidate of choice for this thesis for its potent ability to selectively protect against oxidative-stress induced neuronal cell death in other disease models as well as for its favourable therapeutic profile, comprising high-blood brain barrier permeability, low toxicity, and high solubility (Tanaka et al., 2014). Preliminary nanospectroscopy studies demonstrated that WN1316 effectively crosses the blood-retina barrier in rats (Figure 3.1), hence the compound showed promise that it may be able to exert its neuroprotective effects in the context of glaucoma. Further Western blot experiments showed that WN1316 enhances the expression of HO-1, an endogenous antioxidant regulated by transcription factor Nrf2, in 661W cells treated with increasing concentrations of the oxidative stressor menadione (Figure 3.2 C). WN1316 also appeared to enhance HO-1 expression in a time-dependent manner in intact mouse retinas, with expression peaking at 4

hours post-feeding (Figure 3.2 D). However, the HO-1 protein bands in the intact mouse retinas had migrated faster than the HO-1 control band in 661W cells, raising concerns as to whether the highlighted protein bands in Figure 3.2 B truly represent HO-1. The differences in HO-1 sizes *in vivo* versus *in vitro* may possibly be explained by systemic differences. It could be that protease activity is greater in tissues than in cultured cells, producing truncated HO-1 fragments that may still retain the epitope that is recognized by the primary antibody utilized during immunodetection, leading to lower molecular weight bands. This hypothesis would need to be evaluated in future studies as comparisons of protease activity *in vivo* and *in vitro* have not been well established in the literature. HO-1 has been shown, however, to undergo post-translational modifications in different cellular contexts such as Alzheimer's (AD) disease and cancer (Barone et al., 2012; Jagadeesh et al., 2022). In the context of AD, phosphorylated serine residues in the HO-1 protein were found to be significantly increased in the hippocampus and cerebellum of AD patients with respect to matched controls, and phosphorylation of serine appeared to be a key step in the activation of HO-1 during oxidative stress (Barone et al., 2012). With regards to cancer, HO-1 undergoes acetylation, ubiquitination, and phosphorylation, post-translational modifications that regulate the function, stability, and sub-cellular location of HO-1 (Jagadeesh et al., 2022). It is therefore clear that the size of HO-1 can vary due to post-translational modifications in different disease contexts. Furthermore, given that WN1316's ability to enhance the expression of HO-1 is amplified under conditions of oxidative stress as shown by the results of the 661W Western blot, it may be that WN1316's ability to induce HO-1 protein expression would have been enhanced in the glaucomatous retina where oxidative stress is ongoing. Thus, WN1316 may have been more effective at upregulating HO-1 had the Western blot been performed using retinas from animals that received the magnetic microbead injections.

The magnetic microbead mouse model was chosen for this study for its ability to induce acute elevations in IOP after a single injection, induce both RGC dysfunction and optic nerve axon loss,

and the relative simplicity of the injection procedure (Ito et al., 2016; Visuvanathan et al., 2022). The developers of the microbead model as well as previous glaucoma studies conducted in the Tsilfidis lab that used the same model did not observe the lens and corneal damages caused by the microbead injections that presented in this study. Prior to the main experiment detailed in this thesis, we conducted several preliminary experiments in an attempt to optimize the magnetic microbead model and mitigate these unexpected complications. Specifically, different methods of anesthesia were tested during the magnetic microbead injections (e.g., isoflurane versus injectable anesthetics). The developers of the model had used injectable anesthetics to ensure that the microbeads settle in the iridocorneal angle, so we aimed to determine whether the type of anesthesia influenced microbead distribution and subsequent outcomes for the integrity of the lens and cornea (Ito et al., 2016). We also tested different microbead solution volumes, ultimately reducing the injected volume from 1.5 μL to 0.6 μL after observing that a few animals receiving the lower volume did not develop the same ocular lesions. However, surprisingly, even after proceeding with 0.6 μL injections in the main study, almost all animals still developed lens and corneal damage, indicating that injection volumes were not the source of these ocular lesions.

Rather than modelling POAG, the most common form of glaucoma in which lens and corneal damages typically do not present, it appears that the magnetic microbead model in this study was more reminiscent of a rare and debilitating subtype of glaucoma known as phacomorphic glaucoma (PMG). PMG is a part of a subgroup of secondary glaucomas known as lens-induced glaucoma (LIG), characterized by hyper-mature senile cataracts (HMSCs) (Shah & Meyer, 2025). In PMG, IOP elevations occur due to pupillary block caused by the presence of an intumescent cataractous lens (Shah & Meyer, 2025). Corneal irregularities caused by raised IOP, such as stromal edema, sub-epithelial bullae, and Descemet membrane folds, are also common in LIG; many glaucomatous animals presenting with lens cataracts also exhibited folded or bulging corneas in this study (Shah &

Meyer, 2025). It is challenging to pinpoint exactly how the microbead injections caused the development of LIG in this study, though flaws in surgical technique may have been contributing factors. In the protocol provided by the developers of the magnetic microbead model, the authors state that the microneedle used for the injection of the microbead solution must be placed at a 45º angle in relation to the limbus during the puncture of the cornea, and that care should be taken to ensure that the needle does not enter the posterior chamber or come into contact with the lens or iris (Ito et al., 2016). Moreover, the developers injected the microbead solution over a period of 30-60 seconds, while in this study, the injections were quickly executed in 1-2 seconds (Ito et al., 2016). Hence, variations in the positioning of the microneedle during injections as well as the rapid injection times may have caused the microneedle and microbead solution to contact the lens, causing cataracts formed by penetrating and/or chemical trauma. Penetrating trauma can cause immediate cataract formation, and chemical trauma can induce cataract formation by altering the composition of the lens fibers (Okoye & Gurnani, 2025). These surgical traumas are plausible explanations for the lens damages observed in this study, as cataracts in microbead-injected eyes developed rapidly as they were clearly visible beginning the day after the surgeries while animals were restrained during oral gavage, and in some animals, microbeads were found in the posterior chamber during sampling. Another possible source of ocular trauma may have been the pressing of the handheld magnet against the cornea during the dispersion of the microbeads around the iridocorneal angle. Cataracts induced by blunt trauma display a characteristic rosette or flower-shaped appearance accompanied by degradation of the lens capsule (Okoye & Gurnani, 2025), both of which were observed in some microbead-injected eyes during the sampling procedure. While errors in surgical technique pose as possible explanations for the observed lens and corneal damages, they are not the sole explanation, as several glaucoma studies conducted in the Tsilfidis lab in the past that have utilized the magnetic microbead model of glaucoma did not observe these ocular injuries. Another possibility could be attributed to

flaws in the preparation of the magnetic microbead solution, as a new batch of microbeads were ordered for this project. The magnetic microbeads were coated with epoxy groups, and insufficient removal of epoxy groups during washing could result in clumping of the beads and inflammation (Ito et al., 2016). Overall, a high degree of optimization of the magnetic microbead model is necessary to prevent these ocular damages from confounding experimental findings.

A major goal of this study was to ensure that the magnetic microbead model was effective at promoting sustained elevations in IOP, as elevated IOP is a main risk factor for POAG. In the study conducted by the developers of the magnetic microbead model, IOP levels remained elevated at an average of 20 mmHg up to 6 weeks in microbead-injected eyes (Ito et al., 2016). In this study, the average IOP readings in glaucomatous eyes were higher that what the developers had observed; IOPs were elevated at an average of 25.3 ± 5.9 mmHg in WN1316-treated glaucomatous animals and 24.8 ± 6.2 mmHg (mean ± SEM) in saline-treated glaucomatous animals up to 12 weeks (Figure 3.4). In their protocol, the developers of the magnetic microbead model warn that caution should be taken when IOP measurements in awake mice are greater than 25 mmHg, as extreme IOP elevations can promote ischemic damage and may be painful for the animal (Ito et al., 2016). A glaucoma study that involved the intracameral injection of autologous ghost red blood cells into the anterior chamber to block the TM of Squirrel and Cynomolgus monkeys reported a mean IOP of 53.5 mmHg and a mean peak IOP of 69.8 mmHg, and at these extremely high IOP levels, corneal edema was a common side effect (Quigley & Addicks, 1980). Corneal edema can increase corneal thickness, and central corneal thickness has been shown to artificially increase IOP readings taken by a rebound tonometer (Kohlhaas et al., 2006; Morgan & Tribble, 2015). This may also offer a potential explanation as to why optic nerve axon counts and RGC soma counts were not reduced in microbead-injected eyes at 12-weeks post-surgery; the irregular corneal surface of the microbead-injected eyes may have led to an overestimation of IOP values, hence the true IOPs may not have been sufficient to cause optic nerve

axon loss and RGC soma loss in this study. As mentioned previously, corneal abrasions can also be caused by IOP-independent factors such as chemical, penetrative, or blunt trauma, so it is unclear whether the corneal insults observed in this study were a cause or consequence of high IOP readings. It is much likely the former, however, given that initial elevations in IOP would have likely caused optic nerve axon loss regardless of whether corneal stiffening overestimates subsequent IOP readings.

In addition to evaluating whether the magnetic microbead model accurately resembles clinical POAG in terms of physical presentation and elevation IOP, this thesis aimed to assess if glaucoma induction causes retinal cell dysfunction and if WN1316 treatment could offer functional protection. The pathological hallmark of glaucoma is the progressive dysfunction and loss of RGCs, hence it was not expected for the model to penetrate beyond the GCL, both in terms of functional and structural loss. However, the *in vivo* tests of visual electrophysiology demonstrated that the microbead injections appeared to reduce the functioning of photoreceptors, bipolar cells, and amacrine cells, particularly in WN1316-treated glaucomatous animals. Photoreceptor, bipolar cell, and amacrine cell function is necessary for the functionality of RGCs, as these outer retinal cells relay visual signals to RGCs through neurotransmitters (Addo, 2016). Reductions in the functioning of cells in the ONL and INL were only observed at 3- and 6-weeks post-surgery, as these timepoints included the glaucomatous animals with the greatest severity of ocular (i.e., lens and cornea) damage as observed by fundus imaging. Dysfunction in the outer retina was not reported by the developers of the magnetic microbead model, nor was it observed in a glaucoma study conducted by the Tsilfidis lab that used the same model (Ito et al., 2016; Visuvanathan et al., 2022). However, in these studies, the microbead injections did not cause the same lens and corneal damages as seen in this study, and it may be that these ocular opacities contributed to reductions in a-wave, b-wave, and OP amplitudes; the a- and b-wave mean peak amplitudes have been found to be significantly reduced in human eyes with mature cataracts compared to those of control eyes (Yamauchi et al., 2016). Interestingly, in the sham control

group, particularly at the 3-week timepoint, WN1316 appeared to significantly protect against outer retinal dysfunction. Although these animals did not undergo glaucoma induction, their fundus images still revealed signs of retinal damage, indicated by light-coloured patches. This suggests that even in the absence of elevated IOP, WN1316 may offer neuroprotection under conditions of mild retinal dysfunction, highlighting its potential in preserving retinal function at lesser degrees of damage. Nonetheless, the fact that there was outer retinal dysfunction further supports that optimization of the model is necessary for future studies, as it is possible that protection by WN1316 in glaucoma might have been seen without the added damage to the lens, cornea, and outer retinal cells.

As mentioned previously, determining whether WN1316 could protect against RGC dysfunction was a major goal of this study, as loss of RGC functionality is a primary characteristic of glaucoma. Analysis of the PERG data revealed that there were significant reductions in RGC soma and axon function throughout most experimental timepoints, though the reductions were usually only significant in WN1316-treated glaucomatous animals relative to WN1316-treated sham controls. It is possible that the significant impairments in RGC soma and axon function in WN1316-treated glaucomatous animals were caused by the complications of the microbead model as opposed to WN1316 treatment. According to surgical, sampling, and fundus observation notes, many of the WN1316-treated glaucomatous eyes had seemingly more severe complications than saline-treated glaucomatous eyes; cataracts were usually larger and denser in WN1316-treated glaucomatous eyes, and in some animals, the magnetic microbeads were physically in contact with the lens and scattered throughout the posterior chamber. It is unclear if WN1316 treatment somehow exacerbated the microbead-induced damage, as reports of antioxidant compounds causing harm to ocular structures have not been established in the literature. However, at the 3-week timepoint, WN1316-treated sham animals exhibited preserved RGC soma and axon function compared to saline-treated sham animals, reinforcing the idea of a potential protective effect of WN1316 even in the absence of elevated IOP.

This observation aligns with earlier findings of outer retinal protection in the sham group at the 3-week timepoint and further supports the idea that WN1316 may be capable of preserving retinal function under conditions of mild damage.

Moreover, given that glaucoma is characterized by optic nerve degeneration, it was expected that the model would produce reductions in the components of the VEP tests, as these represent signalling from the optic nerve to the visual cortex. Similar to previous trends in the ERG findings in this study, early arriving signals to the visual cortex, represented by the N1 VEP component, were impaired in WN1316-treated glaucomatous animals at 3- and 6-weeks post-surgery relative to WN1316-treated sham control animals. Again, it is important to note that at these timepoints, the lens and corneal opacities caused by the microbead injections were extremely severe, particularly in the WN1316-treated glaucoma group, hence it remains elusive regarding whether WN1316 treatment truly affected signalling to the visual cortex. Additionally, the VEP signal can be subject to variability due to slight differences in placement of the recording electrode over the visual cortex. Minor deviations in electrode positioning between animals, or even between timepoints in the same animal, can impact signal amplitude, potentially obscuring the effects of the treatment. Moreover, intracortical signalling between the visual cortex and other cortical regions, represented by the P2 VEP amplitude, was not reduced in glaucomatous animals, which suggests that the model was not severe enough to affect intracortical visual signalling. Overall, due to the confounding ocular damages induced by the microbead injections, it remains inconclusive as to whether WN1316 can provide functional protection in glaucoma.

Another major goal of this study was to evaluate if WN1316 treatment could provide structural protection for RGC axons and cell bodies in addition to functional preservation in glaucoma. Surprisingly, at 6-weeks post-surgery, axon counts were significantly reduced only in WN1316-treated

glaucomatous animals, while saline-treated glaucomatous mice showed no significant degeneration (Figure 3.11 I, J). This data corresponds to the ERG trends mentioned previously, in which retinal cell dysfunction was more commonly reduced in WN1316-treated glaucomatous eyes. Again, a possible explanation for the RGC dysfunction and axon loss in WN1316-treated glaucomatous animals could be due to the fact that the damages to the lens and cornea caused by the microbead injections appeared to be more severe in the WN1316-treated glaucomatous groups, as many animals in this group at this timepoint showed magnetic microbeads in the posterior chamber of the eye. However, given that the ERG trends and week 6 axon count data taken together demonstrate that RGCs appear functionally and structurally impaired in WN1316-treated glaucomatous animals, it cannot be ruled out that WN1316 may possibly exacerbate glaucomatous damage, particularly under severe conditions where the lens and cornea have extensive lesions. This is contrary to our initial hypothesis that WN1316 could confer neuroprotection in glaucoma in part due to its potent antioxidative and anti-inflammatory properties. A possibility for this paradox may be that WN1316's mechanism of action may not be compatible with the pathophysiology of advanced glaucoma. A caveat of the antioxidant Nrf2/ARE pathway, which has been previously shown to be upregulated by WN1316 *in vitro* (Tanaka et al., 2014), is that its excessive upregulation can induce reductive stress and promote metabolic vulnerability (Pérez-Torres et al., 2017; Weiss-Sadan et al., 2023). Reductive stress is the counterpart of oxidative stress and is defined as the excessive increase in reducing agents such as glutathione (GSH) and nicotinamide adenine dinucleotide + hydrogen ($NADH^+$), which significantly depletes ROS to sub-optimal levels (Weiss-Sadan et al., 2023). While ROS can be harmful at high levels, ROS serve as critical signalling molecules for processes that are vital to cell survival at basal levels. Hence, excess reducing agents can cause damage to cells by disrupting cell growth, promoting disulfide bonds in proteins, and reducing mitochondrial function and cellular metabolism (Weiss-Sadan et al., 2023). Furthermore, WN1316's ability to suppress gliosis may actually be harmful in the context of glaucoma;

reactive astrocytes may be initially protective as they can promote optic nerve survival and regeneration by mediating epidermal growth factor signalling (Calkins et al., 2017; García-Bermúdez et al., 2021; Harder et al., 2017; Shinozaki et al., 2023, 2024). Future studies should therefore thoroughly investigate how WN1316 alters the retina and optic nerve, at both the cellular and morphological level. Such studies might want to evaluate the expression or protein levels of reducing agents in WN1316-treated animals and compare the findings between glaucomatous animals that display lens and corneal lesions and glaucomatous animals that do not exhibit these ocular abnormalities, and also assess the activation of astrocytes and microglia in WN1316-treated animals through GFAP or Iba-1 staining.

Despite the sustained IOP elevations until 12-weeks post-surgery, RGC axon and soma counts were oddly not reduced in WN1316-treated or saline-treated in glaucomatous animals at the 12-week timepoint. This was highly surprising because sustained IOP elevations have been shown to disrupt the axonal transport of neurotrophic factors and induce axonal ischemia by placing mechanical stress on the optic nerve head, driving RGCs towards apoptosis (Bou Ghanem et al., 2024; Claes et al., 2019; Hurley et al., 2022). The developers of the magnetic microbead mouse model observed a significant 25% reduction in RGC axons as well as a 22% reduction in RGC cell bodies in hypertensive microbead-injected eyes as early as 3-weeks post-surgery, hence it was expected that RGC cell bodies and axons would have been substantially reduced at 12 weeks in microbead-injected eyes (Ito et al., 2016). One possible explanation for the lack of observed RGC soma loss is that cell counts in this study were performed in central retina sections. Evidence suggests that RGC degeneration in glaucoma begins in the peripheral retina and progresses centrally (Liu & Margeta, 2019). If degeneration was localized to the periphery at the time of tissue collection, central sectioning may have missed these RGC losses. However, this explanation alone may be insufficient, as RGC axon counts also did not show reductions at this timepoint, and axon loss is generally thought to precede

RGC soma loss in glaucoma. It therefore would have still been unlikely to observe reductions in RGC soma counts in peripheral retina sections given that RGC axon counts were not reduced in glaucomatous eyes. Nevertheless, including peripheral retina sections or performing soma counts using whole retina flat mounts may therefore provide a more comprehensive measure of RGC loss in future studies using the magnetic microbead model of glaucoma. Another possible explanation for the lack of RGC axon and soma loss in glaucomatous animals at the 12-week time point that was alluded to previously is that the corneal abrasions observed in microbead-injected eyes may have led to an overestimation of IOP values as changes in corneal thickness and an uneven corneal surface can reduce the accuracy of the rebound tonometer, hence the true IOP values may not have been sufficiently elevated to cause substantial RGC axon and soma loss (Ito et al., 2016; Kohlhaas et al., 2006). A study by Cone et al. (2010) that tested the efficacy of polystyrene microbead injections in 2-month-old C57BL6/J mice reported that ocular damages such as enlargement of the cornea, corneal neovascularization, and limbal staphyloma were common and observable as early as 3 days post-bead injection in hypertensive microbead-injected eyes, and reductions in RGC axon and soma counts at 12-weeks post-injection were relatively mild, at 5.2 ± 12.1% and 6.5 ± 8.9% (mean ± SD) respectively. It may therefore be possible that ocular lesions to structures such as the cornea may impede RGC axon and soma loss in inducible models of glaucoma.

Furthermore, it was also surprising to see that glaucomatous RGC somas were not positive for the pro-apoptotic enzyme caspase-3 at 12-weeks post-surgery, suggesting that these RGCs were not undergoing apoptosis at this timepoint. Visuvanathan et al. (2022) observed caspase-3 staining in the GCL of GFP-treated glaucomatous eyes at 6-weeks post-microbead injections, hence it may be that caspase-3 staining was not observed in the 12-week glaucomatous retinas because the initial wave of caspase-3 activity occurred prior to 12 weeks. Alternatively, it could be that the 12-week glaucomatous RGCs were undergoing caspase-independent cell death; a study showed that the

generation of ROS during retinal cell death results in the oxidative inhibition of caspases *in vitro* (Carmody & Cotter, 2000). In addition to apoptosis, RGCs can indeed die through caspase-independent mechanisms such as necroptosis, a regulated cell death pathway that involves a different set of proteins including receptor-interacting protein kinase 1 and 3 (RIPK1, RIPK3), tumor necrosis factor (TNF), and other protein complexes that orchestrate cell leakage, organelle swelling, and inflammation (Thomas et al., 2019). In a rat model of blunt ocular trauma, it was found that the necroptotic proteins RIPK1 and RIPK3 were upregulated specifically in RGCs and treatment with a RIPK1 inhibitor significantly protected against RGC cell death in culture (Thomas et al., 2019). As previously mentioned, many microbead-injected eyes in this study showed signs of blunt ocular trauma that may have been caused during the microbead injection process, which further supports the plausibility that RGCs may have been in the process of undergoing necroptosis rather than apoptosis in this model.

Overall, the overarching takeaway from this study is that going forward, extensive optimization of experimental paradigms will be necessary in order to effectively evaluate WN1316's therapeutic potential in glaucoma. A core confounding variable in this work was the ocular lesions produced by the magnetic microbead injections, namely lens and corneal abrasions, which generated a model that was less reminiscent of clinical POAG and more akin to a rare and elusive subtype of glaucoma known as lens-induced glaucoma (LIG). Thus, modifications to the experimental glaucoma model will be essential for future experiments. With regards to the magnetic microbead model, care should be taken to prevent trauma to the eye that can occur during the injection procedure. During the Association for Research in Vision and Ophthalmology (ARVO) conference that I recently attended, researchers who have also faced challenges with the magnetic microbead model recommended surgical optimization strategies such as performing the injections through the limbus rather than the cornea to prevent the needle and microbeads from contacting the lens, as well as

ensuring that the handheld magnet does not contact the corneal surface to prevent blunt trauma. Other strategies may involve sterilization of the microbeads by gamma irradiation and applying antibiotic ointments to the surgical eye to prevent endophthalmitis (Ito et al., 2016; Morgan & Tribble, 2015). Should these optimization techniques fail to eliminate the confounding ocular damages, future glaucoma studies may want to test potential therapies in alternative models. Though genetic models of glaucoma require long experimental timelines, are typically costly, and can involve significant variation in the glaucoma phenotype, an advantage that they have over inducible models is that they can be more representative of clinical glaucoma given that glaucoma symptoms such as IOP elevations and RGC loss develop slowly over time rather than acutely as in inducible models of glaucoma. An ideal glaucoma model should factor in the synergistic mechanisms involved in glaucomatous pathology, such as IOP elevation and oxidative stress. In one such double transgenic mouse model, with a point mutation in *MYOC* and heterozygous deletion of the superoxide dismutase 2 (SOD2) gene, animals developed outflow pathway impedance, high IOP, optic nerve degeneration, and 37% RGC loss at 10-12 months of age (Joe et al., 2015). Thus, future experimental glaucoma studies may benefit from the use of chronic glaucoma models in the event that inducible models cannot be optimized to prevent confounding ocular lesions.

In summary, this thesis evaluated the neuroprotective potential of a novel antioxidant and anti-inflammatory compound, WN1316, in the mouse magnetic microbead model of glaucoma. While sustained IOP elevations were achieved, unexpected complications such as the observed lens and corneal damage complicated both the progression of glaucomatous pathology and the interpretation of WN1316's ability to protect against functional and structural loss of RGCs. The confounding influence of ocular lesions therefore highlights the need for further optimization of the magnetic microbead model to minimize anterior segment damage and better isolate glaucomatous effects. Although WN1316-treated glaucomatous animals did not exhibit protection at the level of RGC axon

and soma counts, functional data from visual electrophysiology suggested a trend toward preserved outer retinal and RGC function in WN1316-treated sham animals pointing to possible protective effects under milder or non-glaucomatous conditions. Future studies may benefit from incorporating more thorough experiments such as performing Western blots using glaucomatous retinas, evaluating other mechanisms of RGC death such as necroptosis, performing retinal flat-mount analyses, and measuring regional RGC loss. Overall, while this study was not able to definitively establish WN1316's therapeutic potential in glaucoma, it provides a foundation for continued investigation into its role in retinal protection and reinforces the importance of model optimization in preclinical glaucoma research.

REFERENCES

Abu-Amero, K. K., Morales, J., & Bosley, T. M. (2006). Mitochondrial abnormalities in patients with primary open-angle glaucoma. *Investigative Ophthalmology & Visual Science*, *47*(6), 2533–2541. https://doi.org/10.1167/iovs.05-1639

Addo, R. T. (Ed.). (2016). *Ocular Drug Delivery: Advances, Challenges and Applications*. Springer International Publishing. https://doi.org/10.1007/978-3-319-47691-9

Almasieh, M., & Levin, L. A. (2017). Neuroprotection in Glaucoma: Animal Models and Clinical Trials. *Annual Review of Vision Science*, *3*(Volume 3, 2017), 91–120. https://doi.org/10.1146/annurev-vision-102016-061422

Babizhayev, M. A. (1989). Lipid fluorophores of the human crystalline lens with cataract. *Graefe's Archive for Clinical and Experimental Ophthalmology = Albrecht Von Graefes Archiv Fur Klinische Und Experimentelle Ophthalmologie*, *227*(4), 384–391. https://doi.org/10.1007/BF02169418

Barone, E., Di Domenico, F., Sultana, R., Coccia, R., Mancuso, C., Perluigi, M., & Butterfield, D. A. (2012). Heme Oxygenase-1 Post-translational Modifications in the Brain of Subjects with Alzheimer Disease and Mild Cognitive Impairment. *Free Radical Biology & Medicine*, *52*(0), 2292–2301. https://doi.org/10.1016/j.freeradbiomed.2012.03.020

Benitez-Del-Castillo, J., Cantu-Dibildox, J., Sanz-González, S. M., Zanón-Moreno, V., & Pinazo-Duran, M. D. (2019). Cytokine expression in tears of patients with glaucoma or dry eye disease: A prospective, observational cohort study. *European Journal of Ophthalmology*, *29*(4), 437–443. https://doi.org/10.1177/1120672118795399

Berdahl, J. P., Fautsch, M. P., Stinnett, S. S., & Allingham, R. R. (2008). Intracranial pressure in primary open angle glaucoma, normal tension glaucoma, and ocular hypertension: A case-control study. *Investigative Ophthalmology & Visual Science*, *49*(12), 5412–5418. https://doi.org/10.1167/iovs.08-2228

Binibrahim, I. H., & Bergström, A. K. (2017). The role of trabeculectomy in enhancing glaucoma patient's quality of life. *Oman Journal of Ophthalmology*, *10*(3), 150–154. https://doi.org/10.4103/ojo.OJO_61_2016

Boccaccini, A., Cavaterra, D., Carnevale, C., Tanga, L., Marini, S., Bocedi, A., Lacal, P. M., Manni, G., Graziani, G., Sbardella, D., & Tundo, G. R. (2023). Novel frontiers in neuroprotective therapies in glaucoma: Molecular and clinical aspects. *Molecular Aspects of Medicine*, *94*, 101225. https://doi.org/10.1016/j.mam.2023.101225

Bonomi, L., Marchini, G., Marraffa, M., Bernardi, P., De Franco, I., Perfetti, S., Varotto, A., & Tenna, V. (1998). Prevalence of glaucoma and intraocular pressure distribution in a defined population. The Egna-Neumarkt Study. *Ophthalmology*, *105*(2), 209–215. https://doi.org/10.1016/s0161-6420(98)92665-3

Bou Ghanem, G. O., Wareham, L. K., & Calkins, D. J. (2024). Addressing neurodegeneration in glaucoma: Mechanisms, challenges, and treatments. *Progress in Retinal and Eye Research*, *100*, 101261. https://doi.org/10.1016/j.preteyeres.2024.101261

Bridi, R., Crossetti, F. P., Steffen, V. M., & Henriques, A. T. (2001). The antioxidant activity of standardized extract of Ginkgo biloba (EGb 761) in rats. *Phytotherapy Research: PTR*, *15*(5), 449–451. https://doi.org/10.1002/ptr.814

Buffault, J., Labbé, A., Hamard, P., Brignole-Baudouin, F., & Baudouin, C. (2020). The trabecular meshwork: Structure, function and clinical implications. A review of the literature. *Journal Francais D'ophtalmologie*, *43*(7), e217–e230. https://doi.org/10.1016/j.jfo.2020.05.002

Burgoyne, C. F. (2011). A biomechanical paradigm for axonal insult within the optic nerve head in aging and glaucoma. *Experimental Eye Research*, *93*(2), 120–132. https://doi.org/10.1016/j.exer.2010.09.005

Calkins, D. J., Pekny, M., Cooper, M. L., & Benowitz, L. (2017). The challenge of regenerative therapies for the optic nerve in glaucoma. *Experimental Eye Research*, *157*, 28–33. https://doi.org/10.1016/j.exer.2017.01.007

Carmody, R. J., & Cotter, T. G. (2000). Oxidative stress induces caspase-independent retinal apoptosis in vitro. *Cell Death & Differentiation*, *7*(3), 282–291. https://doi.org/10.1038/sj.cdd.4400646

Chen, C., Wei, T., Gao, Z., Zhao, B., Hou, J., Xu, H., Xin, W., & Packer, L. (1999). Different effects of the constituents of EGb761 on apoptosis in rat cerebellar granule cells induced by hydroxyl radicals. *Biochemistry and Molecular Biology International*, *47*(3), 397–405. https://doi.org/10.1080/15216549900201423

Cheng, J., Liang, J., & Qi, J. (2017). Role of nuclear factor (erythroid-derived 2)-like 2 in the age-resistant properties of the glaucoma trabecular meshwork. *Experimental and Therapeutic Medicine*, *14*(1), 791–796. https://doi.org/10.3892/etm.2017.4543

Chi, W., Li, F., Chen, H., Wang, Y., Zhu, Y., Yang, X., Zhu, J., Wu, F., Ouyang, H., Ge, J., Weinreb, R. N., Zhang, K., & Zhuo, Y. (2014). Caspase-8 promotes NLRP1/NLRP3 inflammasome activation and IL-1β production in acute glaucoma. *Proceedings of the National Academy of Sciences of the United States of America*, *111*(30), 11181–11186. https://doi.org/10.1073/pnas.1402819111

Chidlow, G., Ebneter, A., Wood, J. P. M., & Casson, R. J. (2016). Evidence Supporting an Association Between Expression of Major Histocompatibility Complex II by Microglia and Optic Nerve Degeneration During Experimental Glaucoma. *Journal of Glaucoma*, *25*(8), 681–691. https://doi.org/10.1097/IJG.0000000000000447

Cho, H.-K., Kim, S., Lee, E. J., & Kee, C. (2019). Neuroprotective Effect of Ginkgo Biloba Extract Against Hypoxic Retinal Ganglion Cell Degeneration In Vitro and In Vivo. *Journal of Medicinal Food*, *22*(8), 771–778. https://doi.org/10.1089/jmf.2018.4350

Chrysostomou, V., Rezania, F., Trounce, I. A., & Crowston, J. G. (2013). Oxidative stress and mitochondrial dysfunction in glaucoma. *Current Opinion in Pharmacology*, *13*(1), 12–15. https://doi.org/10.1016/j.coph.2012.09.008

Claes, M., De Groef, L., & Moons, L. (2019). Target-Derived Neurotrophic Factor Deprivation Puts Retinal Ganglion Cells on Death Row: Cold Hard Evidence and Caveats. *International Journal of Molecular Sciences*, *20*(17), 4314. https://doi.org/10.3390/ijms20174314

Clemmesen, V., & Alsbirk, P. H. (1971). Primary angle-closure glaucoma (a.c.g.) in Greenland. *Acta Ophthalmologica*, *49*(1), 47–58. https://doi.org/10.1111/j.1755-3768.1971.tb08231.x

Cone, F. E., Gelman, S. E., Son, J. L., Pease, M. E., & Quigley, H. A. (2010). Differential susceptibility to experimental glaucoma among 3 mouse strains using bead and viscoelastic injection. *Experimental Eye Research*, *91*(3), 415–424. https://doi.org/10.1016/j.exer.2010.06.018

Cruess, A. F., Gordon, K. D., Bellan, L., Mitchell, S., & Pezzullo, M. L. (2011). The cost of vision loss in Canada. 2. Results. *Canadian Journal of Ophthalmology. Journal Canadien D'ophtalmologie*, *46*(4), 315–318. https://doi.org/10.1016/j.jcjo.2011.06.006

De Moraes, C. G. V., Juthani, V. J., Liebmann, J. M., Teng, C. C., Tello, C., Susanna, R., & Ritch, R. (2011). Risk factors for visual field progression in treated glaucoma. *Archives of Ophthalmology (Chicago, Ill.: 1960)*, *129*(5), 562–568. https://doi.org/10.1001/archophthalmol.2011.72

Di Meo, F., Cuciniello, R., Margarucci, S., Bergamo, P., Petillo, O., Peluso, G., Filosa, S., & Crispi, S. (2020). Ginkgo biloba Prevents Oxidative Stress-Induced Apoptosis Blocking p53

Activation in Neuroblastoma Cells. *Antioxidants (Basel, Switzerland)*, *9*(4), 279. https://doi.org/10.3390/antiox9040279

Dias, M. S., Luo, X., Ribas, V. T., Petrs-Silva, H., & Koch, J. C. (2022). The Role of Axonal Transport in Glaucoma. *International Journal of Molecular Sciences*, *23*(7), 3935. https://doi.org/10.3390/ijms23073935

Dielemans, I., Vingerling, J. R., Wolfs, R. C., Hofman, A., Grobbee, D. E., & de Jong, P. T. (1994). The prevalence of primary open-angle glaucoma in a population-based study in The Netherlands. The Rotterdam Study. *Ophthalmology*, *101*(11), 1851–1855. https://doi.org/10.1016/s0161-6420(94)31090-6

Do Rhee, K., Wang, Y., Ten Hoeve, J., Stiles, L., Nguyen, T. T. T., Zhang, X., Vergnes, L., Reue, K., Shirihai, O., Bok, D., & Yang, X.-J. (2022). Ciliary neurotrophic factor-mediated neuroprotection involves enhanced glycolysis and anabolism in degenerating mouse retinas. *Nature Communications*, *13*(1), 7037. https://doi.org/10.1038/s41467-022-34443-x

Drance, S., Anderson, D. R., Schulzer, M., & Collaborative Normal-Tension Glaucoma Study Group. (2001). Risk factors for progression of visual field abnormalities in normal-tension glaucoma. *American Journal of Ophthalmology*, *131*(6), 699–708. https://doi.org/10.1016/s0002-9394(01)00964-3

Freitas, A. L., Ushida, M., Almeida, I., Dias, D. T., Dorairaj, S., Kanadani, F. N., & Prata, T. S. (2016). Selective laser trabeculoplasty as an initial treatment option for open-angle glaucoma. *Arquivos Brasileiros De Oftalmologia*, *79*(6), 417–421. https://doi.org/10.5935/0004-2749.20160118

García-Bermúdez, M. Y., Freude, K. K., Mouhammad, Z. A., van Wijngaarden, P., Martin, K. K., & Kolko, M. (2021). Glial Cells in Glaucoma: Friends, Foes, and Potential Therapeutic Targets. *Frontiers in Neurology*, *12*, 624983. https://doi.org/10.3389/fneur.2021.624983

Goldberg, J. L., Beykin, G., Satterfield, K. R., Nuñez, M., Lam, B. L., & Albini, T. A. (2023). Phase I NT-501 Ciliary Neurotrophic Factor Implant Trial for Primary Open-Angle Glaucoma: Safety, Neuroprotection, and Neuroenhancement. *Ophthalmology Science*, *3*(3), 100298. https://doi.org/10.1016/j.xops.2023.100298

Gosling, D., & Meyer, J. J. (2025). Normal Tension Glaucoma. In *StatPearls*. StatPearls Publishing. http://www.ncbi.nlm.nih.gov/books/NBK576377/

Hakim, A., Guido, B., Narsineni, L., Chen, D.-W., & Foldvari, M. (2023). Gene therapy strategies for glaucoma from IOP reduction to retinal neuroprotection: Progress towards non-viral systems. *Advanced Drug Delivery Reviews*, *196*, 114781. https://doi.org/10.1016/j.addr.2023.114781

Hänninen, V. A., Pantcheva, M. B., Freeman, E. E., Poulin, N. R., & Grosskreutz, C. L. (2002). Activation of caspase 9 in a rat model of experimental glaucoma. *Current Eye Research*, *25*(6), 389–395. https://doi.org/10.1076/ceyr.25.6.389.14233

Harder, J. M., Braine, C. E., Williams, P. A., Zhu, X., MacNicoll, K. H., Sousa, G. L., Buchanan, R. A., Smith, R. S., Libby, R. T., Howell, G. R., & John, S. W. M. (2017). Early immune responses are independent of RGC dysfunction in glaucoma with complement component C3 being protective. *Proceedings of the National Academy of Sciences of the United States of America*, *114*(19), E3839–E3848. https://doi.org/10.1073/pnas.1608769114

Henderson, J., O'Callaghan, J., & Campbell, M. (2024). Gene therapy for glaucoma: Targeting key mechanisms. *Vision Research*, *225*, 108502. https://doi.org/10.1016/j.visres.2024.108502

Hirooka, K., Tokuda, M., Miyamoto, O., Itano, T., Baba, T., & Shiraga, F. (2004). The Ginkgo biloba extract (EGb 761) provides a neuroprotective effect on retinal ganglion cells in a rat model of chronic glaucoma. *Current Eye Research*, *28*(3), 153–157. https://doi.org/10.1076/ceyr.28.3.153.26246

Ho, K., Bodi, N. E., & Sharma, T. P. (2024). Normal-Tension Glaucoma and Potential Clinical Links to Alzheimer's Disease. *Journal of Clinical Medicine*, *13*(7), Article 7. https://doi.org/10.3390/jcm13071948

Hurley, D. J., Normile, C., Irnaten, M., & O'Brien, C. (2022). The Intertwined Roles of Oxidative Stress and Endoplasmic Reticulum Stress in Glaucoma. *Antioxidants*, *11*(5), Article 5. https://doi.org/10.3390/antiox11050886

Ito, Y. A., Belforte, N., Cueva Vargas, J. L., & Di Polo, A. (2016). A Magnetic Microbead Occlusion Model to Induce Ocular Hypertension-Dependent Glaucoma in Mice. *Journal of Visualized Experiments: JoVE*, *109*, e53731. https://doi.org/10.3791/53731

Izzotti, A., Bagnis, A., & Sacca, S. (2006). The role of oxidative stress in glaucoma. *Mutation Research/Reviews in Mutation Research*, *612*(2), 105–114. https://doi.org/10.1016/j.mrrev.2005.11.001

Izzotti, A., Saccà, S. C., Cartiglia, C., & De Flora, S. (2003). Oxidative deoxyribonucleic acid damage in the eyes of glaucoma patients. *The American Journal of Medicine*, *114*(8), 638–646. https://doi.org/10.1016/S0002-9343(03)00114-1

Jagadeesh, A. S. V., Fang, X., Kim, S. H., Guillen-Quispe, Y. N., Zheng, J., Surh, Y.-J., & Kim, S.-J. (2022). Non-canonical vs. Canonical Functions of Heme Oxygenase-1 in Cancer. *Journal of Cancer Prevention*, *27*(1), 7–15. https://doi.org/10.15430/JCP.2022.27.1.7

Jain, A., Zode, G., Kasetti, R. B., Ran, F. A., Yan, W., Sharma, T. P., Bugge, K., Searby, C. C., Fingert, J. H., Zhang, F., Clark, A. F., & Sheffield, V. C. (2017). CRISPR-Cas9-based treatment of myocilin-associated glaucoma. *Proceedings of the National Academy of Sciences of the United States of America*, *114*(42), 11199–11204. https://doi.org/10.1073/pnas.1706193114

Jin, Y.-P., Huang, K. Z. Y., Zhao, Q. K., Trope, G. E., Buys, Y. M., El-Defrawy, S., Yan, P., Brent, M. H., & Butty, Z. (2024). Prevalence of glaucoma in Canada: Results from the 2016–2019

Canadian Health Measures Survey. *Canadian Journal of Ophthalmology*, *0*(0). https://doi.org/10.1016/j.jcjo.2024.08.016

Joe, M. K., Nakaya, N., Abu-Asab, M., & Tomarev, S. I. (2015). Mutated myocilin and heterozygous Sod2 deficiency act synergistically in a mouse model of open-angle glaucoma. *Human Molecular Genetics*, *24*(12), 3322–3334. https://doi.org/10.1093/hmg/ddv082

Kaushik, M., Tiwari, P., Dada, T., & Dada, R. (2024). Beyond the optic nerve: Genetics, diagnosis, and promising therapies for glaucoma. *Gene*, *894*, 147983. https://doi.org/10.1016/j.gene.2023.147983

Killer, H. E., Miller, N. R., Flammer, J., Meyer, P., Weinreb, R. N., Remonda, L., & Jaggi, G. P. (2012). Cerebrospinal fluid exchange in the optic nerve in normal-tension glaucoma. *The British Journal of Ophthalmology*, *96*(4), 544–548. https://doi.org/10.1136/bjophthalmol-2011-300663

Killer, H., & Pircher, A. (2018). Normal tension glaucoma: Review of current understanding and mechanisms of the pathogenesis. *Eye*, *32*(5), 924–930. https://doi.org/10.1038/s41433-018-0042-2

Kim, H. S., & Park, C. K. (2005). Retinal ganglion cell death is delayed by activation of retinal intrinsic cell survival program. *Brain Research*, *1057*(1), 17–28. https://doi.org/10.1016/j.brainres.2005.07.005

Klein, B. E., Klein, R., Sponsel, W. E., Franke, T., Cantor, L. B., Martone, J., & Menage, M. J. (1992). Prevalence of glaucoma. The Beaver Dam Eye Study. *Ophthalmology*, *99*(10), 1499–1504. https://doi.org/10.1016/s0161-6420(92)31774-9

Knox, D. L., Eagle, R. C., & Green, W. R. (2007). Optic nerve hydropic axonal degeneration and blocked retrograde axoplasmic transport: Histopathologic features in human high-pressure

secondary glaucoma. *Archives of Ophthalmology (Chicago, Ill.: 1960)*, *125*(3), 347–353. https://doi.org/10.1001/archopht.125.3.347

Kohlhaas, M., Boehm, A. G., Spoerl, E., Pürsten, A., Grein, H. J., & Pillunat, L. E. (2006). Effect of Central Corneal Thickness, Corneal Curvature, and Axial Length on Applanation Tonometry. *Archives of Ophthalmology*, *124*(4), 471–476. https://doi.org/10.1001/archopht.124.4.471

Lambuk, L., Lazaldin, M. A. M., Ahmad, S., Iezhitsa, I., Agarwal, R., Uskoković, V., & Mohamud, R. (2022). Brain-Derived Neurotrophic Factor-Mediated Neuroprotection in Glaucoma: A Review of Current State of the Art. *Frontiers in Pharmacology*, *13*. https://doi.org/10.3389/fphar.2022.875662

Levkovitch-Verbin, H. (2015). Retinal ganglion cell apoptotic pathway in glaucoma. In *Progress in Brain Research* (Vol. 220, pp. 37–57). Elsevier. https://doi.org/10.1016/bs.pbr.2015.05.005

Li, G. Y., & Osborne, N. N. (2008). Oxidative-induced apoptosis to an immortalized ganglion cell line is caspase independent but involves the activation of poly(ADP-ribose)polymerase and apoptosis-inducing factor. *Brain Research*, *1188*, 35–43. https://doi.org/10.1016/j.brainres.2007.10.073

Liu, W. W., & Margeta, M. A. (2019). Imaging Retinal Ganglion Cell Death and Dysfunction in Glaucoma. *International Ophthalmology Clinics*, *59*(4), 41–54. https://doi.org/10.1097/IIO.0000000000000285

Lusthaus, J., & Goldberg, I. (2019). Current management of glaucoma. *The Medical Journal of Australia*, *210*(4), 180–187. https://doi.org/10.5694/mja2.50020

Ma, K., Xu, L., Zhang, H., Zhang, S., Pu, M., & Jonas, J. B. (2010). The effect of ginkgo biloba on the rat retinal ganglion cell survival in the optic nerve crush model. *Acta Ophthalmologica*, *88*(5), 553–557. https://doi.org/10.1111/j.1755-3768.2008.01486.x

Marenna, S., Rossi, E., Huang, S.-C., Castoldi, V., Comi, G., & Leocani, L. (2023). Visual evoked potentials waveform analysis to measure intracortical damage in a preclinical model of multiple sclerosis. *Frontiers in Cellular Neuroscience*, *17*, 1186110. https://doi.org/10.3389/fncel.2023.1186110

Masland, R. H. (2012). The Neuronal Organization of the Retina. *Neuron*, *76*(2), 266–280. https://doi.org/10.1016/j.neuron.2012.10.002

McMonnies, C. (2018). Reactive oxygen species, oxidative stress, glaucoma and hyperbaric oxygen therapy. *Journal of Optometry*, *11*(1), 3–9. https://doi.org/10.1016/j.optom.2017.06.002

Miao, Y., Zhao, G.-L., Cheng, S., Wang, Z., & Yang, X.-L. (2023). Activation of retinal glial cells contributes to the degeneration of ganglion cells in experimental glaucoma. *Progress in Retinal and Eye Research*, *93*, 101169. https://doi.org/10.1016/j.preteyeres.2023.101169

Michels, T. C., & Ivan, O. (2023). Glaucoma: Diagnosis and Management. *American Family Physician*, *107*(3), 253–262.

Miura, G., Wang, M. H., Ivers, K. M., & Frishman, L. J. (2009). Retinal pathway origins of the pattern ERG of the mouse. *Experimental Eye Research*, *89*(1), 49–62. https://doi.org/10.1016/j.exer.2009.02.009

Morgan, J. E., & Tribble, J. R. (2015). Microbead models in glaucoma. *Experimental Eye Research*, *141*, 9–14. https://doi.org/10.1016/j.exer.2015.06.020

Mosinger Ogilvie, J., Deckwerth, T. L., Knudson, C. M., & Korsmeyer, S. J. (1998). Suppression of developmental retinal cell death but not of photoreceptor degeneration in Bax-deficient mice. *Investigative Ophthalmology & Visual Science*, *39*(9), 1713–1720.

Neufeld, A. H., Hernandez, M. R., & Gonzalez, M. (1997). Nitric oxide synthase in the human glaucomatous optic nerve head. *Archives of Ophthalmology (Chicago, Ill.: 1960)*, *115*(4), 497–503. https://doi.org/10.1001/archopht.1997.01100150499009

Neufeld, A. H., Sawada, A., & Becker, B. (1999). Inhibition of nitric-oxide synthase 2 by aminoguanidine provides neuroprotection of retinal ganglion cells in a rat model of chronic glaucoma. *Proceedings of the National Academy of Sciences of the United States of America*, *96*(17), 9944–9948. https://doi.org/10.1073/pnas.96.17.9944

Nucci, C., Di Pierro, D., Varesi, C., Ciuffoletti, E., Russo, R., Gentile, R., Cedrone, C., Duran, M. D. P., Coletta, M., & Mancino, R. (2013). Increased malondialdehyde concentration and reduced total antioxidant capacity in aqueous humor and blood samples from patients with glaucoma. *Molecular Vision*, *19*, 1841–1846.

Okoye, G. S., & Gurnani, B. (2025). Traumatic Cataract. In *StatPearls*. StatPearls Publishing. http://www.ncbi.nlm.nih.gov/books/NBK594251/

Osborne, A., Khatib, T. Z., Songra, L., Barber, A. C., Hall, K., Kong, G. Y. X., Widdowson, P. S., & Martin, K. R. (2018). Neuroprotection of retinal ganglion cells by a novel gene therapy construct that achieves sustained enhancement of brain-derived neurotrophic factor/tropomyosin-related kinase receptor-B signaling. *Cell Death & Disease*, *9*(10), 1007. https://doi.org/10.1038/s41419-018-1041-8

Pang, I.-H., & Clark, A. F. (2020). Inducible rodent models of glaucoma. *Progress in Retinal and Eye Research*, *75*, 100799. https://doi.org/10.1016/j.preteyeres.2019.100799

Pérez-Torres, I., Guarner-Lans, V., & Rubio-Ruiz, M. E. (2017). Reductive Stress in Inflammation-Associated Diseases and the Pro-Oxidant Effect of Antioxidant Agents. *International Journal of Molecular Sciences*, *18*(10), 2098. https://doi.org/10.3390/ijms18102098

Pircher, A., Montali, M., Berberat, J., Remonda, L., & Killer, H. E. (2017). The Optic Canal: A Bottleneck for Cerebrospinal Fluid Dynamics in Normal-Tension Glaucoma? *Frontiers in Neurology*, *8*, 47. https://doi.org/10.3389/fneur.2017.00047

Prabhakaran, G. T., Al-Nosairy, K. O., Tempelmann, C., Wagner, M., Thieme, H., & Hoffmann, M. B. (2021). Functional Dynamics of Deafferented Early Visual Cortex in Glaucoma. *Frontiers in Neuroscience*, *15*, 653632. https://doi.org/10.3389/fnins.2021.653632

Ptito, M., Bleau, M., & Bouskila, J. (2021). The Retina: A Window into the Brain. *Cells*, *10*(12), 3269. https://doi.org/10.3390/cells10123269

Qu, J., Wang, D., & Grosskreutz, C. L. (2010). Mechanisms of Retinal Ganglion Cell Injury and Defense in Glaucoma. *Experimental Eye Research*, *91*(1), 48–53. https://doi.org/10.1016/j.exer.2010.04.002

Quigley, H. A., & Addicks, E. M. (1980). Chronic experimental glaucoma in primates. I. Production of elevated intraocular pressure by anterior chamber injection of autologous ghost red blood cells. *Investigative Ophthalmology & Visual Science*, *19*(2), 126–136.

Ren, R., Jonas, J. B., Tian, G., Zhen, Y., Ma, K., Li, S., Wang, H., Li, B., Zhang, X., & Wang, N. (2010). Cerebrospinal fluid pressure in glaucoma: A prospective study. *Ophthalmology*, *117*(2), 259–266. https://doi.org/10.1016/j.ophtha.2009.06.058

Rimbach, G., Gohil, K., Matsugo, S., Moini, H., Saliou, C., Virgili, F., Weber, S. U., & Packer, L. (2001). Induction of glutathione synthesis in human keratinocytes by Ginkgo biloba extract (EGb761). *BioFactors (Oxford, England)*, *15*(1), 39–52. https://doi.org/10.1002/biof.5520150104

Rotchford, A. P., & Johnson, G. J. (2002). Glaucoma in Zulus: A population-based cross-sectional survey in a rural district in South Africa. *Archives of Ophthalmology (Chicago, Ill.: 1960)*, *120*(4), 471–478. https://doi.org/10.1001/archopht.120.4.471

Saccà, S. C., Pascotto, A., Camicione, P., Capris, P., & Izzotti, A. (2005). Oxidative DNA damage in the human trabecular meshwork: Clinical correlation in patients with primary open-angle

glaucoma. *Archives of Ophthalmology (Chicago, Ill.: 1960)*, *123*(4), 458–463. https://doi.org/10.1001/archopht.123.4.458

Sato, K., Saigusa, D., Kokubun, T., Fujioka, A., Feng, Q., Saito, R., Uruno, A., Matsukawa, N., Ohno-Oishi, M., Kunikata, H., Yokoyama, Y., Yasuda, M., Himori, N., Omodaka, K., Tsuda, S., Maekawa, S., Yamamoto, M., & Nakazawa, T. (2023). Reduced glutathione level in the aqueous humor of patients with primary open-angle glaucoma and normal-tension glaucoma. *Npj Aging*, *9*(1), 28. https://doi.org/10.1038/s41514-023-00124-2

Shah, S. S., & Meyer, J. J. (2025). Lens-Induced Glaucoma. In *StatPearls*. StatPearls Publishing. http://www.ncbi.nlm.nih.gov/books/NBK574524/

Sharif, N. A. (2021). Therapeutic Drugs and Devices for Tackling Ocular Hypertension and Glaucoma, and Need for Neuroprotection and Cytoprotective Therapies. *Frontiers in Pharmacology*, *12*, 729249. https://doi.org/10.3389/fphar.2021.729249

Shinozaki, Y., Kashiwagi, K., & Koizumi, S. (2023). Astrocyte Immune Functions and Glaucoma. *International Journal of Molecular Sciences*, *24*(3), 2747. https://doi.org/10.3390/ijms24032747

Shinozaki, Y., Namekata, K., Guo, X., & Harada, T. (2024). Glial cells as a promising therapeutic target of glaucoma: Beyond the IOP. *Frontiers in Ophthalmology*, *3*. https://doi.org/10.3389/fopht.2023.1310226

Smith, A. M., & Czyz, C. N. (2025). Neuroanatomy, Cranial Nerve 2 (Optic). In *StatPearls*. StatPearls Publishing. http://www.ncbi.nlm.nih.gov/books/NBK507907/

Su, W., Li, Z., Jia, Y., & Zhuo, Y. (2014). Rapamycin is neuroprotective in a rat chronic hypertensive glaucoma model. *PloS One*, *9*(6), e99719. https://doi.org/10.1371/journal.pone.0099719

Sun, X., Dai, Y., Chen, Y., Yu, D.-Y., Cringle, S. J., Chen, J., Kong, X., Wang, X., & Jiang, C. (2017). Primary angle closure glaucoma: What we know and what we don't know. *Progress in Retinal and Eye Research*, *57*, 26–45. https://doi.org/10.1016/j.preteyeres.2016.12.003

Sunderland, D. K., & Sapra, A. (2025). Physiology, Aqueous Humor Circulation. In *StatPearls*. StatPearls Publishing. http://www.ncbi.nlm.nih.gov/books/NBK553209/

Tanaka, K., Kanno, T., Yanagisawa, Y., Yasutake, K., Inoue, S., Hirayama, N., & Ikeda, J.-E. (2014). A novel acylaminoimidazole derivative, WN1316, alleviates disease progression via suppression of glial inflammation in ALS mouse model. *PloS One*, *9*(1), e87728. https://doi.org/10.1371/journal.pone.0087728

Tanimoto, N. (Ed.). (2018). *Mouse Retinal Phenotyping* (Vol. 1753). Springer. https://doi.org/10.1007/978-1-4939-7720-8

Tektas, O.-Y., & Lütjen-Drecoll, E. (2009). Structural changes of the trabecular meshwork in different kinds of glaucoma. *Experimental Eye Research*, *88*(4), 769–775. https://doi.org/10.1016/j.exer.2008.11.025

Tezel, G. (2008). TNF-alpha signaling in glaucomatous neurodegeneration. *Progress in Brain Research*, *173*, 409–421. https://doi.org/10.1016/S0079-6123(08)01128-X

Tezel, G. (2009). The Role of Glia, Mitochondria, and the Immune System in Glaucoma. *Investigative Opthalmology & Visual Science*, *50*(3), 1001. https://doi.org/10.1167/iovs.08-2717

Tezel, G., Chauhan, B. C., LeBlanc, R. P., & Wax, M. B. (2003). Immunohistochemical assessment of the glial mitogen-activated protein kinase activation in glaucoma. *Investigative Ophthalmology & Visual Science*, *44*(7), 3025–3033. https://doi.org/10.1167/iovs.02-1136

Tezel, G., & Wax, M. B. (1999). Inhibition of caspase activity in retinal cell apoptosis induced by various stimuli in vitro. *Investigative Ophthalmology & Visual Science*, *40*(11), 2660–2667.

Tezel, G., & Wax, M. B. (2000). Increased production of tumor necrosis factor-alpha by glial cells exposed to simulated ischemia or elevated hydrostatic pressure induces apoptosis in cocultured retinal ganglion cells. *The Journal of Neuroscience: The Official Journal of the Society for Neuroscience*, *20*(23), 8693–8700. https://doi.org/10.1523/JNEUROSCI.20-23-08693.2000

Tezel, G., Yang, X., & Cai, J. (2005). Proteomic identification of oxidatively modified retinal proteins in a chronic pressure-induced rat model of glaucoma. *Investigative Ophthalmology & Visual Science*, *46*(9), 3177–3187. https://doi.org/10.1167/iovs.05-0208

Thomas, C. N., Thompson, A. M., Ahmed, Z., & Blanch, R. J. (2019). Retinal Ganglion Cells Die by Necroptotic Mechanisms in a Site-Specific Manner in a Rat Blunt Ocular Injury Model. *Cells*, *8*(12), Article 12. https://doi.org/10.3390/cells8121517

Tian, B., Gabelt, B. T., Geiger, B., & Kaufman, P. L. (2009). The role of the actomyosin system in regulating trabecular fluid outflow. *Experimental Eye Research*, *88*(4), 713–717. https://doi.org/10.1016/j.exer.2008.08.008

Tourtas, T., Birke, M. T., Kruse, F. E., Welge-Lüssen, U.-C., & Birke, K. (2012). Preventive effects of omega-3 and omega-6 Fatty acids on peroxide mediated oxidative stress responses in primary human trabecular meshwork cells. *PloS One*, *7*(2), e31340. https://doi.org/10.1371/journal.pone.0031340

Tovar-Vidales, T., Fitzgerald, A. M., & Clark, A. F. (2016). Human trabecular meshwork cells express BMP antagonist mRNAs and proteins. *Experimental Eye Research*, *147*, 156–160. https://doi.org/10.1016/j.exer.2016.05.004

Tripathi, R. C. (1977). Pathologic anatomy in the outflow pathway of aqueous humour in chronic simple glaucoma. *Experimental Eye Research*, *25 Suppl*, 403–407. https://doi.org/10.1016/s0014-4835(77)80035-3

Visuvanathan, S., Baker, A. N., Lagali, P. S., Coupland, S. G., Miller, G., Hauswirth, W. W., & Tsilfidis, C. (2022). XIAP gene therapy effects on retinal ganglion cell structure and function in a mouse model of glaucoma. *Gene Therapy*, *29*(3–4), 147–156. https://doi.org/10.1038/s41434-021-00281-7

Wagner, I. V., Stewart, M. W., & Dorairaj, S. K. (2022). Updates on the Diagnosis and Management of Glaucoma. *Mayo Clinic Proceedings. Innovations, Quality & Outcomes*, *6*(6), 618–635. https://doi.org/10.1016/j.mayocpiqo.2022.09.007

Wang, H., Wang, R., Thrimawithana, T., Little, P. J., Xu, J., Feng, Z.-P., & Zheng, W. (2014). The Nerve Growth Factor Signaling and Its Potential as Therapeutic Target for Glaucoma. *BioMed Research International*, *2014*(1), 759473. https://doi.org/10.1155/2014/759473

Wang, J., & Barton, K. (2017). Aqueous shunt implantation in glaucoma. *Taiwan Journal of Ophthalmology*, *7*(3), 130–137. https://doi.org/10.4103/tjo.tjo_35_17

Wang, M., Li, J., & Zheng, Y. (2020). The Potential Role of Nuclear Factor Erythroid 2-Related Factor 2 (Nrf2) in Glaucoma: A Review. *Medical Science Monitor: International Medical Journal of Experimental and Clinical Research*, *26*, e921514. https://doi.org/10.12659/MSM.921514

Wang, M., & Zheng, Y. (2019). Oxidative stress and antioxidants in the trabecular meshwork. *PeerJ*, *7*, e8121. https://doi.org/10.7717/peerj.8121

Weinreb, R. N., Aung, T., & Medeiros, F. A. (2014). The pathophysiology and treatment of glaucoma: A review. *JAMA*, *311*(18), 1901–1911. https://doi.org/10.1001/jama.2014.3192

Weiss-Sadan, T., Ge, M., Hayashi, M., Gohar, M., Yao, C.-H., de Groot, A., Harry, S., Carlin, A., Fischer, H., Shi, L., Wei, T.-Y., Adelmann, C. H., Wolf, K., Vornbäumen, T., Dürr, B. R., Takahashi, M., Richter, M., Zhang, J., Yang, T.-Y., … Bar-Peled, L. (2023). NRF2 activation induces NADH-reductive stress, providing a metabolic vulnerability in lung cancer. *Cell Metabolism*, *35*(3), 487-503.e7. https://doi.org/10.1016/j.cmet.2023.01.012

Wooff, Y., Man, S. M., Aggio-Bruce, R., Natoli, R., & Fernando, N. (2019). IL-1 Family Members Mediate Cell Death, Inflammation and Angiogenesis in Retinal Degenerative Diseases. *Frontiers in Immunology*, *10*. https://doi.org/10.3389/fimmu.2019.01618

Wu, X., Pang, Y., Zhang, Z., Li, X., Wang, C., Lei, Y., Li, A., Yu, L., & Ye, J. (2019). Mitochondria-targeted antioxidant peptide SS-31 mediates neuroprotection in a rat experimental glaucoma model. *Acta Biochimica Et Biophysica Sinica*, *51*(4), 411–421. https://doi.org/10.1093/abbs/gmz020

Xu, D. G., Crocker, S. J., Doucet, J. P., St-Jean, M., Tamai, K., Hakim, A. M., Ikeda, J. E., Liston, P., Thompson, C. S., Korneluk, R. G., MacKenzie, A., & Robertson, G. S. (1997). Elevation of neuronal expression of NAIP reduces ischemic damage in the rat hippocampus. *Nature Medicine*, *3*(9), 997–1004. https://doi.org/10.1038/nm0997-997

Yamauchi, Y., Mochizuki, J.-I., Hirakata, A., & Uda, S. (2016). Single flash electroretinograms of mature cataractous and fellow eyes. *Clinical Ophthalmology (Auckland, N.Z.)*, *10*, 2031–2034. https://doi.org/10.2147/OPTH.S118677

Yang, J., Yang, P., Tezel, G., Patil, R. V., Hernandez, M. R., & Wax, M. B. (2001). Induction of HLA-DR expression in human lamina cribrosa astrocytes by cytokines and simulated ischemia. *Investigative Ophthalmology & Visual Science*, *42*(2), 365–371.

Zanon-Moreno, V., Marco-Ventura, P., Lleo-Perez, A., Pons-Vazquez, S., Garcia-Medina, J. J., Vinuesa-Silva, I., Moreno-Nadal, M. A., & Pinazo-Duran, M. D. (2008). Oxidative stress in primary open-angle glaucoma. *Journal of Glaucoma*, *17*(4), 263–268. https://doi.org/10.1097/IJG.0b013e31815c3a7f

Zhou, Y., Grinchuk, O., & Tomarev, S. I. (2008). Transgenic mice expressing the Tyr437His mutant of human myocilin protein develop glaucoma. *Investigative Ophthalmology & Visual Science*, *49*(5), 1932–1939. https://doi.org/10.1167/iovs.07-1339